Fabrication and Characterization of Protective Hole Transport Layer for Efficient and Durable Perovskite Solar Cell.

By

Anum Ameer

Fall 2016-MS Energy Systems Engineering

00000171057

Supervised by

Dr. Nadia Shahzad

Center for Advanced Studies in Energy (CAS-EN)

National University of Sciences & Technology (NUST)

H-12, Islamabad, 44000, Pakistan

December 2019

Fabrication and Characterization of Protective Hole Transport Layer for Efficient and Durable Perovskite Solar Cell.

By

Anum Ameer

Fall 2016-MS Energy Systems Engineering

Reg. No: 00000171057

Supervised by

Dr. Nadia Shahzad

A Thesis Submitted to the Center for Advanced Studies in Energy in partial fulfillment of the requirements for the degree of

Masters of Science in ENERGY SYSTEM ENGINEERING

Center for Advanced Studies in Energy (CAS-EN)

National University of Sciences & Technology (NUST)

H-12, Islamabad, 44000, Pakistan

December 2019

THESIS ACCEPTANCE CERTIFICATE

Certified that final copy of MS/MPhil thesis written by **Ms. Anum Ameer**, (Registration No: **00000171057**), of **MS ESE/CAS-EN/NUST** has been vetted by undersigned, found complete in all respects as per NUST Statues/Regulations, is within the similarity indices limit and is accepted as partial fulfillment for the award of MS degree. It is further certified that necessary amendments as pointed out by GEC members of the scholar have also been incorporated in the said thesis.

Signature: _____

Name of Supervisor _____

Date: _____

Signature (HoD ESE): _____

Date: _____

Signature (Dean/Principal): _____

Date: _____

Certificate

This is to certify that work in this thesis has been carried out by **Ms. Anum Ameer** and completed under my supervision in Center for Advanced Studies in Energy (CAS-EN), National University of Sciences and Technology, H-12, Islamabad, Pakistan.

Supervisor:

_____
Dr. Nadia Shahzad
CAS-EN
NUST, Islamabad

GEC member # 1:

_____
Dr. Naseem Iqbal
CAS-EN
NUST, Islamabad

GEC member # 2:

_____
Dr. Pervaiz Akhter
CAS-EN
NUST, Islamabad

GEC member # 3:

_____
Dr. Rabia Liaquat
CAS-EN
NUST, Islamabad

HoD-ESE:

_____
Dr. Naseem Iqbal
CAS-EN
NUST, Islamabad

Principal/ Dean:

_____
Dr. Adeel Waqas
CAS-EN
NUST, Islamabad

Acknowledgement

First of all, I want to thank Allah Almighty, The Most Beneficent, Most Merciful who made me able to gain this goal. I have no words to express my gratitude to my loving family and supportive friends for their prayers, understanding, trust and confidence for me during this whole project. I want to pay my heartiest gratitude to my supervisor Dr. Nadia Shahzad for her guidance, support and motivation, for being helpful, kind, and generous throughout this work. I want to thank the GEC members, Dr. Naseem Iqbal, Dr. Parvez Akhter and Dr. Rabia Liaquat for their guidance and help. I am grateful to Dr. Imran Shahzad for his guidance and support throughout my work at National Centre for Physics (NCP). I am thankful to laboratory engineers and department staff for their help and co-operation for completing this project.

Abstract

Pakistan being an energy deficient country requires to trend toward renewable energy technologies. Solar energy is considered as most proficient form of renewable energy in Pakistan. Perovskite Solar cells were introduced in 2009, since then the efficiencies have surged from single digits to certified 27.3%. Perovskites, being an efficient technology seems to be the key to our energy requirements. Efficient charge transporting mediums add to the efficiency of the Perovskite Solar Cells. In conventional structures, hole transporting layer not only transports holes, it blocks electrons and also protects perovskite from external degradation factors. Hole transporting materials also contribute to increased stability and improved surface coverage of perovskite solar cells. Selection criterion for efficient hole transporting materials include high hole mobility and thermal stability, compatible ionization potential, external degradation factors resistance and low cost. In this work, a bilayer comprising of NiO and MWCNTs has been fabricated as an HTL. NiO HTL was deposited through spin coating and MWCNT thin film was deposited over it through Ultrasonic spray coating on the absorber layer for all the cells. Difference between sintered NiO film and non-sintered NiO film has been studied as well. All the layers were individually characterized and tested using XRD for phase identification, SEM/EDS for surface morphology, UV-Vis spectroscopy to study the optical properties, Hall Effect to check the electrical properties and Contact angle measurement for wettability studies of the samples prepared.

Key words: Photovoltaics, Nickel Oxide, MWCNTs, Hole transporting material, Perovskite Solar cell.

Contents

Abstract v
Contents vi
List of Figures ix
List of Tables xi
List of Abbreviations xii
List of Publications xiii
Chapter 1: Introduction 1
1.1. Energy Scenario 1
1.2. Renewable energy 2
1.3. Solar Cells 3
1.4. Generations of solar cells 3
1.4.1. First Generation Solar Cells 3
1.4.2. Second Generation Solar Cells 3
1.4.3. Third Generation Solar Cells 4
1.5. Perovskite Solar cell 4
1.5.1. Perovskite Solar Cell Working Principle 5
1.5.2. Perovskite Structure 5
1.6. Advantages and limitations of PSCs 6
1.7. Purpose and working of Hole transporting material 6
1.7.1. Characteristics of effective hole transporting materials 7
1.7.2. Typically used hole transporting materials 8
1.8. Thesis Work 8
1.9. Summary 9
References 10
Chapter 2: Literature Review 12
2.1. History 12
2.2. Structure of perovskite solar cells (PSCs) 12
2.2.1. Functional Description of PSC layers 12
2.3. Physics of perovskite solar cells (PSCs) 13
2.3.1. Light absorption 13

2.3.2. Exciton formation and diffusion 13
2.3.3. Charge separation 14
2.3.4. Electron and hole injection following charge collection 14
2.4. Layers of Perovskite Solar Cell (PSC) 14
2.4.1. Electron Transporting Layer 15
2.4.2. Perovskite /Absorber Layer 15
2.4.3. Hole Transporting Layer 16
2.5. Hole Transporting materials in PSCs 17
2.5.1. Organic Hole transporting materials 17
2.5.2. Inorganic HTMs 18
2.6. PSCs Degradation Factors 20
2.7. Summary 21
References 22
Chapter 3: Synthesis Approaches and Characterization Techniques 30
3.1. Nanoparticles Synthesis Approaches 30
3.1.1. Bottom up approach 30
3.1.2. Top Down approach 30
3.2. Material Synthesis Methodologies 31
3.2.1. Sol Gel Method 31
3.2.2. Co precipitation Technique 32
3.2.3. Hydrothermal Technique 32
3.3. Thin Film Deposition Techniques 33
3.3.1. Physical Vapor Deposition 33
3.3.2. Chemical Vapor Deposition (CVD) 34
3.3.3. Solution Based Chemical Processes 35
3.4. Characterization techniques 37
3.4.1. Optical Microscope 37
3.4.2. Scanning Electron Microscope 38
3.4.3. X-Ray Diffraction 39
3.4.4. UV-Visible Spectroscopy 40
3.4.5. Hall Effect 41
3.4.6. Contact Angle Measurement 41
3.5. Summary 42

References 43
Chapter 4: Material and Methodology 45
4.1. Experimentation 45
4.1.1. Synthesis of nickel oxide nanoparticles 45
4.1.2. Characterization of Nickel Oxide nanoparticles 46
4.1.3. HTL Fabrication: 47
4.2. Film Characterization 47
4.3. Summary 48
Chapter 5: Results and Discussion 49
5.1. NiO Nanoparticles fabrication through varying techniques 49
5.1.1. Structural Characterization 49
5.1.2. Morphological Characterization 50
5.2. Optimization of NiO Nanoparticles through variation in process conditions 51
5.2.1. Structural Characterization 52
5.2.2. Morphological Characterization 53
5.3. HTL Characterizations 55
5.3.1. Structural Analysis 55
5.3.2. Morphological Analysis 56
5.3.3. Electrical Properties Investigation 58
5.3.4. Optical Characterization 59
5.3.5. Contact Angle Measurement 60
5.4. Summary 61
References 63
Chapter 6: 67
Conclusion and Recommendations 67
6.1. Conclusion 67
6.2. Future Recommendations 67
Journal Paper 69

List of Figures

Figure 1.1: Pakistan Energy Share. (2018). Source: Ministry of Energy, Power Division.[3] 1
Figure 1.2: Renewable energy Types 2
Figure 1.3: Classification of Solar Cells 3
Figure 1.4: Solar cell Efficiencies. Source: NREL [8] 4
Figure 1.5: Perovskite Solar Cell Working 5
Figure 1.6: (a) n-i-p mesoscopic PSC structure (b) n-i-p planar PSC structure (c) p-i-n planar PSC structure 6
Figure 1.7: Characteristics of effective HTMs 7
Figure 2.1: PSC Structure 12
Figure 2.2: PSC Destabilizing Factors. 20
Figure 3.1: Synthesis Approaches for Nano structures. 30
Figure 3.2: Sol Gel Process 31
Figure 3.3: Co-precipitation Process 32
Figure 3.4: Classification of thin film deposition techniques 33
Figure 3.5: CVD Mechanism 34
Figure 3.6: Spray Pyrolysis 36
Figure 3.7: Optical Microscope Working Mechanism [12] 37
Figure 3.8: SEM Components 38
Figure 3.9: XRD Components 39
Figure 3.10: UV-Vis Spectrophotometer Components 40
Figure 3.11: Hall effect working mechanism 41
Figure 3.12: Varying Contact Angle 42
Figure 4.1: NiO Nanoparticles preparation process flow chart. 46
Figure 4.5: HTL Deposition Process 47
Figure 5.1: XRD Spectra for Sample A & Sample B 50
Figure 5.2:SEM Images (a) Sample prepared through co-precipitation technique (b) Sample prepared through hydrothermal synthesis. 51
Figure 5.3: XRD Spectra for Sample 1, Sample 2, Sample 3, Sample 4 52

Figure 5.4: SEM Images (a) Sample 1 (b) Sample 2 (c) Sample 3 (d) Sample 4 54
Figure 5.5: XRD Spectra for hole transporting layer 56
Figure 5.6: SEM Images (a) NiO thin film (b) MWCNTs thin film 57
Figure 5.7: UV-Vis Spectra of NiO Thin film, MWCNT Thin film and Bi-layer. 60
Figure 5.8: Contact Angles (a) NiO Film (b) Sintered NiO FILM (c) Bi-Layer (d) Sintered Bilayer 61

List of Tables

Table 4.1:Varied Process Conditions during Co-precipitation technique.....46
Table 5.1: Crystallite Size Calculation.....53
Table 5.2:Electrical Characterization Results 59

List of Abbreviations

PSCs	Perovskite solar cells
DSSCs	Dye sensitized solar cells
ITO	Indium tin oxide
FTO	Fluorine tin oxide
HOMO	Highest occupied molecular orbital
LUMO	Lowest unoccupied molecular orbital
HTL	Hole transport layer
ETL	Electron transport layer
HTM	Hole transport material
Voc	Open circuit voltage
Jsc	Short circuit current density
PCE	Power conversion efficiency
XRD	X-ray diffraction
SEM	Scanning electron microscopy
UV-Vis	Ultra Violet Visible
CdTe	Cadmium Telluride
CIGS	Copper Indium Gallium Di-selenide
CIS	Copper Indium sulfide
TiO_2	Titania
CuI	Copper Iodide
CuSCN	Copper thiocyanate
NiO	Nickel Oxide
PEDOT: PSS	Poly (3,4-ethylenedioxythiophene) polystyrene sulfonate
PCBM	[6,6]-phenyl-C61-butyric acid methyl ester
MWCNTs	Multi walled carbon nanotubes

List of Publications

1. **Anum Ameer**, Nadia Shahzad, Imran Shahzad, Bushra Batool, "*Synthesis and Characterization of Nickel Oxide Nanostructures for Solar Cell Application*", presented and accepted for the proceeding of MSNANO-2019, Conference held at GCU, Faisalabad.
2. **Anum Ameer**, Nadia Shahzad, Imran Shahzad, Bushra Batool "*Fabrication and characterization of NiO;MWCNTs based protective hole transporting layer for perovskite solar cell application*" [Submitted to Journal of Solar Energy Materials and Solar Cells]
3. Bushra Batool, Nadia Shahzad, Imran Shahzad**, Anum Ameer**, " *Sintering and pH effect on Low Temperature Processed Tin Oxide Nanoparticles for Perovskite Solar Cells Application"*, presented and accepted for the proceedings of MSNANO-2019.

Chapter 1: Introduction

1.1. Energy Scenario

Fossil fuels which are considered as primary source of energy supply include coal, natural gas and oil. Fossil fuels are not only non-renewable but burning of these fossil fuels is a major contributing factor of greenhouse gas emission in the atmosphere [1]. Steady use of non-renewable energy systems continues to trigger damage towards the earth through consistent discharge of carbon pollution. Global warming has an extensive effect on the environment which has dangerous effects on natural ecosystems. Demand for renewable energy has grown tremendously in recent years [2].

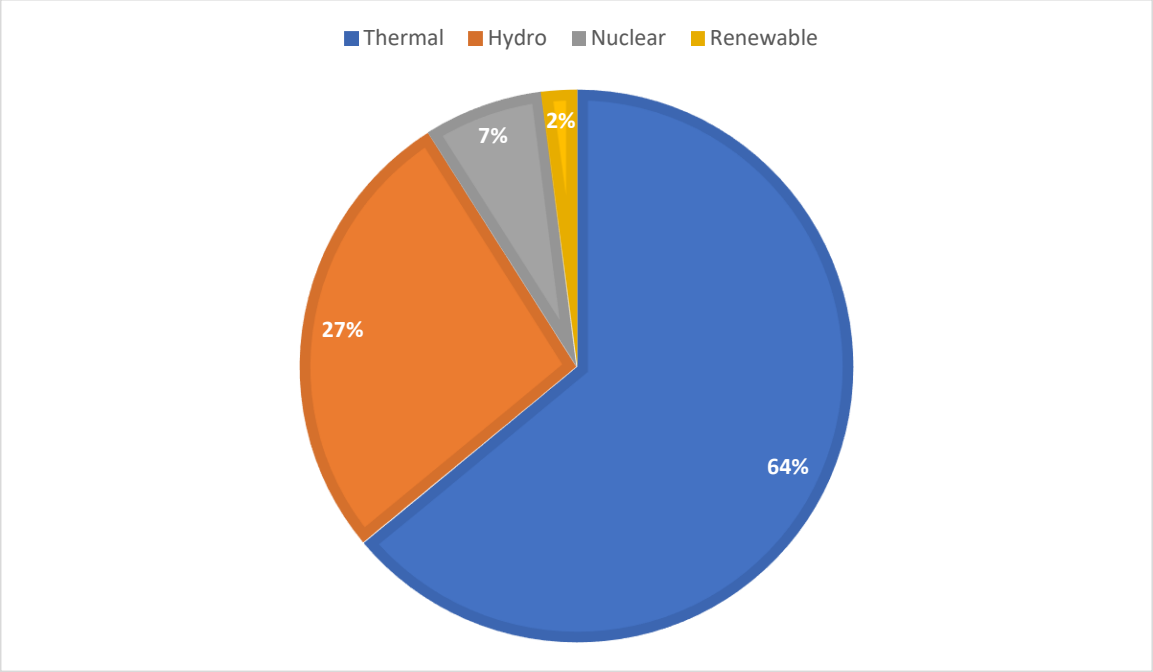

Figure 1.1: Pakistan Energy Share. (2018). Source: Ministry of Energy, Power Division[3].

Pakistan is the 6th largest country by population in the world where energy demand increases more than 9% annually. Electricity demand and supply gap has also increased during past few years. Economic development is caught up due to energy shortage problems. Renewable energy's current share in the total energy mix of the country is

insufficient. Fossil fuels are utilized to fulfill energy needs which lead to environmental hazards. Different renewable energy sources are being explored in Pakistan among which solar energy leads as most suitable source. Sun based energy is affordable, no maintenance or operation cost is required and its average life span is suitable as well. Solar power potential of Pakistan is 1600,000 MW and its geographical placement in the sun belt make it an ideal country for solar power consumption [4].

1.2. Renewable energy

Renewable energy refers to electricity or fuels made from sustainable natural resources. It is sustainable, non-polluting, reliable and efficient. Renewable energy consumption not only contributes to reduced global carbon dioxide emissions, dependence on limited reserves of fossil fuels is also reduced. Solar Energy, Wind Energy, Geothermal Energy, Bioenergy are considered as common renewable energy sources which have the advantage of being renewable, clean forms of energy, with innovative conversion and applications techniques being developed for their utilization [5].

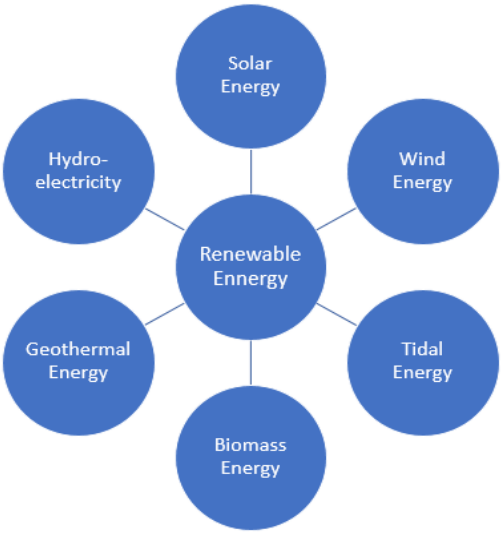

Figure 1.2: Renewable energy Types

Solar energy is a vast and inexhaustible resource. Considering the energy capturing, conversion, and distribution, solar technologies are categorized as either passive or active. Photovoltaic panels and solar thermal collectors are employed in active solar technologies while passive solar technologies consist of building material selection, building orientation, and considers light scattering properties of material as well. Fastest-growing source of alternative energy is solar power in which the process employs solar cells for photovoltaic effect. Solar-thermal power concentrates a large area of sunlight on small region by using lenses and mirrors [6].

1.3. Solar Cells

A solar cell also known as photovoltaic cell uses photovoltaic effect for the conversion of light energy into electricity. Solar cells are the building blocks of photovoltaic modules. Light absorption , electron-hole pairs generation, opposite charge carriers separation and their separate extraction to an external circuit are the basic attributes of a solar cell [7].

1.4. Generations of solar cells

Solar cells can be categorized as first, second and third generation cells.

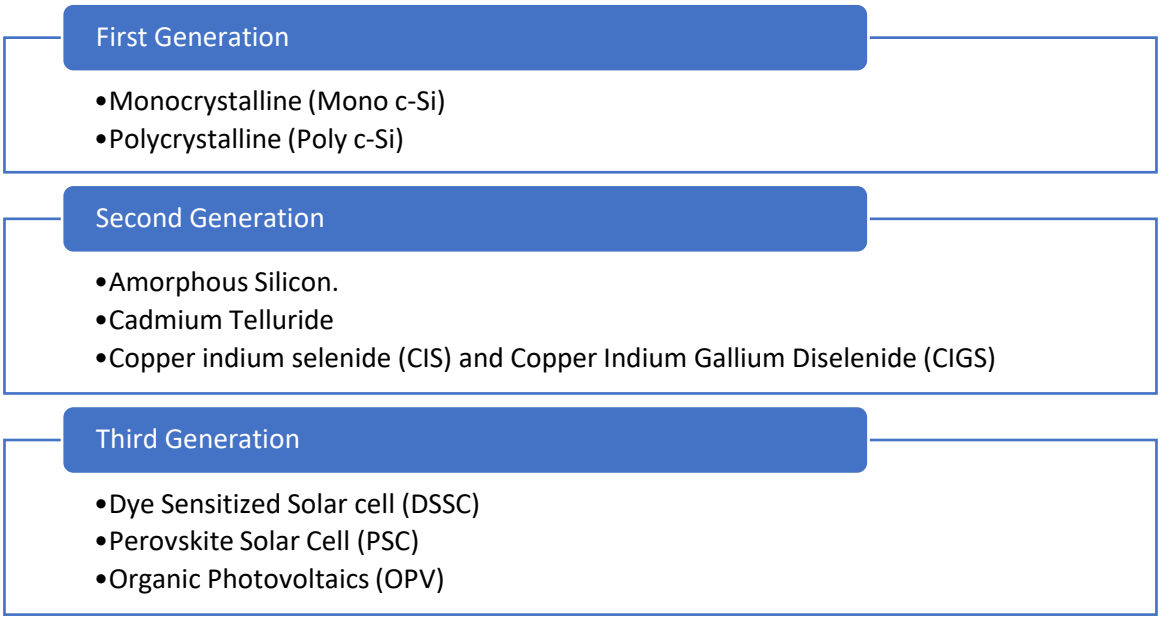

Figure 1.3: Classification of Solar Cells

1.4.1. First Generation Solar Cells

First generation solar cells include silicon based solar cells which have attained an excellent efficiency and are widely used for residential purpose. Silicon solar cells based on silicon wafer and hetero-junction silicon based solar cells have achieved an efficiency of 15%-20%. This category of solar cell includes mono-crystalline, poly-crystalline and amorphous silicon solar cells.

1.4.2. Second Generation Solar Cells

Second generation of solar cell consist of thin-film solar cells, like hetero-junction solar cells, CIGS and CdTe based solar cells. These types of cells are made from thin layers of semi-conductor materials. Because of less cost and less material usage in these types of

solar cells, these cells can be used instead of 1st generation silicon based solar cells. But mass production of this type of solar cells are difficult to achieve, moreover the techniques like vacuum processing and high temperature treatments of thin films require great amount of energy consumption. Efficiency attained by this category of solar cells is around 9%-18%.

1.4.3. Third Generation Solar Cells

Third generation solar cells have been created to achieved higher efficiency at low cost. Quantum dots solar cells, organic solar cells, dye-sensitized solar cells and perovskite solar cells are included in this category of solar cells. These solar cells are low in cost of materials and manufacturing.

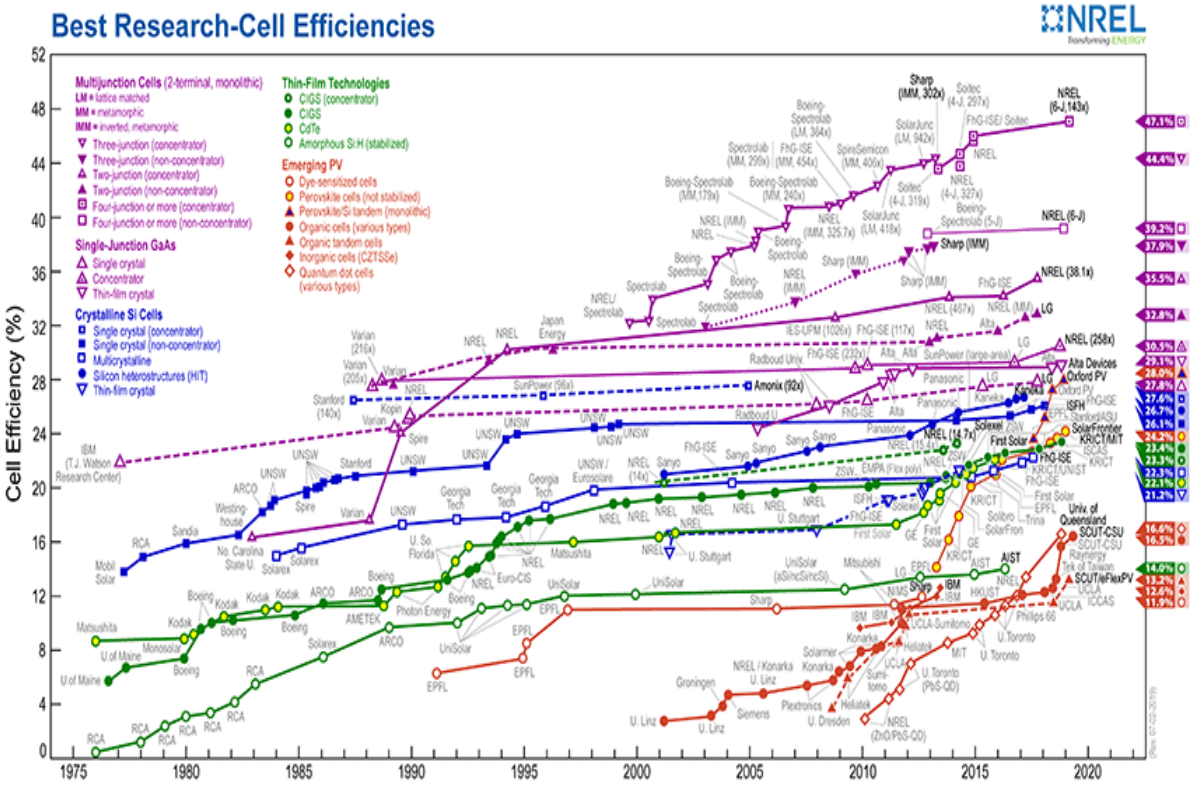

Figure 1.4: Solar cell Efficiencies. Source: NREL [8]

1.5. Perovskite Solar cell

A perovskite solar cell has a light-harvesting active layer sandwiched between two transporting layers known as electron transport layer and hole transport layer which collect the mobile charges. First perovskite solar cell was reported by Miyasaka et al. in

2009. The terms "perovskite" refers to a compound with ABX_3 structure, Where A and B are cations and X is a halogen anion.

1.5.1. Perovskite Solar Cell Working Principle

A perovskite solar cell works when incident light falls on perovskite material and creates electron-hole pair, separation of the charged particles takes place because of low binding energy. Separated charges diffuse through the charge conducting layers, electric current is produced as a result when these charges are collected by their respective electrodes.

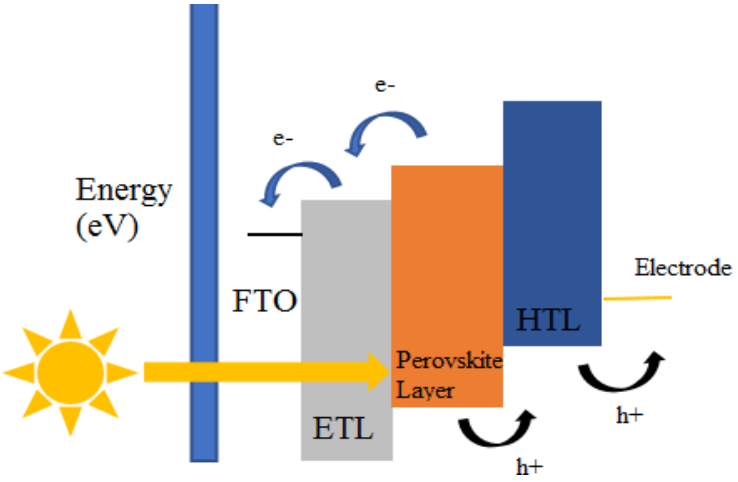

Figure 1.5: Perovskite Solar Cell Working

1.5.2. Perovskite Structure

Perovskite solar cells (PSCs) have two device architectures known as mesostructured and planar device. Perovskite solar cells have layered device structure in which the perovskite layer is sandwiched between two charge transporting layers i.e. hole transporting layer (HTL) and electron transporting layer (ETL). If the top layer is an electron transporting layer (ETL) then it is an n-i-p structure and if the top layer is a hole transporting layer (HTL) then it is p-i-n structure. Mesoscopic solar cell configuration is given as: compact electron transport layer/mesoporous electron transport layer /perovskite/Hole transport layer /electrode. There are two kinds of band configurations for planar type perovskite solar cell known as n-i-p planar structure and p-i-n planar structure. In case of an n-i-p structure, perovskite material is deposited on transparent substrates covered with compact TiO_2 film and an optional mesoporous TiO_2 or Al_2O_3 scaffold layer. In case of a p-i-n

structure, perovskite material is deposited on transparent substrates which are covered with a hole transporting layer. High performance and stability has been depicted by incorporation of both mesoscopic and planar structures in perovskite solar cells [8].

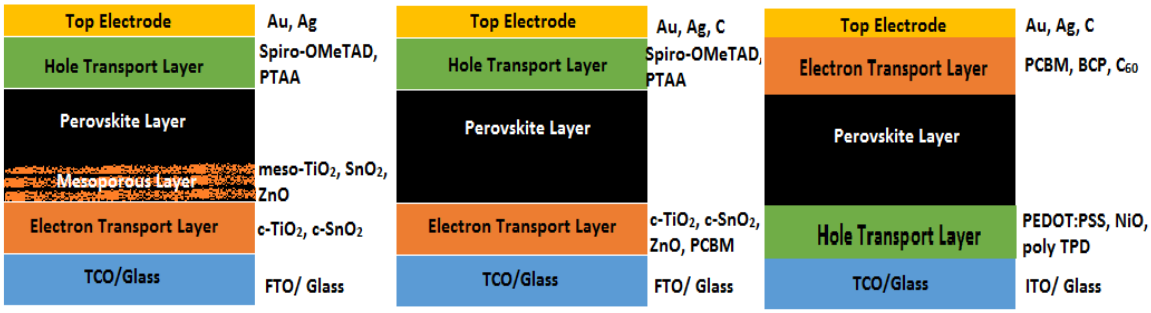

Figure 1.6: (a) n-i-p mesoscopic PSC structure (b) n-i-p planar PSC structure (c) p-i-n planar PSC structure

1.6. Advantages and limitations of PSCs

Advantages:

1. Direct optical band gap (~1.5 Ev) is offered by perovskite material.
2. Long diffusion length and long minority carrier lifetime of perovskite material.
3. Broad absorption range and high absorption coefficient (10^5 cm^{-1}) of perovskite material.
4. High efficiencies (more than 22%) have been delivered by perovskite solar cell.
5. It has fast charge separation process, high dielectric constant, long carrier separation lifetime and long transport distance of electrons and holes.

Limitations:

1. Perovskite solar cell are unstable when exposed to atmospheric conditions such as moisture, heat etc.
2. Perovskite material has toxic contents.

1.7. Purpose and working of Hole transporting material

Hole transporting layer has various purposes in a perovskite solar cell. Hole transfer efficiency is improved due to hole transporting layer. An HTL determines the splitting of the perovskite quasi Fermi-energy levels which effects the open voltage circuit. In the

absence of an HTL, metal (Au)-perovskite interface degradation might take place. Incorporation of a suitable hole transporting materials and light harvesting layer in perovskite solar cells leads to high V_{OC} (1.5-1.61 V). Surface coverage of perovskite solar cell is improved due to HTL and charge recombination is suppressed which results in improved performance. Incorporation of suitable hole transporting layer results in perovskite solar cells with increased stability [9].

1.7.1. Characteristics of effective hole transporting materials

Hole transporting material is considered as an important active material in perovskite solar cell due to its ability of effective hole extraction at the perovskite-hole transporting material interface.

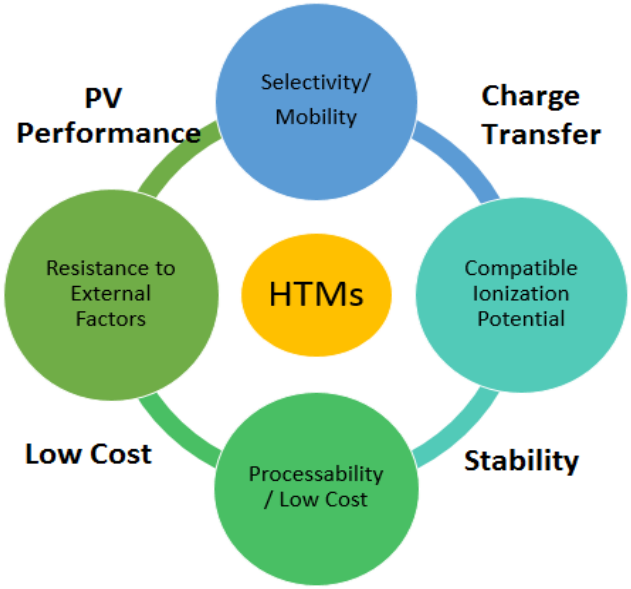

Figure 1.7: Characteristics of effective HTMs

Hole transporting layer should have certain characteristics for effective device operation. It should have high hole mobility and thermal stability. Its ionization potential should be compatible with that of a perovskite material. It should be resistant to external degradation factors. High cost of typically used hole transporting materials makes it one of the most expensive part of PSCs, it should be economic as well. Low electron affinity of hole transporting material might add beneficial electron blocking properties as well. There is a significant impact of hole transporting material mobility on solar cell efficiency.

Significant ohmic losses occur due to low mobility in a hole transporting layer which results in decreased fill factor. Uniform coverage and high mobility of hole transporting layer should be ensured as well for improved power conversion efficiency [9].

1.7.2. Typically used hole transporting materials

Majorly Polymer based hole transporting materials (e.g.: Spiro-OMeTAD, PEDOT: PSS, P3HT etc.) are used which make hole transporting materials as most expensive material component in perovskite solar cells [9]. Nickel oxide known for its corrosion resistance and superior strength has been employed in different material applications by different researchers. Ahmad A.F. et al. synthesized composites of Nickel Oxide and Polycaprolactone through melt blend technique & suggested its applicability in developing absorbing and shielding materials [10]. Dar et al. employed bottom-up approach for electrochemical growth of Nickel oxide nanotubes which exhibited exceptional capacitance properties for supercapacitor applications [11]. Jian-mei LI, et al. developed high corrosion resistance nano-structured nickel film through electrodeposition [12]. A. Rahdar et al. synthesized Nickel Oxide nanostructures through co-precipitation technique, nanostructures calcinated at 500^{o}C exhibited superparamagnetic behavior [13]. S. Zhou et al. synthesized superhydrophobic MWCNTs-Ni/a-C:H nanocomposite film through one-step electrochemical deposition. Nanocomposite film possessed corrosion resistance and self-cleaning properties as well [14]. Y. Yang et al. employed hydrothermally synthesized Nickel Oxide Nano Particles in combination with MWCNTs as hole transporting material in a perovskite solar cell which showed an efficiency of 15.4% [15].

1.8. Thesis Work

My aim is to fabricate a protective Hole Transporting Material for efficient and durable perovskite solar cells comprising of Nickel Oxide and Carbon Nano tubes thin films and to study the properties of the Hole transport material and cell efficiency.

1.9. Summary

Pakistan being an energy deficient country requires to trend toward renewable energy technologies. Solar energy is considered as most proficient form of renewable energy in Pakistan. Perovskite Solar cells were introduced in 2009, since then the efficiencies have surged from single digits to certified 27.3%. Perovskites, being an efficient technology seems to be the key to our energy requirements. Efficient charge transporting mediums result in enhanced efficiency of the Perovskite Solar Cells. Hole Transporting layer not only works as a blocking layer between anode and perovskite layer but also upgrades hole transporting efficiency of the cell. Hole transporting materials contributes in lowering the transportation barrier and blocking the electron transfer between electrode and perovskite for low carrier recombination in order to make the device more efficient. Hole transporting material plays a significant role in enhancing perovskite solar cell efficiency. In conventional structures, hole transporting layer has its share in transportation of holes, electrons blocking, and protection from external factors. Hole transporting materials also contributes to increased stability and better surface coverage of perovskite solar cells.

References

[1] "Fossils Fuels vs. Renewable Energy | Ecology Global Network." [Online]. Available: https://www.ecology.com/2011/09/06/fossil-fuels-renewable-energy-resources/. [Accessed: 14-Nov-2019].

[2] "Declining Costs and Technology Are Powering Renewable Energy Demand - Environment + Energy Leader."[Online].Available:

https://www.environmentalleader.com/2018/09/report-declining-costs-and-technology-are-powering-renewable-energy-demand/. [Accessed: 14-Nov-2019].

[3] "A Review of Pakistan's Energy Policy (Facts & Figures)." [Online]. Available: http://www.pakistaneconomist.com/2019/01/28/a-review-of-pakistans-energy-policy-facts-figures/. [Accessed: 14-Nov-2019].

[4] M. Irfan, Z.-Y. Zhao, M. Ahmad, and M. Mukeshimana, "Solar Energy Development in Pakistan: Barriers and Policy Recommendations," *Sustainability*, vol. 11, no. 4, p. 1206, 2019.

[5] "Examples of renewable resources and alternative energy being used today." [Online]. Available: https://www.solarreviews.com/blog/examples-of-renewable-resources-and-alternative-energy-being-used-today. [Accessed: 14-Nov-2019].

[6] "renewable energy Archives - Universe Today." [Online]. Available: https://www.universetoday.com/tag/renewable-energy/. [Accessed: 14-Nov-2019].

[7] A. Mohammad Bagher, "Types of Solar Cells and Application," *Am. J. Opt. Photonics*, vol. 3, no. 5, p. 94, 2015.

[8] R. Wang, M. Mujahid, Y. Duan, Z. K. Wang, J. Xue, and Y. Yang, "A Review of Perovskites Solar Cell Stability," *Adv. Funct. Mater.*, vol. 1808843, pp. 1–25, 2019.

[9] Z. H. Bakr, Q. Wali, A. Fakharuddin, L. Schmidt-Mende, T. M. Brown, and R. Jose, "Advances in hole transport materials engineering for stable and efficient perovskite solar cells," *Nano Energy*, vol. 34, no. November 2016, pp. 271–305,

2017.

[10] A. F. Ahmad, Z. Abbas, S. A. Aziz, S. J. Obaiys, and M. F. Zainuddin, “Synthesis and characterisation of nickel oxide reinforced with polycaprolactone composite for dielectric applications by controlling nickel oxide as a filler,” *Results Phys.*, vol. 11, no. April, pp. 427–435, 2018.

[11] F. I. Dar, K. R. Moonooswamy, and M. Es-Souni, “Morphology and property control of NiO nanostructures for supercapacitor applications,” *Nanoscale Res. Lett.*, vol. 8, no. 1, pp. 1–7, 2013.

[12] N. Zaghian and B. S. Boroujeny, “The Effect of Saccharin on Microstructure and Corrosion Behavior of Nanocrystalline Nickel Thin Films in Alkaline Solution,” *J. Adv. Mater. Process.*, vol. 5, no. 2, pp. 25–37, 2017.

[13] D. Das and F. Gharib, “Cubic NiO Nanoparticles: Synthesis and Characterization,” *Int. J. Bio-Inorganic Hybrid Nanomater.*, vol. 4, no. 2, pp. 59–64, 2015.

[14] S. Zhou, X. Zhu, L. Ma, Q. Yan, and S. Wang, “Outstanding superhydrophobicity and corrosion resistance on carbon-based film surfaces coupled with multi-walled carbon nanotubes and nickel nano-particles,” *Surf. Sci.*, vol. 677, no. May, pp. 193–202, 2018.

[15] Y. Yang *et al.*, “Ultrasound-spray deposition of multi-walled carbon nanotubes on NiO nanoparticles-embedded perovskite layers for high-performance carbon-based perovskite solar cells,” *Nano Energy*, vol. 42, no. November, pp. 322–333, 2017.

Chapter 2: Literature Review

2.1. History

French Physicist Edmond Becquerel built the first photovoltaic cell in 1839. First solid-state photovoltaic cell was fabricated by Charles Fritts in 1883 with 1% efficiency. Albert Einstein proposed quantum theory of light in 1905 and received Nobel prize in physics in 1921 for explaining photoelectric effect. Modern junction semiconductor solar cells were planted by Russell Ohl in 1946. Calvin souther fuller, Gerald Pearson and Daryl Chapin fabricated the first practical photovoltaic cell in 1954. Solar cells gained major attention in 1958 after being incorporated in a vanguard I satellite. Progress in efficiencies in still under research by various scientists and researchers.

2.2. Structure of perovskite solar cells (PSCs)

Structure of perovskite solar cells (PSCs) is based on improved form of dye-sensitized solar cells (DSSCs) structure [1]. PSCs have hybrid organic-inorganic light absorber material instead of organic molecular dye and solid hole transport material is used instead of liquid electrolyte which has device stability issues [2]. The basic types of PSCs include Meso-super structured, PSCs with mesoscopic TiO_2 scaffold layer and planner heterojunction PSCs without mesoporous layer [3].

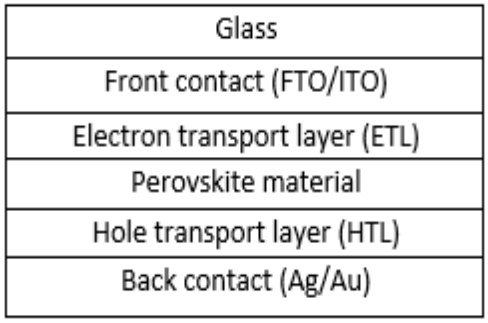

Figure 2.1: PSC Structure.

2.2.1. Functional Description of PSC layers

1. Top glass: Top glass protects complete solar cell from external degradation factors.

2. Indium or Fluorine-doped tin oxide (ITO/FTO): Transparent and electrically conductive coating material is used to coat glass substrate. FTO performs better in solar based applications because of its stability under ambient conditions, high temperature resistivity and being cost effective.
3. Electron transport layer: ETL is the n-type semiconducting layer which works as charge carrier and electron absorber in PSCs. Normally, a uniform and pinhole-free hole blocking layer is employed for enhancing perovskite solar cells efficiency as it works for prevention of direct recombination at interface between light harvesting layer and FTO.
4. Light harvester/sensitizer: Light harvesting layer consist of perovskite material which works for absorption of light and it also facilitates as charge carrier in some configurations.
5. Hole transporting layer: This layer transports holes in perovskite solar cells. Various inorganic and organic hole transporting materials can be employed for this purpose [4].
6. Gold or silver contacts: Contacts are used for electron extraction and transportation in a perovskite solar cell should have high value of conductivity. Contacts selection depends on the highest occupied molecular orbital (HOMO) and lowest unoccupied molecular orbital (LUMO) levels of electron transporting layer and hole transporting layer respectively.

2.3. Physics of perovskite solar cells (PSCs)

The physics of hybrid organic-inorganic lead halide solar cells includes following processes for the conversion of light into electric energy.

2.3.1. Light absorption

Perovskite material is the light absorbing material in Perovskite solar cells (PSCs). When light falls on the perovskite layer, sensitizer absorbs the incident sunlight and electron is excited from the ground state to excited state.

2.3.2. Exciton formation and diffusion

When a light absorber semiconductor material is illumined an exciton can be generated. These generated excitons diffuse in the material and a few numbers of excitons are able

to reach donor/ acceptor junction these excitons have high probability to be dissociated in to charge carriers if the material has short diffusion lengths [5]. In planar bilayer organic photovoltaic cells (OPVs) excitons diffusion is the main efficiency blockage. The bulk hetero junction has mixed donor and acceptor solution therefore donor/ acceptor junction active layers give an efficient exciton dissociation to get rid of diffusion length blockage. Therefore, the short diffusion length restricts the morphologies that can be used to construct efficient solar cell. Hybrid organic-inorganic lead halide has great electronic and optical properties i.e. optimal band gap, high absorption coefficients, high carrier mobility and long diffusion lengths and is used as a light absorber for low cost and efficient solar cells [6][7].

2.3.3. Charge separation

When solar cell absorbs photons, it produces excitons then these excitons are required to separate in to charge carriers for the generation of electrical current [8]. Charge transfer state is the state at which both electron and hole are in front of each other and there is a chance of recombination which leads the excitons to ground state. If the same process happens the loss in efficiency occurs. Recombination is the key reasons for decrease in the efficiency of Photovoltaic devices.

2.3.4. Electron and hole injection following charge collection

After charge separation in the sensitizer the next step is electron injection to the electron transport layer from the conduction band of absorber material. Hole injection occurs when hole created by electron injection is transfer to HOMO energy level of hole transport layer (HTL) [9]. During this process the electron moves from conduction band of active layer to ETL. After that finally charge collection takes place with the help of two electrodes.

2.4. Layers of Perovskite Solar Cell (PSC)

A perovskite solar cell has a light-harvesting active layer sandwiched between two transporting layers known as electron transport layer and hole transport layer which collect the mobile charges.

2.4.1. Electron Transporting Layer

2.4.1.1. Characteristics of ETL

Electron transport layers basic function includes formation of an electron-selective contact with the perovskite layer such that photo-generated electrons extraction efficiency can be improved and hole can be prevented from drifting to the counter electrode. Carrier's separation effect can be enhanced through this phenomenon which will result in reduced recombination. Energy level alignment of an electron transport material with the perovskite active layer, high electron mobility and stable structure are important factors to be considered for the selection of efficient electron transporting material [10]-[12].

2.4.1.2. Materials for ETL

Metal oxides such as TiO_2, ZnO, SnO_2, SiO_2, ZrO_2, can be used as ETLs. TiO_2 has been used extensively as an Electron transport material because of a wide band gap. Rutile and anatase TiO_2 electron transport layer (ETL) has been incorporated and by examining crystalline phase-dependent charge collection it was concluded that rutile TiO_2 electron transporting layer improves the transportation and extraction of electrons to FTO and decrease the recombination as well [13]. for same reasons of increasing charge extraction and preventing recombination another metal oxide layer of materials Such as SnO_2 are fabricated in addition to the compact TiO_2 layer [14]. Acteylacetonate-based additives have been incorporated into TiO_2 for improvement in electron transporting layer of perovskite solar cells, results include improved device performances particularly affecting fill factor and short circuit current (Jsc) [15]. Some research have also been undertaken to investigate the route of fabricating ETLs, like sputtering and anodization processed TiO_2 in comparison with solution processed spin-coated TiO_2 [16].

2.4.2. Perovskite /Absorber Layer

Perovskites material consist of a monovalent cation, a divalent cation, and a halide ion. Commonly, $MAPbI_3$ is the employed as light harvesting material. Mixed cation, mixed halide, and mixed halide–mixed cation is being checked out as possible substitute by researchers and scientists. Monovalent cations modification can result in improved perovskite solar cell performance. Incorporating perovskites with lower band gap than

$MAPbI_3$ can enhance the light-harvesting efficiency of PSCs. Modification of the monovalent cation in a lead halide-based perovskite might result in a change in the Pb–I bond angle, length and, the band structure as well [17]. Research group of Hanusch found $FAPbI_3$ to have more thermal stability than $MAPbI_3$ and $MAPbBr_3$. This supports the concept that incorporating bigger cation in ABX_3 structure at the A site results in stable perovskite structure. Lee et al. observed improvement in moisture stability of $FA_{0.9}Cs_{0.1}PbI_3$ as compared to the results of $FAPbI_3$ [19]. Saliba et al. identified various cationic combination with Rb and with 5% Rb in RbCsMAFA 21.6% efficiency was achieved [21]. Research group of Prochowicz practiced 25% addition of MAI to the reaction mixture resulted in black phase stabilization of $FAPbI_3$, Device formed was 14.98% efficient [18]. Optoelectronic properties of perovskites can be modified by mixing or replacing halogen ion. Improved stability, enhanced carrier transport, and tuned band gap are the results of mixing or replacing halogen ion. [22].

High quality perovskite film has been obtained by employing different film formation techniques such as slot-die coating, spin coating, doctor blade, spray coating, dip coating, vapor-based deposition, inkjet printing etc. Spin coating is commonly adopted for perovskite solar cell fabrication process at lab-scale. Qin et al. employed slot-die coating and obtained 14.7% efficiency [26]. Good controllability and great precision are achieved through ink-jet printing. Negligible material waste during the fabrication process makes ink-jet printing cost effective technique [28].Spray-coating is an apt technique for large-scale fabrication of perovskite solar cells which make it cost effective but the uniformity of film is not guaranteed by this technique [27]. Perovskites poor control of surface morphology affects the performance of the PSC based devices which is considered as a disadvantage of these techniques [29].

2.4.3. Hole Transporting Layer

2.4.3.1. Selection criteria for HTMs in PSCs

Hole transporting material is an important material because of its ability of effective hole extraction at the HTM-absorber layer interface. Hole transporting material should offer high hole mobility, ionization potential should be compatible with that of the perovskite material, thermal stability should be high and it should be resistant to external degradation

factors to ensure long term photovoltaic operation. Cost of hole transporting material is an important concern as well. If the electron affinity of hole transporting material is low, it will enhance the electron blocking properties of hole transporting layer. Efficiency of the solar cell is affected by the mobility of hole transporting material as well. Considerable ohmic losses occur across the hole transporting layer due to low mobility, this results in low fill factor (FF). Charge carrier mobility also affects the short circuit photocurrent (J_{SC}). Thus, Uniform coverage and high mobilities of HTM should be ensured for efficient PSCs.

2.5. Hole Transporting materials in PSCs

Hole transporting material in PSCs can be categorized as organic and inorganic hole transporting materials. Small molecules-based HTMs, polymer-based HTMs and oligomers are the three categories of organic hole transporting materials.

2.5.1. Organic Hole transporting materials

2.5.1.1. Small molecules-based hole transporting materials

Solid state dye sensitized solar cells (s-DSSCs) have commonly employed Spiro-OMeTAD as hole transporting material and have achieved an efficiency of up to 7.2% [10][30]. In case of PSCs incorporation of spiro-OMeTAD as hole transporting material resulted in high efficiency up to 20% [31][32]. However, good pore filling and high efficiency have been achieved by incorporation of spiro-OMeTAD but its drawbacks include low conductivity ($\sim 10^{-5}$ S cm^{-1}) and low hole mobility ($\sim 10^{-4}$ cm^2 V^{-1} s^{-1}). Transporting properties of spiro-OMeTAD have been improved due to dopants but it has resulted in its increased sensitivity to humidity. Doped spiro-OMeTAD based solar cells quickly degrade in humid surroundings [33]. High cost of spiro-OMeTAD and its extensive synthetic processes makes hole transporting material most expensive component in PSCs.

2.5.1.2. Polymer hole transport materials

Polymer materials are cost-effective and stable hole transporting materials with high hole mobility as compared to dopant-free small molecules in PSCs. P3HT, PEDOT: PSS and PTAA employed as hole transporting material in PSCs were efficient up to 15.3%, 18.1%

and 20.2% respectively. Perovskite solar cells based on P3HT hole transporting layer have low hole mobility (3×10^{-4} cm^2 V^{-1} s^{-1}) shows lower PV performance as compared to doped spiro-OMeTAD HTM based PSCs [34]. Carbon nano-materials incorporation [35][36] and Li salts additives [17][37] have been employed in order to raise hole mobility. Hole mobility of PTAA is 1×10^{-2} to 1×10^{-3} cm^2 V^{-1} s^{-1} which is higher when compared that of P3HT i.e. $\sim3\times10^{-4}$ cm^2 V^{-1} s^{-1} [38]. A research group reports the incorporation of $FAPbI_3$ microstructures and PTAA as hole transporting material, resultantly up to 20% efficiency was achieved [39]. PEDOT: PSS is known for good film forming properties, high work function i.e. ~5.2 eV and transparency, this refers that it is an adequate choice as being employed as hole transporting material [23]. PEDOT: PSS requires low-temperature processing, it is an adequate choice for flexible or low temperature processed perovskite solar cells. PEDOT: PSS has hygroscopic behavior as well as it is an inefficient electron blocking material, this makes it the reason of chemically unstable hole transporting material [40][22]. Acidic nature of PEDOT: PSS also causes substrate corrosion [41].

2.5.1.3. Oligomer HTMs

Strong optical properties of an oligomer contribute to efficient perovskite solar cells. Research group of Peng incorporated oligomer S197 as hole transporting material, it has high hole mobility i.e. $\sim5.1\times10^{-4}$ cm^2V^{-1} $s^{-1,}$ low molecular weight and it proved to be effective hole transporting layer with efficiency up to 12% [42].

2.5.2. Inorganic HTMs

Polymer hole transporting material-based PSCs have been more efficient than 15%. Polymer based hole transporting materials have low hole mobility and are unstable in atmospheric conditions [43][44]. Incorporation of inorganic hole transporting materials leads to long term operation of PSCs and makes it cost-effective as well. Inorganic hole transporting materials include GO, Cu_2O, PbS, CuI, NiO, CuSCN, MoO_3 and quantum dots have been found capable to be incorporated as HTM in PSCs.

Copper thiocyanate (CuSCN): Copper thiocyanate **(**CuSCN) shows good optical properties, high chemical stability and high mobility (~0.01–0.1 cm^2 V^{-1} s^{-1}) which make it an adequate choice to be incorporated as HTM in PSCs [47]–[49]. Ye et. al. incorporated

CuSCN as HTM in an inverted planar PSC and found it to be 16% efficient which is the highest efficiency achieved by using CuSCN hole transporting layer [50].

Copper Iodide (CuI): Copper iodide (CuI) was the first inorganic HTM incorporated in a PSC which proved to be 6% efficient [45]. High recombination rate has been observed by lowering V_{OC} of ~300 mV in copper iodide based dye sensitized solar cells [46].

Graphene oxide (GO): Graphene Oxide has good electronic conductivity, high charge mobility, high optical transmittance and superior thermal conductivity which refer to it as being an adequate choice to be incorporated as hole transporting material in PSCs [57]–[60]. Graphene oxide has been incorporated as a buffer layer between spiro-OMeTAD and absorber layer in PSC which resulted in improved hole extraction, stable device performance and high efficiency up to 18.2% [61].

Cuprous oxide (Cu_2O): Cuprous oxide has long carrier diffusion length, high hole mobility and direct band gap of ~2.17 eV which make it an adequate choice to be incorporated as HTM in heterojunction solar cells [51][52]. 13% efficiency has been achieved by employing Cu_2O HTM in PSC [53].

Vanadium oxide (VO_X): Vanadium oxide is not considered an adequate choice for being employed as HTM in PSCs because it requires high temperature processing [66]. Research group of Haitao used V_2O_x as a buffer layer between PEDOT: PSS and absorber layer in PSC, resultantly hysteresis-free device was formed with efficiency up to 17.5% which is higher as compared to the efficiency achieved by pristine PEDOT: PSS and pristine V_2O_x [67].

Molybdenum oxide (MoO_3): Molybdenum oxide is non-toxic and stays stable under ambient conditions which are good qualities for HTM of PSCs. Incorporation of MoO_3 layer between hole transporting layer and metal contact in conventional perovskite solar cell structure leads to diminished contact resistance, improved stability and increased efficiency of the device [64][65].

Tungsten oxide (WO_X): Tungsten oxide has been reported as low temperature inorganic HTM for PSCs. Research group of Zhiwei fabricated WO_3 nanocrystals for incorporation as HTM in inverted PSC, resultantly 7.68% efficiency was achieved [68]. A research group reported incorporation of UV-ozone treated WO_3 for improving the surface coverage of perovskite layer, resultantly 9.8% efficiency was achieved [69].

Nickel oxide (NiO): Nickel oxide is considered a potential material for inverted PSC owing to its good hole conductivity, large energy gap, and deep valence band. NiO is abundant, cost-effective and potentially stable material for perovskite solar cell. Research group of Irwin compared incorporation of NiO with PEDOT: PSS as hole transporting layer, resultantly performance of polymer bulk-heterojunction solar cells was higher for NiO hole transporting material [70]. Highest efficiency reported by incorporating an inorganic HTM in an inverted planar PSC was 17.3% reported by Seok et al., this group of researchers prepared NiO nanostructured film through pulsed laser deposition method and employed it as hole transporting layer for PSC [72].

Nanocrystals and Quantum dots: $CuInS_2$ and Cu_2ZnSnS_4 nanocrystals have low temperature solution processability and direct band gap of 1.5 eV which makes it an appropriate choice for incorporation in solar cells [73][74]. Quantum dots (QDs) sensitized solar cells have broadened light harvesting to near-infrared region which can prove to be a good strategy for perovskite solar cells as well [69]. Mei et al. reported $CuInS_2$, quantum dot hole transporting layer based mesoporous PSC which provided an efficiency of 6.57%. This hole transporting layer was made efficient by modification in the surface of $CuInS_2$ quantum dots by cation exchange to form $CuInS_2$/ZnS core/ shell quantum dots, resultantly 8.38% efficiency was achieved [76].

2.6. PSCs Degradation Factors

Important factors which influence the success of photovoltaic technology are long term stability, high efficiency and low cost. Various intrinsic and extrinsic factors destabilize perovskite solar cells. Intrinsic factors which destabilize a perovskite solar cell include hysteresis, structural instability, charge transporting mediums and their interfaces with light harvesting layer. Electrical biasing, UV irradiation, prolonged light soaking, temperature, humidity and oxygen are the extrinsic destabilizing factors [77][78].

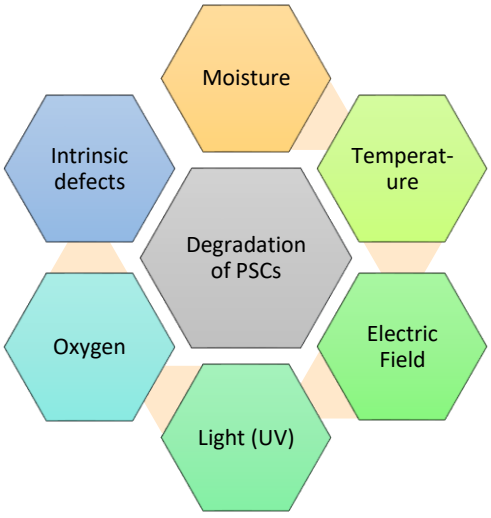

Figure 2.2: PSC Destabilizing Factors.

Different temperatures and pressures significantly impact perovskite crystalline phases which might affect device stability [79]. Active layers crystals decompose when exposed to light, humidity, moisture and temperature. Planar perovskite solar cell structure contains hole transporting layer as a top layer, it acts as protective layer as well. Inefficient hole transporting layer is considered as one of the dominant factors which destabilize the devise. Small molecules based organic material i.e. spiroOMeTAD, conducting polymers such as PEDOT: PSS, P3HT, PTAA and inorganic materials such as NiO, CuO etc. have proved to be successful hole transporting materials. Organic HTMs cause degradation in PSCs because of their sensitivity oxygen and moisture [80]–[83].

2.7. Summary

This chapter started with brief history of solar cells, perovskite solar cell structure was discussed, Brief functional description of perovskite solar cell layers was given. Working mechanism of each layer were explained. Materials used for electron transport layer and light harvesting layer/perovskite layer were discussed. Selection criterion for efficient hole transporting materials include high hole mobility, high thermal stability, compatible ionization potential, low cost and resistance to external degradation factors. Various organic and inorganic materials employed as hole transporting layer and their properties and efficiencies were discussed briefly. Different intrinsic and extrinsic factors destabilize perovskite solar cells which include hysteresis, structural instability, charge transporting mediums and their interfaces with light harvesting layer, electrical biasing, UV irradiation, prolonged light soaking, temperature, humidity and oxygen.

References

[1] M. Antonietta Loi and J. C. Hummelen, "Hybrid solar cells: Perovskites under the Sun," *Nat. Mater.*, vol. 12, no. 12, pp. 1087–1089, 2013.

[2] G. P. Smestad, "Education and solar conversion: Demonstrating electron transfer," *Sol. Energy Mater. Sol. Cells*, vol. 55, no. 1–2, pp. 157–178, 1998.

[3] M. Grätzel, "The light and shade of perovskite solar cells," *Nat. Mater.*, vol. 13, no. 9, pp. 838–842, 2014.

[4] P. Gao, M. Grätzel, and M. Kazeeruddin, "Environmental Science Organohalide lead perovskites for photovoltaic," *Energy Environ. Sci.*, vol. 1, no. c, pp. 2448–2463, 2014.

[5] P. Peumans and S. R. Forrest, "Separation of geminate charge-pairs at donor-acceptor interfaces in disordered solids," *Chem. Phys. Lett.*, vol. 398, no. 1–3, pp. 27–31, 2004.

[6] J. S. Yeo *et al.*, "Highly efficient and stable planar perovskite solar cells with reduced graphene oxide nanosheets as electrode interlayer," *Nano Energy*, vol. 12, pp. 96–104, 2015.

[7] P. Qin *et al.*, "Inorganic hole conductor-based lead halide perovskite solar cells with 12.4% conversion efficiency," *Nat. Commun.*, vol. 5, no. May, pp. 1–6, 2014.

[8] P. Peumans, A. Yakimov, and S. R. Forrest, "Small molecular weight organic thin-film photodetectors and solar cells," *J. Appl. Phys.*, vol. 93, no. 7, pp. 3693–3723, 2003.

[9] I. Chung, B. Lee, J. He, R. P. H. Chang, and M. G. Kanatzidis, "All-solid-state dye-sensitized solar cells with high efficiency," *Nature*, vol. 485, no. 7399, pp. 486–489, 2012.

[10] J. Burschka *et al.*, "Tris(2-(1 H -pyrazol-1-yl)pyridine)cobalt(III) as p-type dopant for organic semiconductors and its application in highly efficient solid-state dye-sensitized solar cells," *J. Am. Chem. Soc.*, vol. 133, no. 45, pp. 18042–18045, 2011.

[11] F. Huang *et al.*, "Perovskite Solar Cells: Effect of the Microstructure of the Functional Layers on the Efficiency of Perovskite Solar Cells (Adv. Mater. 20/2017)," *Adv. Mater.*, vol. 29, no. 20, May 2017.

[12] G. Yang, H. Tao, P. Qin, W. Ke, and G. Fang, "Recent progress in electron transport layers for efficient perovskite solar cells," *J. Mater. Chem. A*, vol. 4, no. 11, pp. 3970–3990, 2016.

[13] Y. Wang, J. Wan, J. Ding, J.-S. Hu, and D. Wang, "A Rutile TiO $_2$ Electron Transport Layer for the Enhancement of Charge Collection for Efficient Perovskite Solar Cells," *Angew. Chemie Int. Ed.*, vol. 58, no. 28, pp. 9414–9418, Jul. 2019.

[14] M. M. Tavakoli, P. Yadav, R. Tavakoli, and J. Kong, "Surface Engineering of TiO $_2$ ETL for Highly Efficient and Hysteresis-Less Planar Perovskite Solar Cell (21.4%) with Enhanced Open-Circuit Voltage and Stability," *Adv. Energy Mater.*, vol. 8, no. 23, p. 1800794, Aug. 2018.

[15] H.-H. Wang *et al.*, "Improving the TiO 2 electron transport layer in perovskite solar cells using acetylacetonate-based additives †," Journal of Material Chemistry A. 2015.

[16] J. Choi, S. Song, M. T. Hörantner, H. J. Snaith, and T. Park, "Well-Defined Nanostructured, Single-Crystalline TiO $_2$ Electron Transport Layer for Efficient Planar Perovskite Solar Cells," *ACS Nano*, vol. 10, no. 6, pp. 6029–6036, Jun. 2016.

[17] W. S. Yang *et al.*, "High-performance photovoltaic perovskite layers fabricated through intramolecular exchange," *Science (80-.).*, vol. 348, no. 6240, pp. 1234–1237, 2015.

[18] M. Saliba *et al.*, "Cesium-containing triple cation perovskite solar cells: Improved stability, reproducibility and high efficiency," *Energy Environ. Sci.*, vol. 9, no. 6, pp. 1989–1997, 2016.

[19] Y. Liu *et al.*,"Two-Inch-Sized Perovskite $CH_3NH_3PbX_3$ (X = Cl, Br, I) Crystals: Growth and Characterization," *Adv. Mater.*, vol. 27, no. 35, pp. 5176–5183, 2015.

[20] J. P. Correa-Baena *et al.*, "The rapid evolution of highly efficient perovskite solar cells," *Energy Environ. Sci.*, vol. 10, no. 3, pp. 710–727, 2017.

[21] M. Saliba *et al.*, "Incorporation of rubidium cations into perovskite solar cells improves photovoltaic performance," *Science (80-.).*, vol. 354, no. 6309, pp. 206–209, 2016.

[22] J. A. Chang *et al.*, "Nano Lett. 2012, 12, 1863−1867.pdf," *ACS Nano*, no. 2 pp. 8–

12, 2012.

[23] T. Krishnamoorthy *et al.*, “Lead-free germanium iodide perovskite materials for photovoltaic applications,” *J. Mater. Chem. A*, vol. 3, no. 47, pp. 23829–23832, 2015.

[24] M. Abd Mutalib *et al.*, “Progress towards highly stable and lead-free perovskite solar cells,” *Mater. Renew. Sustain. Energy*, vol. 7, no. 2, pp. 1–13, 2018.

[25] I. Kopacic *et al.*, “Enhanced Performance of Germanium Halide Perovskite Solar Cells through Compositional Engineering,” *ACS Appl. Energy Mater.*, vol. 1, no. 2, pp. 343–347, 2018.

[26] J. A. Alberola-Borràs *et al.*, “Perovskite Photovoltaic Modules: Life Cycle Assessment of Pre-industrial Production Process,” *iScience*, vol. 9, pp. 542–551, 2018.

[27] N. Marinova, S. Valero, and J. L. Delgado, “Organic and perovskite solar cells: Working principles, materials and interfaces,” *J. Colloid Interface Sci.*, vol. 488, pp. 373–389, 2017.

[28] F. Mathies, H. Eggers, B. S. Richards, G. Hernandez-Sosa, U. Lemmer, and U. W. Paetzold, “Inkjet-Printed Triple Cation Perovskite Solar Cells,” *ACS Appl. Energy Mater.*, vol. 1, no. 5, pp. 1834–1839, 2018.

[29] B. Chen, M. Yang, S. Priya, and K. Zhu, “Origin of J-V Hysteresis in Perovskite Solar Cells,” *J. Phys. Chem. Lett.*, vol. 7, no. 5, pp. 905–917, 2016.

[30] N. Cai *et al.*, “An organic D-π-A dye for record efficiency solid-state sensitized heterojunction solar cells,” *Nano Lett.*, vol. 11, no. 4, pp. 1452–1456, 2011.

[31] H. Zhou *et al.*, “Interface engineering of highly efficient perovskite solar cells,” *Science (80-.).*, vol. 345, no. 6196, pp. 542–546, 2014.

[32] S. D. S. Cells *et al.*, “Hole Transport Materials with Low Glass Transition Temperatures and High Solubility for Application in solid state DSC,” *ACS Nano*, no. 2, pp. 1455–1462, 2012.

[33] S. Cho *et al.*, “Single-Crystalline Thin Films for Studying Intrinsic Properties of BiFeO3-SrTiO3 Solid Solution Photoelectrodes in Solar Energy Conversion,” *Chem. Mater.*, vol. 27, no. 19, pp. 6635–6641, 2015.

[34] M. Cai, V. T. Tiong, T. Hreid, J. Bell, and H. Wang, “An efficient hole transport

material composite based on poly(3-hexylthiophene) and bamboo-structured carbon nanotubes for high performance perovskite solar cells," *J. Mater. Chem. A*, vol. 3, no. 6, pp. 2784–2793, 2015.

[35] H. Chen *et al.*, "Efficient panchromatic inorganic-organic heterojunction solar cells with consecutive charge transport tunnels in hole transport material," *Chem. Commun.*, vol. 49, no. 66, pp. 7277–7279, 2013.

[36] G. Namkoong, P. Boland, K. Lee, and J. Dean, "Design of organic tandem solar cells using PCPDTBT: PC61 BM and P3HT: PC71BM," *J. Appl. Phys.*, vol. 107, no. 12, 2010.

[37] T. W. Lee, Y. Chung, O. Kwon, and J. J. Park, "Self-organized gradient hole injection to improve the performance of polymer electroluminescent devices," *Adv. Funct. Mater.*, vol. 17, no. 3, pp. 390–396, 2007.

[38] M. Jørgensen, K. Norrman, S. A. Gevorgyan, T. Tromholt, B. Andreasen, and F. C. Krebs, "Stability of polymer solar cells," *Adv. Mater.*, vol. 24, no. 5, pp. 580–612, 2012.

[39] K. Norrman, M. V. Madsen, S. A. Gevorgyan, and F. C. Krebs, "Degradation patterns in water and oxygen of an inverted polymer solar cell," *J. Am. Chem. Soc.*, vol. 132, no. 47, pp. 16883–16892, 2010.

[40] X. Li *et al.*, "A comparative study of o, p -dimethoxyphenyl-based hole transport materials by altering π-linker units for highly efficient and stable perovskite solar cells," *J. Mater. Chem. A*, vol. 5, no. 21, pp. 10480–10485, 2017.

[41] S. Nezu *et al.*, "Light soaking and gas effect on nanocrystalline TiO2/Sb 2S3/CuSCN photovoltaic cells following extremely thin absorber concept," *J. Phys. Chem. C*, vol. 114, no. 14, pp. 6854–6859, 2010.

[42] J. A. Christians, R. C. M. Fung, and P. V. Kamat, "An inorganic hole conductor for Organo-lead halide perovskite solar cells. improved hole conductivity with copper iodide," *J. Am. Chem. Soc.*, vol. 136, no. 2, pp. 758–764, 2014.

[43] V. P. S. Perera and K. Tennakone, "Recombination processes in dye-sensitized solid-state solar cells with CuI as the hole collector," *Sol. Energy Mater. Sol. Cells*, vol. 79, no. 2, pp. 249–255, 2003.

[44] B. O'Regan, D. T. Schwartz, S. M. Zakeeruddin, and M. Grätzel, "Electrodeposited

nanocomposite n-p heterojunctions for solid-state dye-sensitized photovoltaics," *Adv. Mater.*, vol. 12, no. 17, pp. 1263–1267, 2000.

[45] P. Pattanasattayavong *et al.*, "Electric field-induced hole transport in copper(i) thiocyanate (CuSCN) thin-films processed from solution at room temperature," *Chem. Commun.*, vol. 49, no. 39, pp. 4154–4156, 2013.

[46] P. Pattanasattayavong *et al.*, "Hole-transporting transistors and circuits based on the transparent inorganic semiconductor copper(I) thiocyanate (CuSCN) processed from solution at room temperature," *Adv. Mater.*, vol. 25, no. 10, pp. 1504–1509, 2013.

[47] S. Ye *et al.*, "CuSCN-Based Inverted Planar Perovskite Solar Cell with an Average PCE of 15.6%," *Nano Lett.*, vol. 15, no. 6, pp. 3723–3728, 2015.

[48] M. D. Irwin, D. B. Buchholz, A. W. Hains, R. P. H. Chang, and T. J. Marks, "p-Type semiconducting nickel oxide as an efficiency-enhancing anode interfacial layer in polymer bulk-heterojunction solar cells," *Proc. Natl. Acad. Sci. U. S. A.*, vol. 105, no. 8, pp. 2783–2787, 2008.

[49] A. Garcia, G. C. Welch, E. L. Ratcliff, D. S. Ginley, G. C. Bazan, and D. C. Olson, "Improvement of interfacial contacts for new small-molecule bulk-heterojunction organic photovoltaics," *Adv. Mater.*, vol. 24, no. 39, pp. 5368–5373, 2012.

[50] E. A. Gibson *et al.*, "A p-type NiO-based dye-sensitized solar cell with an open-circuit voltage of 0.35 v," *Angew. Chemie - Int. Ed.*, vol. 48, no. 24, pp. 4402–4405, 2009.

[51] Y. Wang *et al.*, "Towards printed perovskite solar cells with cuprous oxide hole transporting layers: A theoretical design," *Semicond. Sci. Technol.*, vol. 30, no. 5, p. 54004, 2015.

[52] S. Chen *et al.*, "A graphene oxide/oxygen deficient molybdenum oxide nanosheet bilayer as a hole transport layer for efficient polymer solar cells," *J. Mater. Chem. A*, vol. 3, no. 36, pp. 18380–18383, 2015.

[53] G. A. M. Ali, M. M. Yusoff, K. F. Chong, and S. A. Makhlouf, "Structural and electrochemical characteristics of graphene nanosheets as supercapacitor electrodes," *Rev. Adv. Mater. Sci.*, vol. 41, no. 1, pp. 35–43, 2015.

[54] M. C. Lemme, S. Member, T. J. Echtermeyer, M. Baus, and H. Kurz, "<A

Graphene Field Effect Device.pdf>," vol. 28, no. 4, pp. 1–12, 2007.

[55] S. V. Morozov *et al.*, "Giant intrinsic carrier mobilities in graphene and its bilayer," *Phys. Rev. Lett.*, vol. 100, no. 1, pp. 11–14, 2008.

[56] A. A. Balandin *et al.*, "Superior thermal conductivity of single-layer graphene," *Nano Lett.*, vol. 8, no. 3, pp. 902–907, 2008.

[57] J. H. Seol *et al.*, "Two-dimensional phonon transport in supported graphene," *Science (80-.).*, vol. 328, no. 5975, pp. 213–216, 2010.

[58] R. R. Nair *et al.*, "Fine structure constant defines visual transparency of graphene," *Science (80-.).*, vol. 320, no. 5881, p. 1308, 2008.

[59] A. Agresti *et al.*, "Graphene Interface Engineering for Perovskite Solar Modules: 12.6% Power Conversion Efficiency over 50 cm 2 Active Area," *ACS Energy Lett.*, vol. 2, no. 1, pp. 279–287, 2017.

[60] W. Marchal *et al.*, "Steering the properties of MoOx hole transporting layers in OPVs and OLEDs: Interface morphology vs. electronic structure," *Materials (Basel).*, vol. 10, no. 2, pp. 1–17, 2017.

[61] N. K. Elumalai, A. Saha, C. Vijila, R. Jose, Z. Jie, and S. Ramakrishna, "Enhancing the stability of polymer solar cells by improving the conductivity of the nanostructured MoO3 hole-transport layer," *Phys. Chem. Chem. Phys.*, vol. 15, no. 18, pp. 6831–6841, 2013.

[62] D. Kabra, L. P. Lu, M. H. Song, H. J. Snaith, and R. H. Friend, "Efficient single-layer polymer light-emitting diodes.," *Adv. Mater.*, vol. 22, no. 29, pp. 3194–3198, 2010.

[63] J. Kim *et al.*, "Efficient planar-heterojunction perovskite solar cells achieved via interfacial modification of a sol-gel ZnO electron collection layer," *J. Mater. Chem. A*, vol. 2, no. 41, pp. 17291–17296, 2014.

[64] Y. Zhao, A. M. Nardes, and K. Zhu, "Effective hole extraction using MoOx-Al contact in perovskite CH3NH3PbI3 solar cells," *Appl. Phys. Lett.*, vol. 104, no. 21, 2014.

[65] Q. Guo *et al.*, "Low-temperature solution-processed vanadium oxide as hole transport layer for efficient and stable perovskite solar cells," *Phys. Chem. Chem. Phys.*, vol. 20, no. 33, pp. 21746–21754, 2018.

[66] Z. Li, "Stable perovskite solar cells based on WO_3 nanocrystals as hole transport layer," *Chem. Lett.*, vol. 44, no. 8, pp. 1140–1141, 2015.

[67] I. Aguilera, P. Palacios, and P. Wahnón, "Enhancement of optical absorption in Ga-chalcopyrite-based intermediate-band materials for high efficiency solar cells," *Sol. Energy Mater. Sol. Cells*, vol. 94, no. 11, pp. 1903–1906, 2010.

[68] Y. Hou *et al.*, "Low-Temperature Solution-Processed Kesterite Solar Cell Based on in Situ Deposition of Ultrathin Absorber Layer," *ACS Appl. Mater. Interfaces*, vol. 7, no. 38, pp. 21100–21106, 2015.

[69] W. Liu, D. B. Mitzi, M. Yuan, A. J. Kellock, S. Jay Chey, and O. Gunawan, "12% Efficiency CuIn(Se,S)2 photovoltaic device prepared using a hydrazine solution process," *Chem. Mater.*, vol. 22, no. 3, pp. 1010–1014, 2010.

[70] J. R. Manders *et al.*, "NiOfilm.pdf," *Phys. Chem. Chem. Phys.*, vol. 15, no. 18,pp. 2993–3001, 2013.

[71] A. Nattestad *et al.*, "Highly efficient photocathodes for dye-sensitized tandem solar cells," *Nat. Mater.*, vol. 9, no. 1, pp. 31–35, 2010.

[72] Y. S. Lee *et al.*, "Nitrogen-doped cuprous oxide as a p-type hole-transporting layer in thin-film solar cells," *J. Mater. Chem. A*, vol. 1, no. 48, pp. 15416–15422, 2013.

[73] C. Chen *et al.*, "Efficient perovskite solar cells based on lowtemperature .pdf," pp. 1–8, 2014.

[74] T. Zhao *et al.*, "Advanced Architecture for Colloidal PbS Quantum Dot Solar Cells Exploiting a CdSe Quantum Dot Buffer Layer," *ACS Nano*, vol. 10, no. 10, pp. 9267–9273, 2016.

[75] M. Lv *et al.*, "Colloidal CuInS<inf>2</inf> Quantum Dots as Inorganic Hole-Transporting Material in Perovskite Solar Cells," *ACS Appl. Mater. Interfaces*, vol. 7, no. 31, pp. 17482–17488, 2015.

[76] A. Fakharuddin, R. Jose, T. M. Brown, F. Fabregat-Santiago, and J. Bisquert, "A perspective on the production of dye-sensitized solar modules," *Energy Environ. Sci.*, vol. 7, no. 12, pp. 3952–3981, 2014.

[77] A. Mei *et al.*, "A hole-conductor-free, fully printable mesoscopic perovskite solar cell with high stability," *Science (80-.).*, vol. 345, no. 6194, pp. 295–298, 2014.

[78] T. Baikie *et al.*, "Synthesis and crystal chemistry of the hybrid perovskite

(CH_3NH_3)PbI_3 for solid-state sensitised solar cell applications," *J. Mater. Chem. A*, vol. 1, no. 18, pp. 5628–5641, 2013.

[79] G. Niu, X. Guo, and L. Wang, "Review of recent progress in chemical stability of perovskite solar cells," *J. Mater. Chem. A*, vol. 3, no. 17, pp. 8970–8980, 2015.

[80] X. Dong *et al.*, "Improvement of the humidity stability of organic-inorganic perovskite solar cells using ultrathin Al_2O_3 layers prepared by atomic layer deposition," *J. Mater. Chem. A*, vol. 3, no. 10, pp. 5360–5367, 2015.

[81] K. Kim and D. J. Siegel, "Correlating lattice distortions, ion migration barriers, and stability in solid electrolytes," *J. Mater. Chem. A*, vol. 7, no. 7, pp. 3216–3227, 2019.

[82] I. Hwang, I. Jeong, J. Lee, M. J. Ko, and K. Yong, "Enhancing Stability of Perovskite Solar Cells to Moisture by the Facile Hydrophobic Passivation," *ACS Appl. Mater. Interfaces*, vol. 7, no. 31, pp. 17330–17336, 2015.

[83] L. Zheng *et al.*, "A hydrophobic hole transporting oligothiophene for planar perovskite solar cells with improved stability," *Chem. Commun.*, vol. 50, no. 76, pp. 11196–11199, 2014.

Chapter 3: Synthesis Approaches and Characterization Techniques

3.1. Nanoparticles Synthesis Approaches

Basically, two approaches are used for nanomaterial synthesis known as top down approach and bottom up approach.

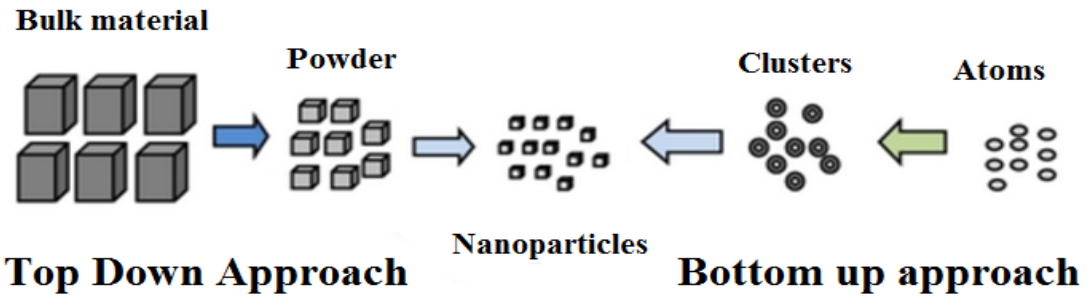

Figure 3.1: Synthesis Approaches for Nano structures.

3.1.1. Bottom up approach

Bottom up approach involves physical forces which operate at nanoscale during the self-assembly process to combine basic units into large stable structures. This approach includes techniques such as Chemical reduction, Electrochemical synthesis, Photochemical synthesis, Sono-chemical routes, Solvothermal synthesis, Interfacial synthesis, Micelles and microemulsions, Biological methods, Thermolysis, Hybrid methods, Solvated metal atom dispersion.

3.1.2. Top Down approach

Top down approach involves bulk initial structures and reduce them to nanostructures. This approach includes techniques such as High-energy ball milling, Wire explosion, Arc discharge, Inert-gas condensation, Laser ablation and Ion sputtering. High-energy ball milling uses ball milling to break down large structures into nanostructures. Wire explosion uses a sudden high current pulse which results in an explosion to produce conducting nanomaterials. Arc discharge method uses alternating current (AC) or direct

current (DC) arcs to evaporate materials for the formation of nanostructures. Inert-gas condensation method condenses evaporated atoms in a matrix to achieve particle growth. Laser ablation method uses high-energy laser to induce evaporation and nanostructures are formed. Ion sputtering method uses impact of high energy ions to cause evaporation for the production of nanostructures.

3.2. Material Synthesis Methodologies

3.2.1. Sol Gel Method

Sol Gel method works when a colloidal or concentrated solution of the reactants known as the 'sol' is prepared and further concentrated to form the gel. The gel is heat-treated to form the product. It is useful technique for producing Nano crystals/particles. First step of this method is the hydrolysis that can be done mixing of water or suitable solvent for making precursor solutions followed by constant stirring using magnetic stirrer. Second step is drying of solution at required temperature in oven for required time period. Third step is washing and filtration of resulting powder for obtaining final material crystals. Sol gel method is a low temperature process with achievable particle size and morphological control at low temperature. Process Drawbacks include requirement of Extra care and monitoring during the complete process and the use of polar solvent and other raw materials when metal alkoxides are employed which make the process expensive. The organic reagents used in the process, can cause the product to capture high carbon and this would resist densification during the annealing process.

Figure 3.2: Sol Gel Process

3.2.2. Co precipitation Technique

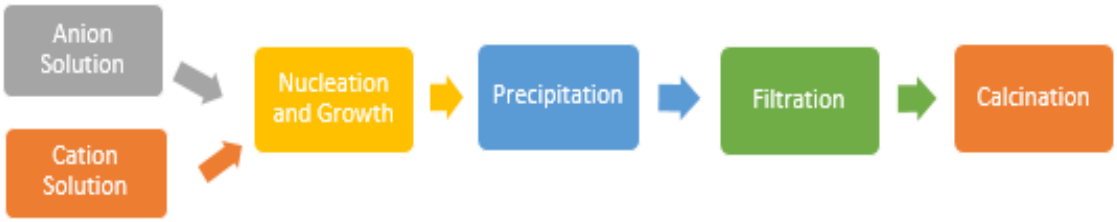

Figure 3.3: Co-precipitation Process

Coprecipitation reactions involves nucleation, growth, coarsening, and/or agglomeration processes taking place simultaneously. Nucleation is considered as a key step in this procedure. Morphology, size and properties of the products are affected due to aggregation. Co precipitation is a simple, low temperature, energy efficient process with easy control of composition and particle size. If the reactants have varied precipitation rates, this reaction does not work well.

3.2.3. Hydrothermal Technique

Synthesis of substances through chemical reactions in a sealed heated solution above the ambient pressure and temperature is known as hydrothermal synthesis. Single crystals hydrothermal synthesis relies on the solubility of minerals in hot water under high pressure. An autoclave is used for crystal growth. Chemical activity of the reactant can be improved through this process. Hydrothermal synthesis can be employed to obtain materials which cannot be synthesized through solid-state reaction. Hydrothermal synthesis can be employed to produce the products of intermediate state, metastable state and other specific condensed states. Reaction time, temperature, surfactant type, precursor type and solvent type are the parameters through which shape distribution, size control and product crystallinity can be achieved precisely. High temperature procedure and costly autoclaves are the disadvantages of this process [1].

3.3. Thin Film Deposition Techniques

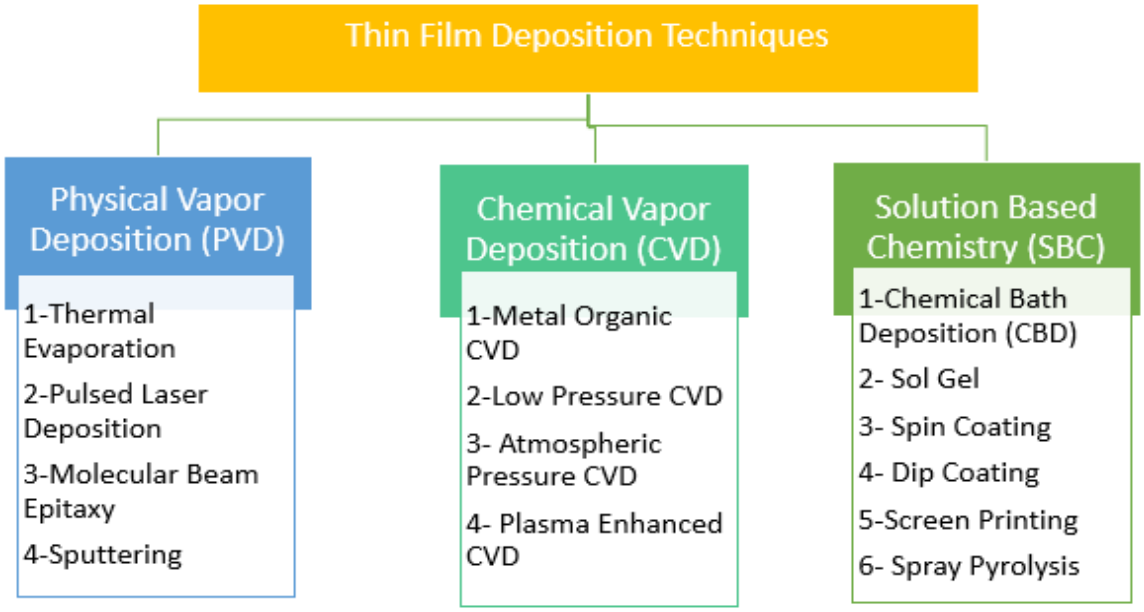

Figure 3.4: Classification of thin film deposition techniques

3.3.1. Physical Vapor Deposition

Thin film deposition process in which atom by atom growth takes place on the substrate is known as physical vapor deposition technique. Material atomization or vaporization takes place from a solid source, known as target. Target is transformed into atomic particles through thermal physical procedure, these atomic particles are focused to the substrates in vacuum environment, physical coating takes place due to projected atoms condensation. This technique results in improved composition control and high flexibility of the deposited films [2][3]. PVD reactors consists of two electrodes which are connected to high voltage power supply present in a vacuum chamber [4]. Evaporation and sputtering are frequently employed physical vapor deposition methods for the fabrication of thin films. Magnetron sputtering process involves the application of high voltage in the vacuum chamber which results in the release of atomic size particles from the target leading to the fabrication of fine layers of target material. This technology employs cathodic cleaning technique for contamination removal. E-beam evaporation employs target as an evaporation source, energetic e-beams are used for evaporating target

material. Plasma is created in deposition chamber which accelerates the evaporated material resulting in film deposition onto substrate material [4]–[6].

Advantages of physical vapor deposition technique include improvement in corrosion and wear resistance of the deposited film, low maintenance of equipment and environmentally friendly procedure. Coats produced through physical vapor deposition have excellent adhesion, graduated properties, homogeneity and precise morphology [7]. Mono-layered, multi-layered and multi-graduated coating systems can be done through physical vapor deposition. Coating characteristics can be varied continuously throughout the film, this is considered as most important characteristic of physical vapor deposition process [8].

3.3.2. Chemical Vapor Deposition (CVD)

Chemical vapor deposition (CVD) process involves the transportation of volatile precursors to the reaction chamber through vapor phase, where heated substrate is used to decompose these precursors. Hot-wall reactors, cold-wall reactors, process at sub-torr total pressures to above atmospheric pressures, varied temperature ranges (200-1600°C) and process with or without carrier gases are the variants of this technique.

3.3.2.1. CVD Mechanism

CVD Mechanism begins with convective and diffusive transportation of reactants to the reaction zone which lead to gas phase reactions followed by transport of reactants to the substrate surface, after that chemical and physical adsorption takes place leading to the surface reactions for film formation then volatile byproducts are desorbed and lastly transportation of by products from the reaction zone.

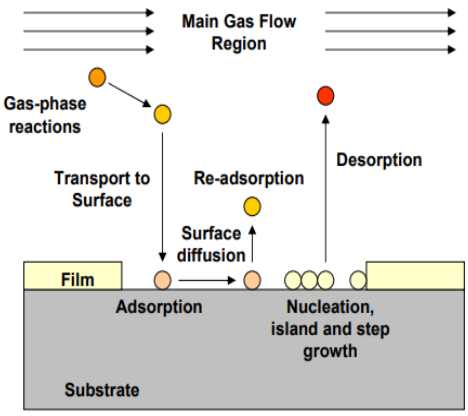

Figure 3.5: CVD Mechanism

3.3.2.2. Types of CVD processes

CVD processes involve the use of plasmas, photons, ions, hot filaments, lasers, or combustion reactions in order to decrease deposition temperatures or improve deposition rates. Atmospheric Pressure chemical vapor deposition (APCVD) is used to deposit thin

film at atmospheric pressure. It has low operating cost but due to greater gas density and residence time this process is prone to oxidation. Low Pressure chemical vapor deposition (LPCVD) is used to deposit thin film at low pressure (10-1000 Pa) due to which unwanted gas phase reactions are reduced and the mass transfer rate of gaseous reactants is elevated than that of surface reaction rate. High purity, excellent uniformity and good step coverage are attained through this process. Metal Organic chemical vapor deposition (MOCVD) uses metal organic compounds as precursor which are highly volatile at moderate to low temperature therefore low reaction temperature (750-1100 K) is maintained. Expensive precursors are difficult to purify due to their volatility. Laser Chemical vapor deposition (LCVD) uses focused laser beam for heating the substrate and film deposition in a single step process. Plasma Enhanced chemical vapor deposition (PECVD) involves plasma production and applies it for thin film deposition.

Advantages of chemical vapor deposition process include conformal film fabrication, wide variety of deposition materials, high purity of deposited films, high deposition rates, and no requirement of high vacuum but CVD precursors are the main cause of limiting CVD process, precursors can be highly toxic, volatile, corrosive or explosive. CVD reaction byproducts can be harmful as well. Metal-organic precursors for the process can be quite costly. Film deposition at elevated temperatures is also a limiting factor for the process [9].

3.3.3. Solution Based Chemical Processes

Solution based chemical process includes techniques which employ liquid phase as mass transport media for precursors transportation. Low temperature processing and product homogeneity are the advantages of these techniques. Variation in factors such as viscosity, composition, solution concentration, pH etc. are used for morphological control of the films. Multiple coating techniques such as dip coating, spin coating, and spray coating are used for film deposition.

3.3.3.1. Dip coating

Dip coating is a simple, flexible and cost-effective solution deposition technique which is applicable on complex shaped and large area-based substrates. In this process substrate is immersed in the solution, film forms and substrate are taken out from the solution and

dried. Film obtained through dip coating has thickness in micrometer range. Gravitational forces, viscous drag, inertial force, surface tension, disjoining pressure are the important factors which influence film formation and quality.

3.3.3.2. Spin coating

Spin coating is considered as a simple method for the deposition of uniform thin films. Spin coater consists of a vacuum chuck which holds the substrate while coating solution is dispensed on it for film formation. Particular rotation speed is set for particular duration considering the deposition of required film thickness. Centrifugal force enables thin and uniform coating by spinning out excess solution from substrate surface. Static and dynamic dispense spin coating are the main two methods for fabricating thin films by using spin coating technique. Dynamic dispense spin coating technique is better as compared to static dispense spin coating, it ensures using limited solution and controlled process. Substrate rotation at high speed results in even film formation. Film quality depends on parameters such as spin speed, spin duration. Film thickness depends on the factors like solvent evaporation rate and solution concentration, which further depends upon the vapor pressure, solution viscosity, temperature and humidity. Spin speed is significant factor as it effects the thickness of film that can be formed from a desired solution. Film uniformity, reproducibility, process simplicity, varied substrate materials, and reasonable cost are the major advantages of this process. Requirement of flat and smooth substrate is considered as a drawback of this process.

3.3.3.3. Spray Pyrolysis

Spray coating technique employs an atomizer which converts liquid precursor solution into fine aerosol which are then deposited on a substrate surface. The substrate temperature can be controlled. Different spray techniques involve multiple atomization methods, varied film morphologies are produced accordingly. Spray pyrolysis film deposition process involves precursor solution atomization, aerosol transport, droplet evaporation and film formation.

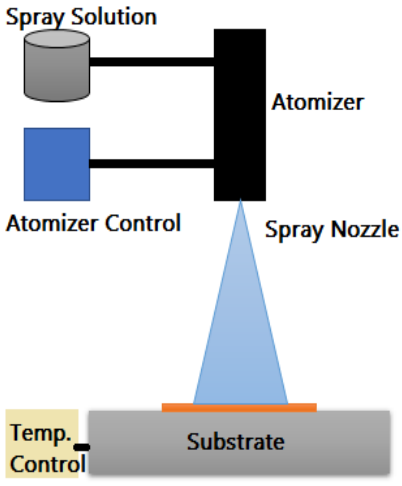

Figure 3.6: Spray Pyrolysis

Spray pyrolysis is easy, cost effective technique which results in high quality and uniform film formation. It is suitable technique for mass production as well.

Techniques employed by spray pyrolysis include air blast, ultrasonic, or electrostatic methods. Different atomizers provide different droplet size, atomization rate, and droplet initial velocity. Initial droplet velocity influences the droplets reaching rate to the substrate surface. Ultrasonic nozzles apply minor energy to produce low radius droplet with slight atomization rate. Air blast atomizer applies high speed air for converting precursor solution in aerosol. Applied air pressure has direct influence on the diameter of droplet produced. Increased liquid pressure results in increased droplet diameter. Two types nozzles are used for electrostatic Spray Deposition, cone-jet mode and the multi-jet mode. A cone jet mode nozzle dispenses liquid in a single convex shape jet while in a multi jet mode nozzle multiple jets with small diameter are dispensed from the nozzle tip. Forces such as are gravitational force, thermophoretic force, electrical force and stokes force act on the droplet and decide its path while it is passing through the ambient.

3.4. Characterization techniques

3.4.1. Optical Microscope

Optical microscope is also referred as light microscope. It uses visible light and a setup of lenses for magnification. Ocular lens, objective turret, objective lenses, coarse adjustment knobs, fine adjustment knobs, object holder, illuminator, diaphragm and condenser are the basic components of an optical microscope.

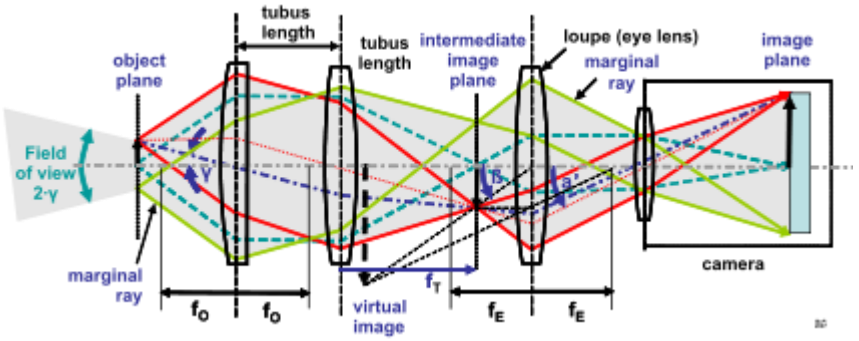

Figure 3.7: Optical Microscope Working Mechanism

Modern microscopes have complex components. Optical path should be set up and controlled accurately in order to ensure proper working of an optical microscope. It has a simple operating principle. An objective lens is a high-powered magnifying glass with short focal length which is used to obtain a highly magnified real image of the object. Optical microscopy is widely used in nanophysics, microelectronics, microbiology, biotechnology and pharmaceutic research.

3.4.2. Scanning Electron Microscope

Scanning electron microscope uses electrons to observe the morphology of a sample at higher resolution, higher magnification and depth of focus. In scanning electron microscope electron beam is used instead of visible light and because of the fact that electron has wavelength about 1000 time shorter than visible light so SEM tendency to magnify the material surface is much higher than simple microscope. The electron beam is generated thermionically by using electron gun fixed on a tungsten filament cathode. The tungsten metal has the highest melting point and lowest vapor pressure so it can be used for electron beam generation via heating thermionic electron guns. The focusing and controlling of electron beam is achieved by using condenser lenses of diameter range ~4–50 Å and deflection coils respectively. The schematic diagram of SEM is shown in Figure 3.10 which shows the complete flow of process from the start i.e. generation of electron beam to end i.e. the beam strikes the sample. Generated signals consisting of secondary electrons are analyzed with the help of detector and the output is displayed. When the electron beam hits the sample surface different types of signals are generated which carry information about film or surface morphology. These signals include X-rays, secondary electrons and back scattered electrons. These signals can be detected by specific detectors and analyzed for getting

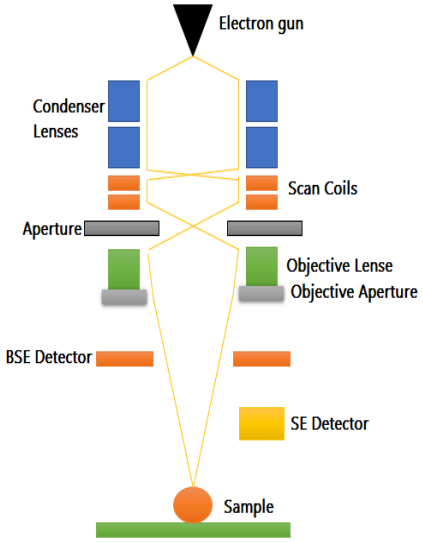

Figure 3.8: SEM Components

results. The chemical composition of material is analyzed by back scattered electrons while secondary electrons gives surface morphology.

3.4.3. X-Ray Diffraction

X-ray diffraction is an analytical technique used for crystalline material phase identification, sample purity and information regarding unit cell dimensions. When crystalline materials are irradiated by X-rays, they interact with atoms of the material and refract X-rays of characteristic energy. An individual pattern is generated by each material. In a mixture of materials, each substance gives its own pattern independently. XRD works on the principal of constructive interference of refracted X-rays. Fig.3.9 shows working of XRD machine.

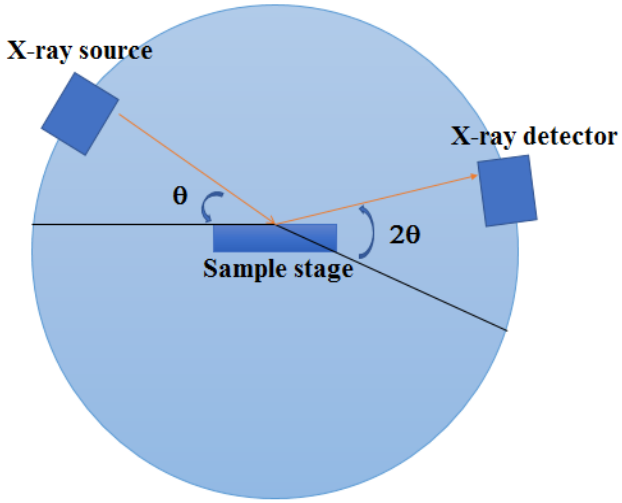

Figure 3.9: XRD Components

When X-rays interact with matter, three phenomena may occur, Ionization, fluorescence and diffraction. In XRD, when X-rays hit atoms, the electrons in atoms start vibrating with frequency same as the frequency of striking X-rays. The constructive interference occurs due to angles with high scattering and is given by Bragg's law i.e. $n\lambda = 2d \sin\theta$, where λ = X-ray beam wavelength, d = crystal lattice interplanar spacing, θ = X-ray beam angle of incidence over the crystal plane n = 0,1,2,3…Focused X-ray beam scatters after its interaction with planes of atoms, these scattered radiations form diffraction patterns which are related to materials structure. Information regarding materials crystal structure can be attained from the obtained peak positions, peak-width, intensity and shape.

3.4.4. UV-Visible Spectroscopy

UV/VIS/NIR spectroscopy is an analytical technique for determining the optical properties such as transmittance, absorbance and reflectance. UV-Vis spectroscopy analysis technique is a very important technique in which visible (400 nm- 700nm) and ultraviolet (190 nm-400 nm) regions of the electromagnetic spectrum are used to obtain information about organic molecules. Other than absorption or transmittance spectra this technique is also used for determining impurities, saturation, unsaturation and heteroatoms existence in the material. Qualitative analysis can be performed to determine the type of compounds present in the specimen. The spectrum obtained by UV-VIS spectrophotometer is compared to spectra of known compounds.

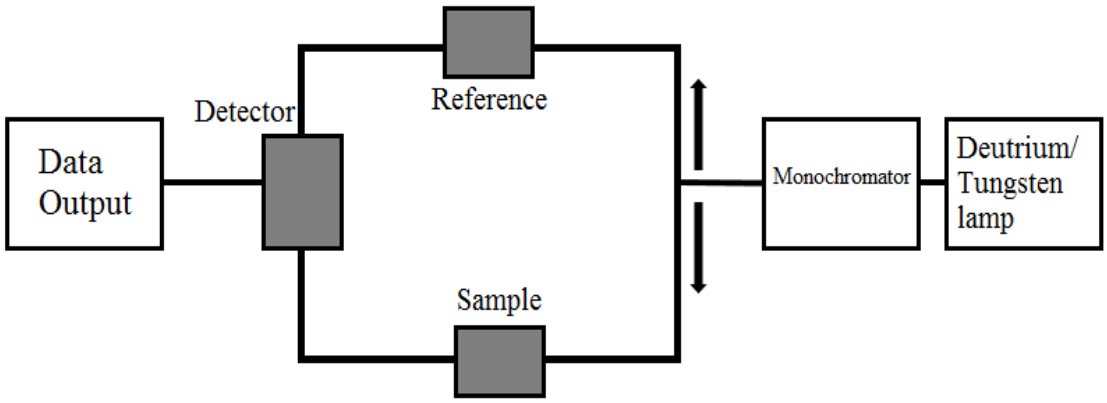

Figure 3.10: UV-Vis Spectrophotometer Components

When a sample is placed under the UV-Vis spectrum the electrons get excited to higher antibonding orbitals. Lesser the energy gap between HOMO and LUMO of a material, easier is the excitation of electrons by longer wavelength radiations. When a molecule with an energy equal to gap between HOMO-LUMO is exposed to radiation with a wavelength corresponding to that energy, the electron is jumped from HOMO to LUMO. This is referred to as electronic transition bonding to anti-bonding and denoted by $\sigma - \sigma^*$. The graph between absorption or transmittance of light on X-axis and different wavelengths on Y-axis is obtained and analyzed.

3.4.5. Hall Effect

Electric field enables the movement of charges in a conductor due to which electric current is produced. If magnetic field is applied in perpendicular direction to the direction of movement of charges, these charges distribute such that opposite charges lie on opposite faces of the conductor leading to the production of potential difference due to which further charge movement is opposed. This leads to the production of steady electrical potential in the conductor. This phenomenon is known as Hall effect. Sign of the potential determine the positive or negative charge of the carriers.

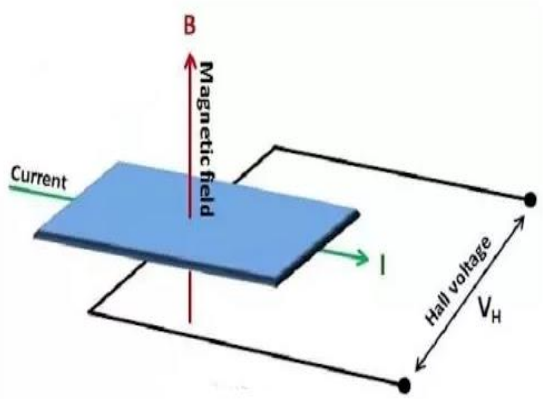

Figure 3.11: Hall effect working mechanism

If we take a region where electric field E and magnetic field B act at right angles to each other. When electron movement takes place at right angles to both fields and field strength is adjusted such that opposite and equal forces act on the electron such that Ee=ev/d =Bev. During Hall effect phenomenon, electric field is generated by the movement of electron towards one side of the specimen and produced electric field should be adequate enough to balance the force produced by magnetic field. The voltage across the specimen at this point is known as Hall voltage (V_H), equationally written as $eV_H/d = Bev$. Since $I = nAve$ where n is the number of charge carriers per cubic meter and A the cross-sectional area of the specimen, d its width and t its thickness then $V_H = BI/net$. Hall voltage value depends on the flux density, current, electron charge, number of charge carriers and specimen thickness.

3.4.6. Contact Angle Measurement

Angle created between liquid and solid surface when both materials come in contact together is known as contact angle. Contact angle created in the solid and liquid interface

is influenced by properties of the liquid, solid and their adhesion, cohesion and repulsion forces. Contact angle measurement is a common method to find the wettability of a material or surface. Contact angle and wettability share indirect relation i.e. materials with large wetting tendency have small contact angles and vice versa. Contact angle of 0° depicts complete wetting. Angle formed between 0°- 90° depicts that the surface is hydrophilic. Angle formed between 90°- 180° depicts that the surface is hydrophobic. Ultra-hydrophobic surfaces are strongly liquid-repellent with contact angle ~180°. Drop shape analysis, Wilhelmy plate method, Wash-burn method, Top-view distance method are the techniques employed for contact angle measurement.

Figure 3.12: Varying Contact Angle

3.5. Summary

Details of the experimental method, material synthesis and working principle of different characterization techniques have been explained. Thin films coating by using low-cost solution-based techniques like dip coating, spin and blade coating etc. are inexpensive as compared to vacuum based techniques like HR thermal evaporation and electron beam method etc. After nanoparticle synthesis and film fabrication, it is required to characterize the compound and films. Different material characterization techniques like XRD, SEM, UV-Vis spectroscopy, Hall effect, contact angle measurement have been employed to study the Structural, morphological, optical, electrical and wettability properties of films. The information obtained from these characterization data are utilized to optimize better conditions.

References

[1] A. V. Rane, K. Kanny, V. K. Abitha, and S. Thomas, "Methods for Synthesis of Nanoparticles and Fabrication of Nanocomposites," in *Synthesis of Inorganic Nanomaterials*, Elsevier, 2018, pp. 121–139.

[2] D. M. Mattox, *The Foundations of Vacuum Coating Technology*. 2003.

[3] H. Wasa, Kiyotaka, Kitabatake, Makoto, Adachi, *Thin Films Material Technology*. Springer-Verlag Berlin Heidelberg, 2004.

[4] V. Imbeni, C. Martini, E. Lanzoni, G. Poli, and I. M. Hutchings, "Tribological behaviour of multi-layered PVD nitride coatings," *Wear*, vol. 250, no. 251, pp. 997–1002, 2001.

[5] "Coatings Technology Handbook - CRC Press Book." [Online]. Available: https://www.crcpress.com/Coatings-Technology-Handbook/Tracton/p/book/9781574446494. [Accessed: 18-Nov-2019].

[6] P. M. Martin, *Handbook of Deposition Technologies for Films and Coatings : Science, Applications and Technology*. Elsevier Science, 2009.

[7] A. Baptista, F. J. G. Silva, J. Porteiro, J. L. Míguez, G. Pinto, and L. Fernandes, "On the Physical Vapour Deposition (PVD): Evolution of Magnetron Sputtering Processes for Industrial Applications," *Procedia Manuf.*, vol. 17, pp. 746–757, 2018.

[8] A. Baptista, F. Silva, J. Porteiro, J. Míguez, and G. Pinto, "Sputtering Physical Vapour Deposition (PVD) Coatings: A Critical Review on Process Improvement and Market Trend Demands," *Coatings*, vol. 8, no. 11, p. 402, 2018.

[9] H. H. Gatzen, V. Saile, and J. Leuthold, *Micro and Nano Fabrication*. 2015.

[10] "Chapter 17 New technologies," *Pergamon Mater. Ser.*, vol. 11, pp. 475–517, 2007.

[11] B. D. (Bernard D. Cullity, *Elements of x-ray diffraction*. Addison-Wesley Publishing Company, Inc, 1978.

Chapter 4: Material and Methodology

4.1. Experimentation

A number of experiments were performed to meet the research objectives. The detail of experiments is given below:

1. Synthesis of nickel oxide nanoparticles by varying techniques and process conditions.
2. Characterization of nanoparticles through XRD, SEM in order to select the best for film deposition.
3. NiO and MWCNTs film fabrication
4. Characterization of thin films by XRD, SEM, Hall effect and UV-Vis analysis, Contact angle measurement.

4.1.1. Synthesis of nickel oxide nanoparticles

Material:

Nickel di chloride hexahydrate ($NiCl_2.6H_2O$) 99.9% trace metals basis, Sodium hydroxide (NaOH), Sodium Carbonate (Na_2Co_3) were bought from Sigma Aldrich. Ethanol and Distilled water have been utilized as the solvent. Ethylene glycol and glucose have been used as template.

Methodology:

I. Hydrothermal Synthesis:

Nickel dichloride Hexahydrate (1.782 gm) was added to 75 ml Distilled Water. Sodium Citrate (0.1 M) solution prepared and added dropwise to $NiCl_2.6H_2O$ solution at constant stirring. Hydrothermal Synthesis done at 180 C for 12 hours followed by hot plate drying. Sample was calcinated at 350 C for 4 hours, crushed and again calcinated at 500 C for 4 hours.

II. Co-precipitation Technique:

Nickel di chloride Hexahydrate solution was prepared by adding 1.18 gm $NiCl_2.6H_2O$ to 50 ml Ethanol. Solution was magnetically stirred at room

temperature for an hour. NaOH 0.1 M solution was added during the stirring until PH reached particular level. Varied templates were used and samples was calcinated at varied temperatures, crushed and collected. Process has been shown in flow diagram.

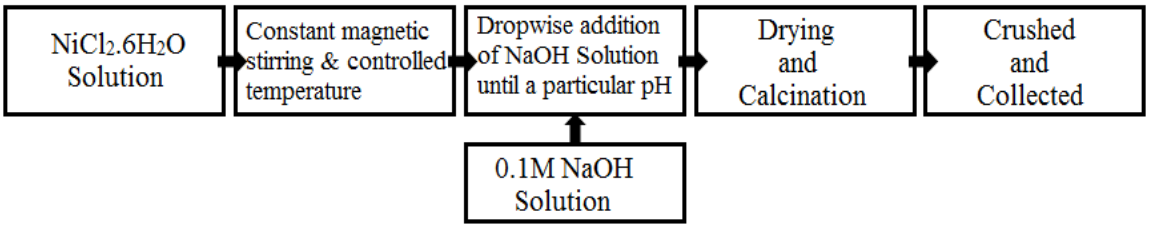

Figure 4.1: NiO Nanoparticles preparation process flow chart.

Table 0.1:Varied Process Conditions during Co-precipitation technique.

Sample No.	Material	Template	Process Conditions	Calcination Temperature
1	$NiCl_2.6H_2O$ NaOH	Ethylene Glycol ($C_2H_6O_2$)	Room temperature. pH: 10	500 °C
2	$NiCl_2.6H_2O$ NaOH	Ethylene Glycol ($C_2H_6O_2$)	Temperature: 60°C. pH: 11	500 °C
3	$NiCl_2.6H_2O$ NaOH	Glucose	Temperature: 60°C pH: 11	500 °C
4	$NiCl_2.6H_2O$ NaOH	Ethylene Glycol ($C_2H_6O_2$)	Temperature: 70°C. pH: 11	800 °C

4.1.2. Characterization of Nickel Oxide nanoparticles

i. **XRD:** X-ray diffraction was performed for purity examination and phase identification of NiO nanoparticles synthesized with varying templates and varying sintering temperatures by using using X-ray Diffractometer (XRD) (Model: D8 Advance, Bruker) with monochromatic CuKα at a scanning rate of 10^0/min and scan angle of $2\theta=20\text{-}70^0$.

ii. **SEM/EDS:** Morphological analysis of NiO nanoparticles was carried out by employing Scanning Electron Microscopy (SEM) (Model: Vega3, Tescan) while

corresponding elemental compositions obtained through Energy Dispersive Spectroscopy (EDS).

4.1.3. HTL Fabrication:

HTL is a bi-layer comprising of NiO thin film and MWCNTs thin film.

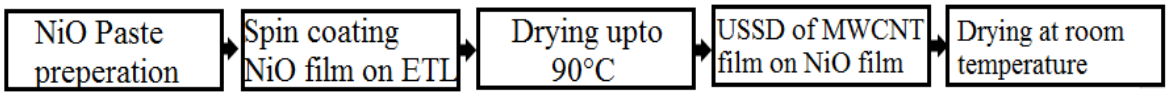

Figure 4.2: HTL Deposition Process

Step 1: Fabrication of NiO Thin film:

Nickel oxide nanoparticles 1 gm were finely crushed with 3 ml ethanol by using a mortar and pestle until a fine paste was achieved. NiO paste was spin coated at r1 1500 rpm – r2 3000 rpm for t1=t2=30seconds. Thin film was dried at 90 in an oven.

Step 2: Deposition of MWCNT Thin film on NiO Thin film:

CNTs thin film has been prepared by ultrasonic spray coating. MWCNT solution has been prepared by adding 10 mg CNTs in 10 ml Ethanol. SDS (Sodium Dodecyl Sulphate) has been used as a surfactant. Solution was magnetically stirred for one hour followed by sonication for 2 hours. Homogeneous Ink formed resultantly was deposited at the rate of 1mg/min through ultrasonic spray coating at medium ultrasonic power.

4.2. Film Characterization

I. **XRD:** X-ray Diffractometer (XRD) (Model: D8 Advance, Bruker) with monochromatic CuKα with scanning rate of 10^0/min and scan angle of $2\theta=20\text{-}70^0$ has been employed for the phase identification and purity analysis of synthesized films.

II. **SEM/EDS:** Morphological analysis of synthesized films was carried out by employing Scanning Electron Microscopy (SEM) (Model: Vega3, Tescan) while corresponding elemental compositions obtained through Energy Dispersive Spectroscopy (EDS)

III. **UV-Vis Spectroscopy:** The optical properties of the film were studied using a UV-3600 plus UV-VIS NIR Spectrophotometer. The Transmittance and Absorbance spectra were measured for the fabricated films.

IV. **Hall Effect:** The Electrical conductivity of the prepared film was measured using Hall Effect measurement system (Ecopia HMS-3000). The results obtained confirmed the p/n type of the material, charge mobility, conductivity and resistivity.

V. **Contact Angle Measurement:** To understand the hydrophobicity, contact angle was measured by using a Kruss Drop Shape Analyzer DSA100.

4.3. Summary

This chapter explained all the experiments carried out for this research. NiO nanoparticles have been synthesized by varying techniques and process conditions. Suitable nanoparticles identified through structural and morphological characterizations were incorporated as HTM. A bilayer comprising of NiO and MWCNTs has been employed as an HTL. NiO HTL was deposited through spin coating and MWCNT thin film was deposited over it through Ultrasonic spray coating on the absorber layer for all the cells. NiO thin film has been sintered at 90^0 to study the difference between sintered and non-sintered films. All the layers were individually characterized and tested using XRD for phase identification, SEM/EDS for surface morphology, UV-Vis spectroscopy to study the optical properties, Hall Effect to check the electrical properties and Contact angle measurement for wettability studies of the samples prepared.

Chapter 5: Results and Discussion

This chapter discusses results obtained by characterizations of the NiO nanoparticles and films fabricated after varying techniques optimizing process conditions.

5.1. NiO Nanoparticles fabrication through varying techniques

Nickel oxide nanoparticles synthesized through co-precipitation technique and hydrothermal synthesis have been subjected to structural and morphological characterizations.

5.1.1. Structural Characterization

XRD (D8 Advance, BRUKER) was incorporated for structural characterization, 2Θ angle is used from 30° to 70°. Sample A shows the XRD graph of nanoparticles prepared through co-precipitation technique. Sample B shows the XRD graph of nanoparticles prepared through hydrothermal synthesis. The characteristic peaks for sample A and B seen at 2θ of 37.0°. 43.1°, 62.6° could be indexed to (111), (200), and (220) diffraction planes respectively. XRD pattern reflections can be attributed to cubic phase of NiO (JCPD card no.# 03-065-5745). Information obtained through XRD data has been justified from literature. L.G.Teoh et al. synthesized NiO nanoparticles through sol gel method and three characteristic peaks referred to diffraction planes (110), (200) and (220) (JCPDS card No. 87-0712) represent face-centered cubic (fcc) structure of nickel [1]. XRD patterns of NiO synthesized by Barakat A. et al. reveals similar diffraction peaks which can be referred to face-centered cubic phase of NiO (JCPDS card No. 73-1523) [2]. Rahdar A. et al. fabricated nanostructured Nickel oxide by co-precipitation method. XRD pattern revealed the face-centered cubic (FCC) structure of NiO and ensured high degree of crystallinity as well [3]. Pilban J. et al. produced Nickel oxide nanoparticles through a facile sol gel method, calcined it at varied temperatures of 300, 400, 500 C and obtained similar diffraction peaks through XRD corresponding to the face-centered-cubic (fcc) structure of the NiO [4]. Peak position of NiO nanoparticles synthesized by Qiao et al. can be referred to crystal planes (111), (200), (220), (311) and (222) (JCPDS, No. 04-0835) [5]. These diffraction peaks are attributable to the face-centered cubic crystalline

structure of NiO with relative peak position and characteristic peaks intensity as well. Increase in sharpness of XRD peaks indicates the crystalline nature of the particles.

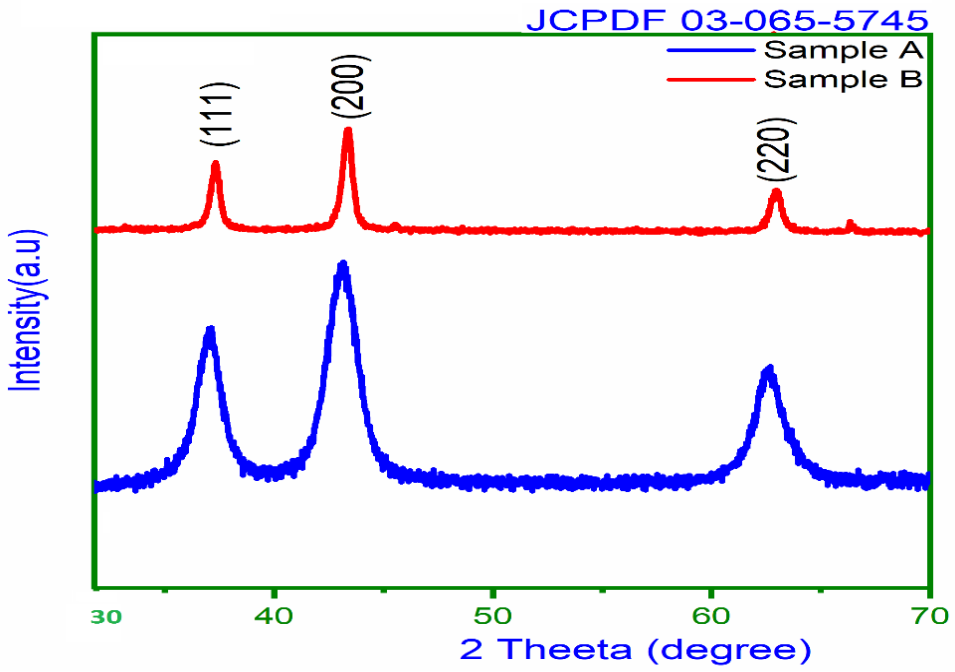

Figure 5.1: XRD Spectra for Sample A & Sample B

5.1.2. Morphological Characterization

SEM (VEGA 3 LMU, TESCAN) was used to understand the surface morphology and surface quality. Studies have been done using SEM, at a magnification of up to 500 nm with an accelerating voltage of about 20 kV and a magnification of about 50 kX. SEM Results of Co-precipitation prepared sample showed needle like structure width varying from 64.19 nm up to 97.61 nm and length up to 901.71 nm was found while the SEM Results of hydrothermally synthesized sample showed clusters of small particles attached to large particles. Particle size of radius ranging from 34.89 nm, 71.20 nm were found at 500 nm Scale. Information obtained through SEM has been justified from literature. H. Xiao et al. also used $NiCl_2.6H_2O$ as precursor and fabricated large scale ultrathin NiO nanoflakes through combining a hydrothermal reaction and a thermal annealing process [6]. A. Manikandan et al. fabricated NiO Nano sized flakes, the average size and void space diameter of single NiO nanoflake was found to be 15–20 nm [7]. Nanostructured nickel oxide (NiO) synthesized by similar hydrothermal route by using similar chloride precursor yielded attractive nanosphere which were made up of fine nanoflakes [8]. Q.

Zhou et al. also used typical hydrothermal procedure to synthesize hierarchical NiO nanostructures, which are constructed by many ultrathin nanoflakes with thickness ranging from 10 to 15nm [9]. Research group of S. Safa observed that morphology and size of NiO nanostructures can be controlled effectively by changing the hydrothermal temperature [10]. Rahdar et al. also used co-precipitation method with similar precursors i.e. $NiCl_2.6H_2O$ and NaOH and synthesized nanostructured nickel oxide (NiO) in spherical shape, average size of the NiO nanoparticles is 24 nm [3]. The formed NPs show agglomeration at different locations due to large surface energy and high reactivity [11].

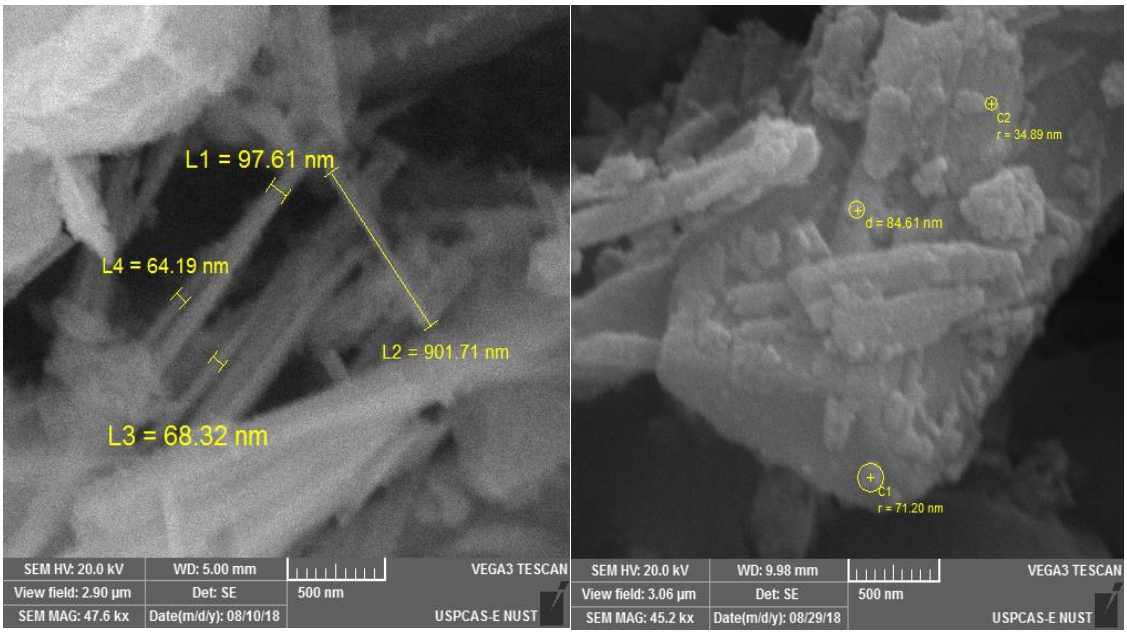

Figure 5.2:SEM Images (a) Sample prepared through co-precipitation technique (b) Sample prepared through hydrothermal synthesis.

5.2. Optimization of NiO Nanoparticles through variation in process conditions

Uniform and fine structured NiO nanoparticles obtained by optimizing process conditions during co-precipitation technique have been subjected to structural and morphological characterizations in order to select the best material for further film deposition.

5.2.1. Structural Characterization

5.2.1.1. X-ray Diffraction Spectroscopy

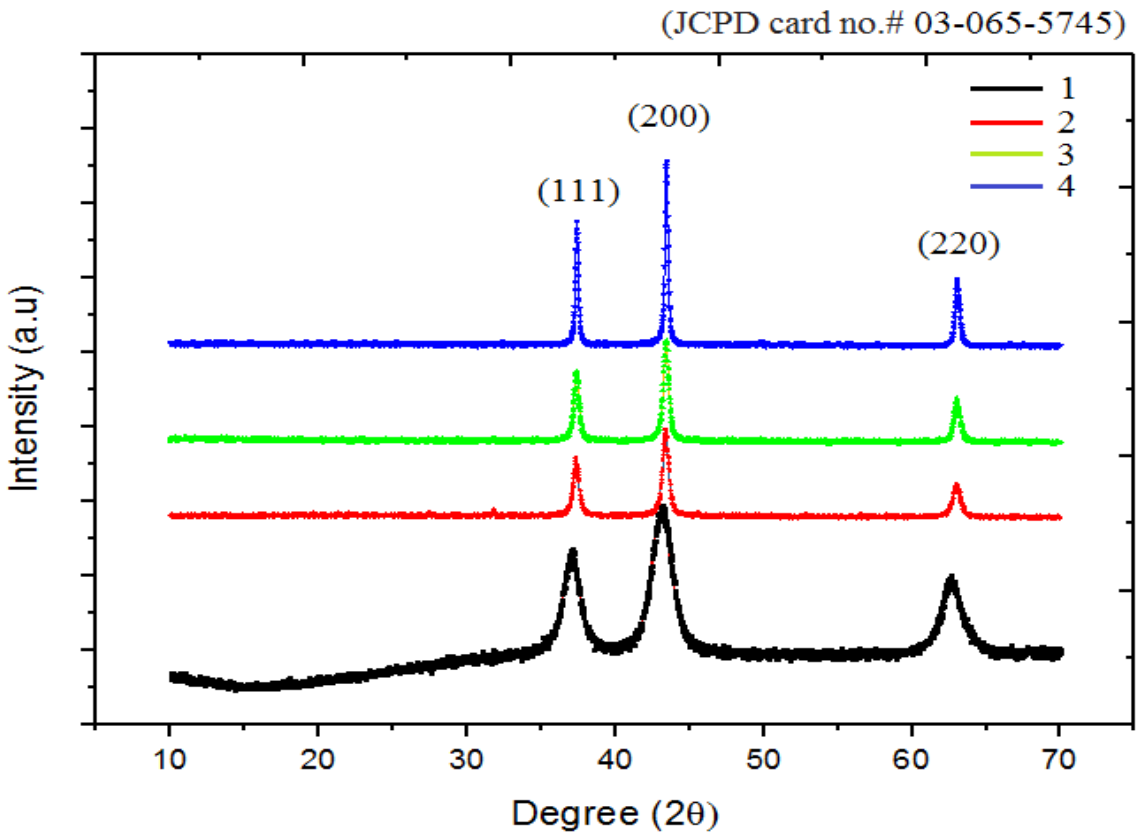

Figure 5.3: XRD Spectra for Sample 1, Sample 2, Sample 3, Sample 4

XRD (D8 Advance, BRUKER) was incorporated for structural characterization, 2Θ angle is used from 10° to 70°. XRD patterns of the synthesized Nickel Oxide nanoparticles are shown in Figure 5.3. The characteristic peaks seen at 2θ of 37.0°. 43.1°, 62.6° could be indexed to (111), (200), and (220) diffraction planes respectively. Reflections in the XRD pattern are attributable to cubic phase of NiO (JCPD card no.# 03-065-5745). XRD results have been justified through literature. Rahdar A. et al. also synthesized nanostructured Nickel oxide (NiO) by co-precipitation method. XRD pattern revealed the face-centered cubic (FCC) structure of NiO and ensured high degree of crystallinity. Results have been compared before and after calcination, NiO nanoparticles calcined at 500 C exhibit high crystalline quality as compared to non-calcined samples [3][12]. Research group of Pilban synthesized Nickel oxide nanoparticles through a facile sol gel method, calcined at varied temperatures of 300, 400, 500 °C and compared the results. Similar diffraction peaks

obtained through XRD at crystal planes (111), (200), (220), (311), and (222) correspond to face-centered-cubic structure of NiO [4]. XRD Spectra indicates that diffraction peaks intensity has improved with the calcination temperature, which indicates that nickel oxide prepared at a higher calcination temperature exhibit better crystallinity. No peaks from other phases are detected ensuring high purity of the product.

5.2.1.2. Crystallite Size Calculation

Scherrer equation was used to calculate average crystallite size;

$$Dp = (0.94 \times \lambda) / (\beta \times \cos\theta)$$

Where, Dp = Average Crystallite size, β = Line broadening in radians, θ = Bragg angle, λ = X-Ray wavelength.

Table 0.1: Crystallite Size Calculation

Sample 1:

Pos. [°2Th.]	FWHM	Crystal size
37.0310	0.9446	9.26
43.1166	1.2595	7.09
62.5951	1.1520	8.45

Sample 2:

Pos. [°2Th.]	FWHM	Crystal size
37.3298	0.9446	9.28
43.3694	0.9446	9.46
62.9826	1.1520	8.45

Sample 3:

Pos. [°2Th.]	FWHM	Crystal size
37.3545	0.9446	9.28
43.3923	0.9446	9.46
63.0247	1.1520	8.45

Sample 4:

Pos. [°2Th.]	FWHM	Crystal size
37.3864	0.9446	9.28
43.4183	0.9446	9.46
63.0445	1.1520	8.45

The average crystallite size calculated using the Scherrer equation is about 8.27 nm, 9.063 nm, 9.063 nm, 9.06 nm for sample 1, sample 2, sample 3, sample 4 respectively.

5.2.2. Morphological Characterization

SEM (VEGA 3 LMU, TESCAN) was used to understand the surface morphology and surface quality. Studies have been done using SEM, at a magnification of up to 500 nm with an accelerating voltage of about 20 kV and a magnification of about 50 kX. Scanning electron microscope images of samples are given in fig. 5.4. SEM images of sample 1

resulted in flake like structure with width varying from 64.19 nm up to 97.61 nm and length up to 901.71 nm was found. SEM images of Sample 2 showed Grain Like Nano structures with Grain size of d= 27.28 nm, 28.50 nm, 25.53 nm observed at 500 nm scale. SEM images of Sample 3 showed Grain Like Nano structure with Grain size of d= 23.62 nm, 25.79 nm, 27.08 nm observed at 500 nm scale. SEM images of Sample 4 showed Grain Like Nano structures with Grain size of d= 32.27nm, 37.17 nm, 39.20 nm observed at 500 nm scale.

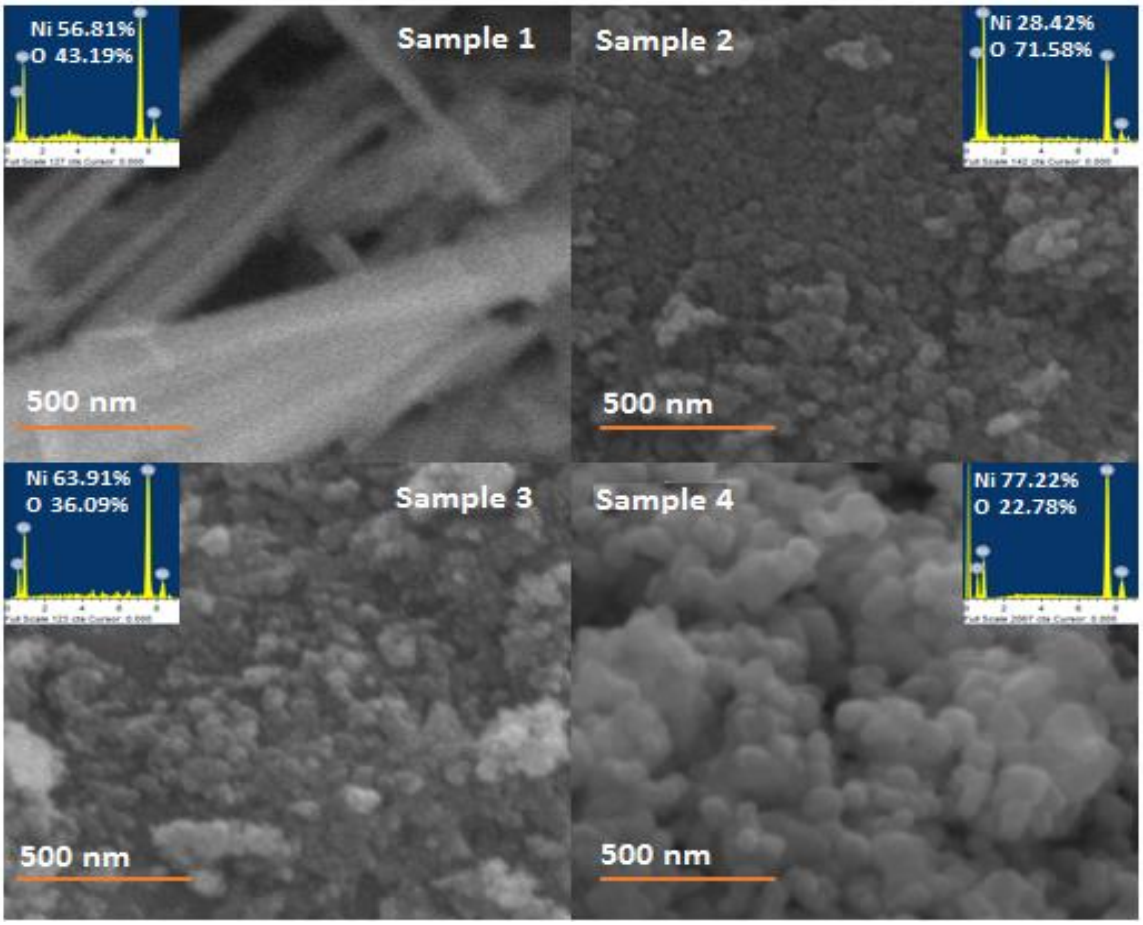

Figure 5.4: SEM Images (a) Sample 1 (b) Sample 2 (c) Sample 3 (d) Sample 4

Results obtained through morphological characterization have been justified through literature. S.V. Ganachari et al. synthesized NiO nanoparticles at low temperature. The particles obtained have irregular spherical shape in nanosized range of 20-40 nm [13]. Uniform and well dispersed cubic nickel oxide (NiO) nanoparticles with size 40–50nm have been synthesized by N. Dharmaraj et al. SEM image show similar uniform sized

grain like structure with diameter around 40–50nm obtained due to heat treatment [14]. Research group of A.Rahdar synthesized nanostructured Nickel oxide (NiO) by using same technique and same precursors i.e. co-precipitation method , $NiCl_2.6H_2O$ and NaOH respectively. SEM results indicated spherical shape of nanoparticles with average size~24nm [3]. S. Sagadevan et al. also used co-precipitation technique for NiO nanoparticles synthesis, SEM images showed small and homogeneous spherical shaped grains [15]. NiO nanoparticles synthesized by research group of Khalaji are approximately spherical with the diameter varying between 35 and 60 nm [16]. Similar structure has been observed in this work.

5.3. HTL Characterizations

NiO film deposited by spin coating, MWCNT film fabricated through ultrasonic spray coating and Bi-layer which is formed by combining NiO film and MWCNT film have been subjected to structural, morphological, electrical and optical characterization.

5.3.1. Structural Analysis

XRD (D8 Advance, BRUKER) was incorporated for structural characterization, 2θ angle is used from 10° to 70°. The characteristic peaks seen at 2θ of 37.0°. 43.1°, 62.6° could be indexed to (111), (200), and (220) diffraction planes respectively. XRD pattern reflections can be attributed to cubic phase of NiO (JCPD card no.# 03-065-5745). Peak appeared at 26° can be indexed to (002) plane of MWCNTs. The other peaks observed in non-sintered films at 2θ of 31.6° have been identified as Ni_2O_3 corresponds to [002] crystal planes. Peaks observed at 2θ of 45.315° have been identified for Ni [111] phase. These peaks have disappeared after sintering, this shows that sintering has converted Ni and Ni_2O_3 to NiO. Shrivastav et al. observed similar peaks for Ni and Ni_2O_3 in his work for fabrication NiO [17]. High peak intensity indicates that the NiO nanoparticles are of high crystallinity. Z. Liu et al used NiO nanocrystals dispersed in chlorobenzene to spin coat a 30 nm-thick layer of a NiO film at 3000 rpm, synthesized NiOx film exhibit diffraction peak at 36.9°, 42.9°, 62.2°, which are attributable to crystal planes (111), (200) and (220) of NiO, respectively [18]. Similar XRD spectra for spin coated NiO film has been observed by Kwon U et al. XRD spectrum showed intense peaks at 2θ = 37.2°, 43.3°,

and 62.9°, which are assigned to (111), (200), (220) planes of NiO cubic crystal structure [19].

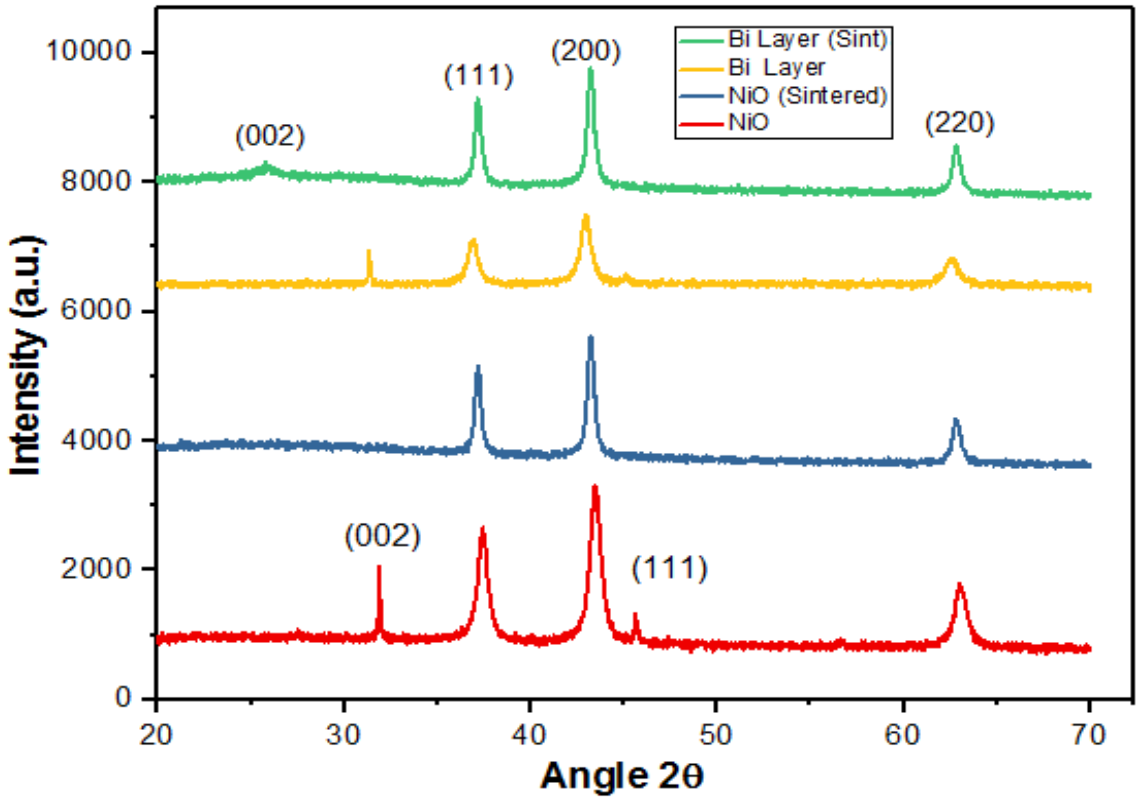

Figure 5.5: XRD Spectra for hole transporting layer

5.3.2. Morphological Analysis

SEM (VEGA 3 LMU, TESCAN) was used to understand the surface morphology and surface quality. Studies have been done using SEM, at a magnification of up to 500 nm with an accelerating voltage of about 20 kV and a magnification of about 50 kX. SEM images show that a uniform film of NiO nanoparticles has been obtained through spin coating at r1=700rpm -r2=3000rpm for t1=t2=30 seconds. Uniform film of MWCNTs has been obtained through Ultrasonic spray coating. SEM images of MWCNT film shows MWCNT films were coated uniformly and densely on NiO film by forming well-interconnected network structure.

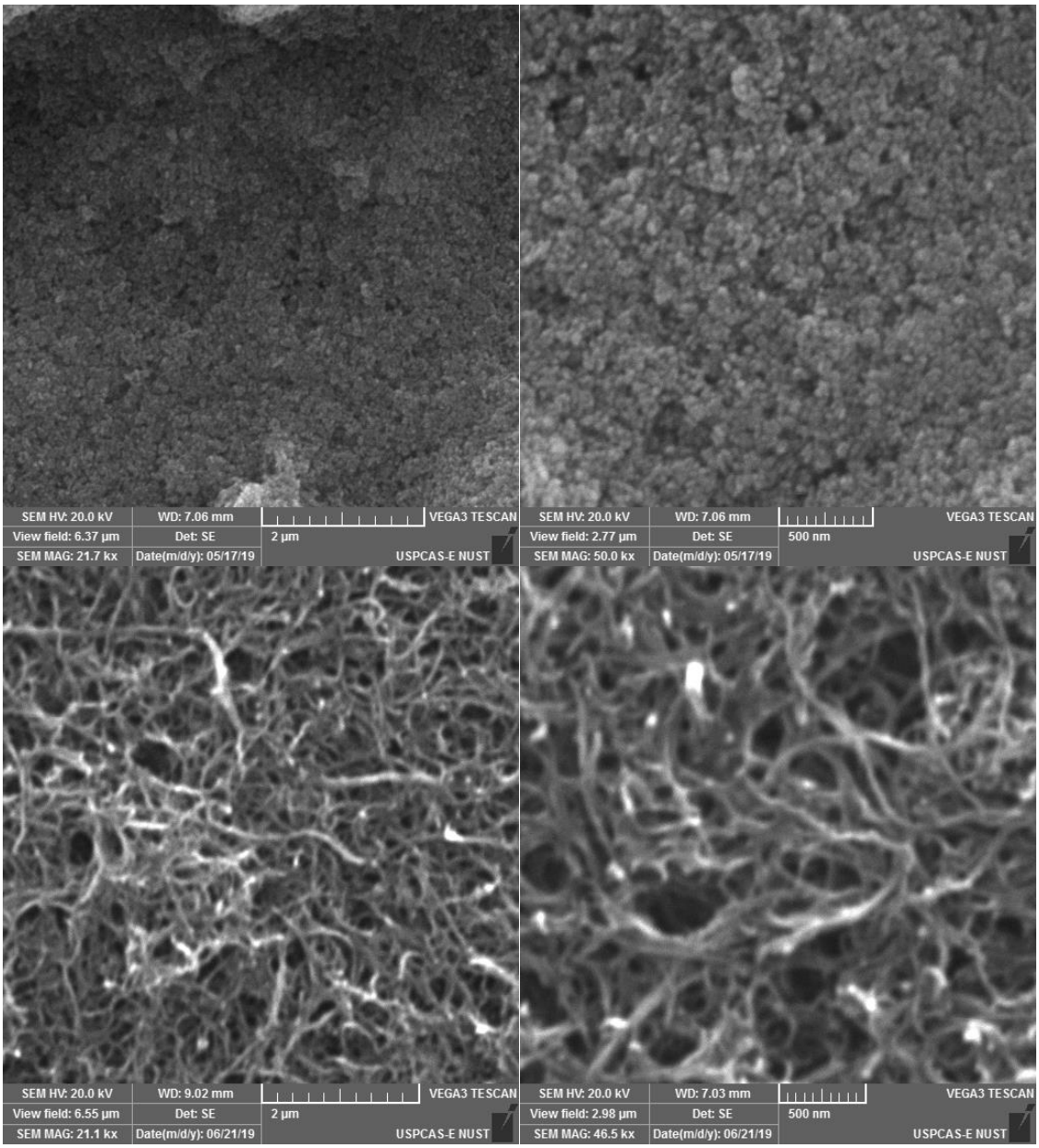

Figure 5.6: SEM Images (a) NiO thin film (b) MWCNTs thin film

Morphological characterization results in this work has been justified through literature. Z. Liu et al used NiO nanocrystals dispersed in chlorobenzene to spin coat a 30 nm-thick layer of a NiO film at 3000 rpm for 30 s, annealed it at 150 °C, resultantly similar film structure was observed through SEM [18]. Kwon U et al. spin-coated NiO nanoparticles at 3000 rpm for 30 s, similar morphology was observed in SEM images [19]. Research group of M. Ruscello used similar solvent for NiO nanoparticles i.e. ethanol, spin-coated at 2000 rpm for 40 s, annealed at 100 C and treated it with oxygen plasma. Fine NiO film

was observed in SEM images [20]. M. Wasik et al. also used sodium dodecyl sulfate as a surfactant for MWCNT Solution, the thin films forming random networks were formed by employing vacuum filtration method. Similar morphology of random MWCNT network was observed in SEM results [21]. J. Di et al. also prepared MWCNT film with similar morphology of random MWCNT network [22]. Research group of Young J. fabricated similar structurally stable multiwalled carbon nanotube thin films through spin-coating [23]. Y. Yang et al. fabricated NiO and MWCNTs bi-layer by using ultrasound spray method while using chlorobenzene as a solvent. Morphology observed through SEM results shows random MWCNT Network on NiO nanoparticles [24].

5.3.3. Electrical Properties Investigation

Ecopia Hall Effect Measurement System (HMS-3000 ver. 3.2) was used to understand the conductivity of the films. In order to examine electrical properties of NiO thin films, we measured the conductivity, resistivity, carrier concentrations and the Hall mobility using Hall-effect measurements. Tabulated data shows that non-sintered NiO film offers high resistivity i.e. 6.481×10^{4} Ω cm and low conductivity i.e. 1.543×10^{-5}/ Ω cm, on the other hand sintered NiO film offers conductivity~1.067×10^{-6}/ Ω cm and resistivity~9.370×10^{5} Ω cm. Electrical properties can be co-related with film thickness. Electrical resistivity of nickel oxide thin films has been reported in the range of $10 - 10^{6}$ (Ω·cm) [25]. The Hall resistivity decreases with increase in film thickness of Nickel [26]. Bulk concentration for non-sintered NiO film was found to be $1.036 \times 10^{12}/cm^{3}$, it was found to be 1.288×10^{12} $/cm^{3}$ for sintered NiO film. It is an p-type material. Research group of Chanae studied the effect of sintering on NiO film, film resistivity was 24.7 Ω·cm before sintering, it decreased to 4.23 Ω·cm after sintering~100 ºC. Nio film was found to have increased conductivity i.e. 1.78×10^{16} cm^{-3} after sintering, before sintering the value for conductivity was 2.41×10^{15} cm^{-3} .Decrease in mobility from 104 $cm^{2}V^{-1}s^{-1}$ to 82.85 $cm^{2}V^{-1}s^{-1}$ was observed before and after sintering respectively [27]. Research group of JianRen reported that hybrid films conductivity depends on the conductive network formed by the MWCNTs. MWCNTs provide network for the electron transfer due to which electrical resistance decreases [28]. Bulk concentration for CNT film was found to be $7.715 \times 10^{18}/cm^{3}$ which shows it is an p-type material as well but bulk concentration for bi-layer with non-sintered NiO film was found to be $5.22 \times 10^{18}/cm^{3}$, which increased to

$7.872x10^{19}/cm^3$ with sintered NiO film. It is an p-type film and it can be incorporated as an HTL in PSCs. Bi-layer has improved results as compared to NiO film, sintering has enhanced the electrical properties for both NiO film and bi-layer as well. Bi-layer shows p-type behavior with decreased resistivity, improved conductivity, and carrier concentration.

Table 0.2:Electrical Characterization Results

Parameters	NiO Film	NiO Film (Sintered)	MWCNT Film	Bi Layer (NiO & MWCNTs)	Bi Layer (sintered)
Resistivity (Ω cm)	$6.481x10^{4}$	$9.370x10^{5}$	$9.867x10^{-1}$	$5.382x10^{0}$	$1.555x10^{-1}$
Conductivity (1/ Ω cm)	$1.543x10^{-5}$	$1.067x10^{-6}$	$1.014x10^{0}$	$1.858x10^{-1}$	$5.994x10^{0}$
Mobility ($cm^2 V_s^{-1}$)	$9.299x10^{1}$	5.174x10	$8.200x10^{-1}$	$2.229x10^{-1}$	$4.753x10^{-1}$
Carrier Concentration (cm^{-3})	$1.036x10^{12}$	$1.288x10^{12}$	$7.715x10^{18}$	$5.22x10^{18}$	$7.872x10^{19}$

5.3.4. Optical Characterization

For optical characterization, UV-VIS-NIR Spectrophotometer (UV-3600 Plus, SHIMADZU) is used to understand the absorbance and percent transmittance of the layers. Non sintered NiO film shows <1% transmittance in visible region. Bi-layer with non-sintered NiO film shows transmittance ~1%. Transmittance for MWCNT film was found to be ~4% in visible region. Sintering effect improved transmittance for NiO Film ~11%. Transmittance of bi-layer with sintered NiO film was ~4%. Optical characterization results in this work have been justified through literature. Oscillations arise in transmittance spectra because of refractive index difference between thin films and substrate [29]. Abdel et al. reported that with increase in Ni concentration, transmittance of the Ni-doped ZnO decreased because of increased lattice defects [30]. Research group of Safwat A. observed an anomalous behavior at low substrate temperature that is disappearing absorption edge and lowering of the transmittance [31]. Absorption edge disappears in the films deposited at low temperature leading to decreased

transmittance; by lowering substrate temperature bigger clusters are formed and the scattered radiation increase because of surface roughness. This can be a reason of low transmittance in this work as well. Anyaegbunam et al. reports that decrease in transmittance can be linked with being metal oxide since the metal films reflect the incident radiation. The decrease in transmittance could also be attributed to increased molarity of the solution. Generally, optical transmittance increases with decrease in film thickness. This behavior may be ascribed to the stoichiometry and perfection of the films. The reduction in the optical transmittance due to irradiation might result from increase in nickel to oxygen ratio and it can be related to increased lattice defects [32].

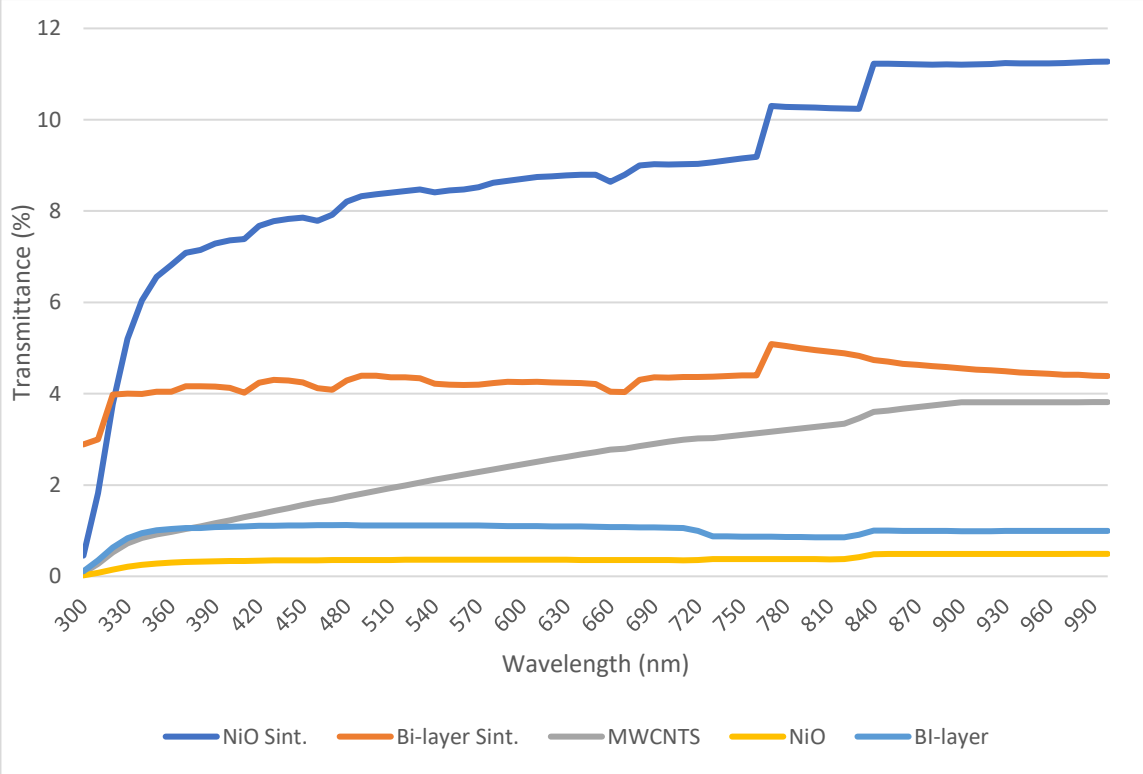

Figure 5.7: UV-Vis Spectra of NiO Thin film, MWCNT Thin film and Bi-layer.

5.3.5. Contact Angle Measurement

Contact angle for the fabricated NiO film and Bi-layer was observed before and after sintering by using a Kruss Drop Shape Analyzer DSA100. A 3-µm sized water droplet was poured upon the surface of slide. The contact angle of non-sintered NiO film was found to be <10°. After step sintering from 30°- 90° the contact angle improved to ~40°. The contact angle of bi-layer with non-sintered NiO film was found to be ~49°. The

contact angle of bi-layer with sintered NiO film improved from 49° to 68.4°. Contact angle could be improved if the sintering temperature is raised but in this work the film is being deposited on perovskite layer, raising temperature above 90° can destroy the perovskite layer.

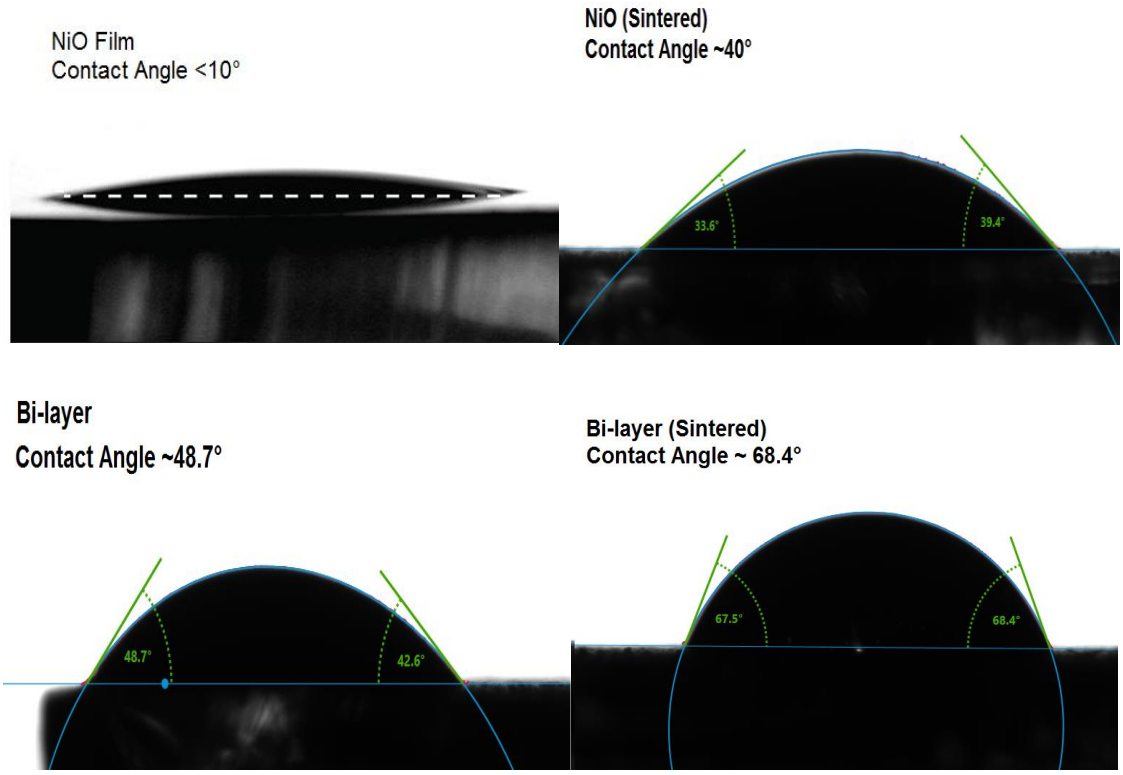

Figure 5.8: Contact Angles (a) NiO Film (b) Sintered NiO FILM (c) Bi-Layer (d) Sintered Bilayer

5.4. Summary

Results obtained by characterizations of the NiO nanoparticles and films fabricated after varying techniques optimizing process conditions have been discussed in this chapter. Nickel oxide nanoparticles synthesized through co-precipitation technique and hydrothermal synthesis have been subjected to structural and morphological characterizations. Nanoparticles synthesized through co-precipitation showed better results to be incorporated as HTM. NiO film deposited by spin coating, MWCNT film fabricated through ultrasonic spray coating and Bi-layer which is formed by combining NiO film and MWCNT film have been subjected to structural, morphological, electrical and optical characterization. Difference between sintered NiO film and non-sintered NiO

film has been studied as well. Contact angle measurement has been done for wettability studies of the fabricated films. Resultantly sintered NiO film showed better results to be incorporated as HTL.

References

[1] S. Ganeshan, R. Dhanalakshmi, and R. Vijayalakshmi, "Synthesis and characterization of LiCoO2 by sol gel method," *Int. J. ChemTech Res.*, vol. 7, no. 3, pp. 1085–1089, 2015.

[2] A. Barakat *et al.*, "One step synthesis of NiO nanoparticles via solid-state thermal decomposition at low-temperature of novel aqua(2,9-dimethyl-1,10-phenanthroline)NiCl2 complex," *Int. J. Mol. Sci.*, vol. 14, no. 12, pp. 23941–23954, 2013.

[3] D. Das and F. Gharib, "Cubic NiO Nanoparticles: Synthesis and Characterization," *Int. J. Bio-Inorganic Hybrid Nanomater.*, vol. 4, no. 2, pp. 59–64, 2015.

[4] S. Pilban Jahromi *et al.*, "Influence of particle size on performance of a nickel oxide nanoparticle-based supercapacitor," *RSC Adv.*, vol. 5, no. 18, pp. 14010–14019, 2015.

[5] Z. Wei, H. Qiao, H. Yang, C. Zhang, and X. Yan, "Characterization of NiO nanoparticles by anodic arc plasma method," *J. Alloys Compd.*, vol. 479, no. 1–2, pp. 855–858, 2009.

[6] H. Xiao, F. Qu, and X. Wu, "Ultrathin NiO nanoflakes electrode materials for supercapacitors," *Appl. Surf. Sci.*, vol. 360, pp. 8–13, 2016.

[7] G. Raja, S. Gopinath, R. A. Raj, A. K. Shukla, M. S. Alhoshan, and K. Sivakumar, "Comparative investigation of CuFe2O4 nano and microstructures for structural, morphological, optical and magnetic properties," *Phys. E Low-Dimensional Syst. Nanostructures*, vol. 83, pp. 69–73, 2016.

[8] K. Mahendraprabhu and P. Elumalai, "Nanoscience and Nanotechnology : An International Journal ISSN : 2278-1374 Original Article Influence of precursors on formation of NiO nanostructures in hydrothermal synthesis," vol. 5, no. 2, pp. 29–33, 2015.

[9] Q. Zhou, Z. Lu, Z. Wei, L. Xu, Y. Gui, and W. Chen, "Hydrothermal synthesis of

hierarchical ultrathin NiO nanoflakes for high-performance CH4 sensing," *Front. Chem.*, vol. 6, no. MAY, pp. 2–5, 2018.

[10] S. Safa, R. Hejazi, M. Rabbani, and R. Azimirad, "Hydrothermal synthesis of NiO nanostructures for photodegradation of 4-nitrophenol," *Desalin. Water Treat.*, vol. 57, no. 46, pp. 21982–21989, 2016.

[11] A. Shamim, Z. Ahmad, S. Mahmood, U. Ali, T. Mahmood, and Z. A. Nizami, "Synthesis of nickel nanoparticles by sol-gel method and their characterization," *Open J. Chem.*, vol. 2, no. 1, pp. 16–20, 2019.

[12] H. Yan *et al.*, "Solution growth of NiO nanosheets supported on Ni foam as high-performance electrodes for supercapacitors," *Nanoscale Res. Lett.*, vol. 9, no. 1, pp. 1–7, 2014.

[13] R. D. and V. A. Sharanabasava V.Ganachari, Ravishankar Bhat, "Synthesis and characterization of nickel oxide nanoparticles by self-propagating low temperature combustion method," *Recent Res. Sci. Technol.*, vol. 04, no. 04, pp. 50–53, 2012.

[14] N. Dharmaraj, P. Prabu, S. Nagarajan, C. H. Kim, J. H. Park, and H. Y. Kim, "Synthesis of nickel oxide nanoparticles using nickel acetate and poly(vinyl acetate) precursor," *Mater. Sci. Eng. B Solid-State Mater. Adv. Technol.*, vol. 128, no. 1–3, pp. 111–114, 2006.

[15] S. Sagadevan and J. Podder, "Investigations on structural, optical, morphological and electrical properties of nickel oxide nanoparticles," *Int. J. Nanoparticles*, vol. 8, no. 3–4, pp. 289–301, 2015.

[16] A. D. Khalaji, K. Jafari, and S. M. Rad, "Synthesis of NiO nanoparticles via a solid state thermal decomposition of nickel(II) schiff base complex Ni(caph) (N3)(NO3) as a new precursor," *Synth. React. Inorganic, Met. Nano-Metal Chem.*, vol. 45, no. 6, pp. 875–878, 2015.

[17] N. Srivastava and P. C. Srivastava, "Realizing NiO nanocrystals from a simple chemical method," *Bull. Mater. Sci.*, vol. 33, no. 6, pp. 653–656, 2010.

[18] Z. Liu *et al.*, "Nickel oxide nanoparticles for efficient hole transport in p-i-n and n-

i-p perovskite solar cells," *J. Mater. Chem. A*, vol. 5, no. 14, pp. 6597–6605, 2017.

[19] U. Kwon *et al.*, "Solution-Processible Crystalline NiO Nanoparticles for High-Performance Planar Perovskite Photovoltaic Cells," *Sci. Rep.*, vol. 6, no. April, pp. 1–10, 2016.

[20] M. Ruscello *et al.*, "Nanocomposite of nickel oxide nanoparticles and polyethylene oxide as printable hole transport layer for organic solar cells," *Sustain. Energy Fuels*, vol. 3, no. 6, pp. 1418–1426, 2019.

[21] M. Wąsik *et al.*, "Ultraviolet to far-infrared transmission properties of thin film multi-walled carbon nanotube random networks," *Journal of Materials Science*, vol. 52, no. 6. pp. 3086–3094, 2017.

[22] J. Di *et al.*, "Dry-processable carbon nanotubes for functional devices and composites," *Small*, vol. 10, no. 22, pp. 4606–4625, 2014.

[23] Y. J. Kim, S. J. Yu, and Y. G. Jeong, "Carbon nanotube/polyimide bilayer thin films with high structural stability, optical transparency, and electric heating performance," *RSC Adv.*, vol. 6, no. 36, pp. 30106–30114, 2016.

[24] Y. Yang *et al.*, "Ultrasound-spray deposition of multi-walled carbon nanotubes on NiO nanoparticles-embedded perovskite layers for high-performance carbon-based perovskite solar cells," *Nano Energy*, vol. 42, no. November, pp. 322–333, 2017.

[25] A. J. Hassan, "Study of Optical and Electrical Properties of Nickel Oxide (NiO) Thin Films Deposited by Using a Spray Pyrolysis Technique," *J. Mod. Phys.*, vol. 05, no. 18, pp. 2184–2191, 2014.

[26] M. K. Dasoundhi, R. P. Jena, D. Kumar, and A. Lakhani, "Anomalous hall effect in nickel thin film at low temperatures," *AIP Conf. Proc.*, vol. 2100, no. April, 2019.

[27] C. Park, J. Kim, K. Lee, S. K. Oh, H. J. Kang, and N. S. Park, "Electronic, Optical and Electrical Properties of Nickel Oxide Thin Films Grown by RF Magnetron Sputtering," *Appl. Sci. Converg. Technol.*, vol. 24, no. 3, pp. 72–76, 2015.

[28] J. Huang, S. C. Her, X. Yang, and M. Zhi, “Synthesis and characterization of multi-walled carbon nanotube/graphene nanoplatelet hybrid film for flexible strain sensors,” *Nanomaterials*, vol. 8, no. 10, 2018.

[29] S. T. Tan *et al.*, “Blueshift of optical band gap in ZnO thin films grown by metal-organic chemical-vapor deposition,” *J. Appl. Phys.*, vol. 98, no. 1, pp. 1–5, 2005.

[30] M. S. Abdel-Wahab, A. Jilani, I. S. Yahia, and A. A. Al-Ghamdi, “Enhanced the photocatalytic activity of Ni-doped ZnO thin films: Morphological, optical and XPS analysis,” *Superlattices Microstruct.*, vol. 94, pp. 108–118, 2016.

[31] S. A. Mahmoud, A. Shereen, and M. A. Tarawnh, “Structural and Optical Dispersion Characterisation of Sprayed Nickel Oxide Thin Films,” *J. Mod. Phys.*, vol. 02, no. 10, pp. 1178–1186, 2011.

[32] F. N. C. Anyaegbunam and C. Augustine, “A study of optical band gap and associated Urbach energy tail of chemically deposited metal oxides binary thin films,” *Dig. J. Nanomater. Biostructures*, vol. 13, no. 3, pp. 847–856, 2018.

Chapter 6:

Conclusion and Recommendations

6.1. Conclusion

- Nickel oxide nanoparticles were synthesized by varying techniques and process conditions. Best results in terms of morphological and structural characterization were achieved for nanoparticles synthesized through co-precipitation technique.
- Thin film comprising of nickel oxide nanoparticles was deposited through spin coating, at r1 1500 rpm - r2 3000 rpm for t1=t2=30seconds.
- A Bi-layer comprising of NiO and MWCNTs was deposited by ultrasonic spray deposition of MWCNTs on NiO thin film.
- Sintered and non-sintered NiO film and bi-layer were tested through structural, morphological, electrical, optical characterization. Contact angle measurement has been done for wettability study of the film. Comparatively, Bi-layer with sintered NiO film has showed better results to be employed as an HTL in perovskite solar cell.

6.2. Future Recommendations

- Similar HTL can be employed in an inverted PSC structure and results can be compared with this work.
- Similar HTL can be employed in DSSCs and results can be compared with this work.
- Solvent can be varied, optimization in NiO solution and change in film deposition technique might bring better results.

In case of inverted PSCs, HTL can be sintered at high temperature and effects of sintering can be observed, in the case of planar PSCs, HTLs cannot be processed above certain temperature. Raising sintering temperature can bring good results as well. Results can be compared with this work. Solvent can be varied for same process as well. Chlorobenzene

can be a good choice for the solvent, change in film deposition technique can bring good results in terms of film characteristics as well.

Journal Paper

Fabrication and Characterization of NiO nanoparticles by varying techniques for NiO:MWCNT based Hole Transporting Layer for Solar Cell Applications.

Anum Ameer [1], Nadia Shahzad [1], Bushra Batool [1], M. Imran Shahzad [2]

[1]US-Pakistan Centre for Advanced Studies in Energy (USPCAS-E), National University of Science and Technology (NUST), Islamabad, Pakistan.

[2]Nano Science & Technology Department (NS & TD), National Centre for Physics (NCP), 44000-Islamabad, Pakistan.

Corresponding Author: Anumameer1@yahoo.com

Abstract:

NiO is known for superior strength, super hydrophobicity, corrosion resistance, low cost which are required in effective HTMs. NiO as a wide band gap p-type semiconductor is believed to enhance hole extraction, block electron leakage and reduce the nonradiative recombination. Special structure and properties of nickel oxide nanoparticles make it applicable in different areas such as for fuel cells, electrochromic coatings, as p-type conductive films, as counter electrodes etc. Nickel oxide nanoparticles can also serve as a less expensive and effective hole transporting material for perovskite solar cells (PSCs). Hole transporting materials are important constituents in PSCs as they selectively transport charges, influence photovoltaic parameters, determine device stability and influence its cost. In this study nickel oxide nanostructures have been grown by varying techniques and process conditions, nanoparticles have been characterized through XRD (X-ray diffraction), SEM (Scanning electron microscopy) and the nanoparticles with best results have been used to fabricate films. NiO:MWCNTs based films have been deposited and sintered NiO based films has been compared with non-sintered NiO film. MWCNTs are known for their suitable work function, good filming ability, high conductivity, which add strength to the properties of HTL. Samples have been characterized through XRD (X-ray diffraction), SEM (Scanning electron microscopy), Hall effect, UV-Vis Spectroscopy,

Contact Angle Measurement for phase identification, morphological and electrical, optical and wettability studies respectively. The obtained results indicated that sintered nickel oxide-based hole transporting layer can serve as a potential candidate for solar cell application.

Keywords: Nickel oxide, MWCNTs, Fabrication, Hole Transporting Layer, Sintering, Solar Cell Applications.

1. Introduction

A solar cell also known as photovoltaic cell uses photovoltaic effect for the conversion of light energy into electricity. Solar cells are the building blocks of photovoltaic modules. Light absorption , electron-hole pairs generation, opposite charge carriers separation and their separate extraction to an external circuit are the basic attributes of a solar cell [1]. A perovskite solar cell has a light-harvesting active layer sandwiched between two transporting layers known as electron transport layer and hole transport layer which collect the mobile charges. Hole transporting layer has various purposes in a perovskite solar cell. Hole transfer efficiency is improved due to hole transporting layer. An HTL determines the splitting of the perovskite quasi Fermi-energy levels which effects the open voltage circuit. In the absence of an HTL, metal (Au)-perovskite interface degradation might take place. Incorporation of a suitable hole transporting materials and light harvesting layer in perovskite solar cells leads to high V_{OC} (1.5-1.61 V). Surface coverage of perovskite solar cell is improved due to HTL and charge recombination is suppressed which results in improved performance. Incorporation of suitable hole transporting layer results in perovskite solar cells with increased stability [2]. Hole transporting material is an important material because of its ability of effective hole extraction at the HTM-absorber layer interface. Hole transporting material should offer high hole mobility, ionization potential should be compatible with that of the perovskite material, thermal stability should be high and it should be resistant to external degradation factors to ensure long term photovoltaic operation. Cost of hole transporting material is an important concern as well. If the electron affinity of hole transporting material is low, it will enhance the electron blocking properties of hole transporting layer. Efficiency of the solar cell is affected by the mobility of hole transporting material as well. Considerable ohmic losses occur across the hole transporting layer due to low mobility, this results in low fill factor (FF). Charge carrier mobility also affects the short circuit photocurrent (J_{SC}). Thus, Uniform coverage and high mobilities of HTM should be ensured for efficient PSCs. NiO is known for superior strength, super hydrophobicity, corrosion resistance, low cost which are required in effective HTMs. NiO as a wide band gap p-type semiconductor is believed to enhance hole extraction, block electron leakage and reduce the nonradiative recombination. Valence band for NiO lies at -5.4 eV, valence band for perovskite layer

lies at -5.5 eV. Upward band bending in the valence band between perovskite and NiO favors fast hole extraction and transportation from perovskite layer to NiO. Conduction band value of NiO is much higher i.e. -1.8eV than that of perovskite i.e. -4.0 eV, so electrons could not go through from perovskite layer to NiO layer because of the energy barrier, and this blocks the electron leakage and reduces the non-radiative re-combination effectively. MWCNTs are known for their suitable work function, good filming ability, high conductivity, which will add to the properties of HTL.

2. Literature Review

Hole transporting material in PSCs can be categorized as organic and inorganic hole transporting materials. Small molecules-based HTMs, polymer-based HTMs and oligomers are the three categories of organic hole transporting materials. Majorly Polymer based hole transporting materials (e.g.: Spiro-OMeTAD, PEDOT: PSS, P3HT etc.) are used which make hole transporting materials as most expensive material component in perovskite solar cells [2]. Nickel oxide known for its corrosion resistance and superior strength has been employed in different material applications by different researchers. Ahmad A.F. et al. synthesized composites of Nickel Oxide and Polycaprolactone through melt blend technique & suggested its applicability in developing absorbing and shielding materials [3]. Dar et al. employed bottom-up approach for electrochemical growth of Nickel oxide nanotubes which exhibited exceptional capacitance properties for supercapacitor applications [4]. Jian-mei LI, et al. developed high corrosion resistance nano-structured nickel film through electrodeposition [5]. A. Rahdar et al. synthesized Nickel Oxide nanostructures through co-precipitation technique, nanostructures calcinated at 500^{o}C exhibited superparamagnetic behavior [6]. S. Zhou et al. synthesized superhydrophobic MWCNTs-Ni/a-C:H nanocomposite film through one-step electrochemical deposition. Nanocomposite film possessed corrosion resistance and self-cleaning properties as well [7]. Nickel oxide is considered a potential material for inverted PSC owing to its good hole conductivity, large energy gap, and deep valence band. NiO is abundant, cost-effective and potentially stable material for perovskite solar cell. Research group of Irwin compared incorporation of NiO with PEDOT: PSS as hole transporting layer, resultantly performance of polymer bulk-heterojunction solar cells was

higher for NiO hole transporting material [8]. Highest efficiency reported by incorporating an inorganic HTM in an inverted planar PSC was 17.3% reported by Seok et al., this group of researchers prepared NiO nanostructured film through pulsed laser deposition method and employed it as hole transporting layer for PSC [9]. Y. Yang et al. employed hydrothermally synthesized Nickel Oxide Nano Particles in combination with MWCNTs as hole transporting material in a perovskite solar cell which showed an efficiency of 15.4% [10].

3. Material and Methodology

Nickel di chloride hexahydrate ($NiCl_2.6H_2O$) 99.9% trace metals basis, Sodium hydroxide (NaOH), were bought from Sigma Aldrich. Ethanol and Distilled water have been utilized as the solvent. Ethylene glycol and glucose have been used as template.

3.1.Nanoparticles Synthesis

I. Hydrothermal Synthesis:

Nickel dichloride Hexahydrate (1.782 gm) was added to 75 ml Distilled Water. Sodium Citrate (0.1 M) solution prepared and added dropwise to $NiCl_2.6H_2O$ solution at constant stirring. Hydrothermal Synthesis done at 180 C for 12 hours followed by hot plate drying. Sample was calcinated at 350 C for 4 hours, crushed and again calcinated at 500 C for 4 hours.

II. Co-precipitation Technique:

Nickel di chloride Hexahydrate solution was prepared by adding 1.18 gm $NiCl_2.6H_2O$ to 50 ml Ethanol. Solution was magnetically stirred at room temperature for an hour. NaOH 0.1 M solution was added during the stirring until PH reached particular level. Varied templates were used and samples was calcinated at varied temperatures, crushed and collected.

Table 1:Varied Process Conditions during Co-precipitation technique.

Sample No.	Material	Template	Process Conditions	Calcination Temperature
1	$NiCl_2.6H_2O$ NaOH	Ethylene Glycol ($C_2H_6O_2$)	Room temperature. pH: 10	500 °C
2	$NiCl_2.6H_2O$ NaOH	Ethylene Glycol ($C_2H_6O_2$)	Temperature: 60°C. pH: 11	500 °C
3	$NiCl_2.6H_2O$ NaOH	Glucose	Temperature: 60°C pH: 11	500 °C
4	$NiCl_2.6H_2O$ NaOH	Ethylene Glycol ($C_2H_6O_2$)	Temperature: 70°C. pH: 11	800 °C

3.2. Film Fabrication

HTL is a bi-layer comprising of NiO thin film and MWCNTs thin film.

Step 1: Fabrication of NiO Thin film:

Nickel oxide nanoparticles 1 gm were finely crushed with 3 ml ethanol by using a mortar and pestle until a fine paste was achieved. NiO paste was spin coated at r1 1500 rpm – r2 3000 rpm for t1=t2=30seconds. Thin film was dried at 90 in an oven.

Step 2: Deposition of MWCNT Thin film on NiO Thin film:

CNTs thin film has been prepared by ultrasonic spray coating. MWCNT solution has been prepared by adding 10 mg CNTs in 10 ml Ethanol. SDS (Sodium Dodecyl Sulphate) has been used as a surfactant. Solution was magnetically stirred for one hour followed by sonication for 2 hours. Homogeneous Ink formed resultantly was deposited at the rate of 1mg/min through ultrasonic spray coating at medium ultrasonic power.

4. Results and Discussion

NiO film deposited by spin coating, MWCNT film fabricated through ultrasonic spray coating and Bi-layer which is formed by combining NiO film and MWCNT film have been subjected to structural, morphological, electrical and optical characterization.

4.1. NiO Nanoparticles fabrication through varying techniques

Nickel oxide nanoparticles synthesized through co-precipitation technique and hydrothermal synthesis have been subjected to structural and morphological characterizations.

4.1.1. Structural Characterization

XRD (D8 Advance, BRUKER) was incorporated for structural characterization, 2Θ angle is used from 30° to 70°. Sample A shows the XRD graph of nanoparticles prepared through co-precipitation technique. Sample B shows the XRD graph of nanoparticles prepared through hydrothermal synthesis. The characteristic peaks for sample A and B seen at 2θ of 37.0°. 43.1°, 62.6° could be indexed to (111), (200), and (220) diffraction planes respectively. XRD pattern reflections can be attributed to cubic phase of NiO (JCPD card no.# 03-065-5745). Information obtained through XRD data has been justified from literature. L.G.Teoh et al. synthesized NiO nanoparticles through sol gel method and three characteristic peaks referred to diffraction planes (110), (200) and (220) (JCPDS card No. 87-0712) represent face-centered cubic (fcc) structure of nickel [11]. XRD patterns of NiO synthesized by Barakat A. et al. reveals similar diffraction peaks which can be referred to face-centered cubic phase of NiO (JCPDS card No. 73-1523) [12]. Rahdar A. et al. fabricated nanostructured Nickel oxide by co-precipitation method. XRD pattern revealed the face-centered cubic (FCC) structure of NiO and ensured high degree of crystallinity as well [6]. Pilban J. et al. produced Nickel oxide nanoparticles through a facile sol gel method, calcined it at varied temperatures of 300, 400, 500 C and obtained similar diffraction peaks through XRD corresponding to the face-centered-cubic (fcc) structure of the NiO [13]. Peak position of NiO nanoparticles synthesized by Qiao et al. can be referred to crystal planes (111), (200), (220), (311) and (222) (JCPDS, No. 04-0835) [14]. These diffraction peaks are attributable to the face-centered cubic crystalline structure of NiO with relative peak position and characteristic peaks intensity as well. Increase in sharpness of XRD peaks indicates the crystalline nature of the particles.

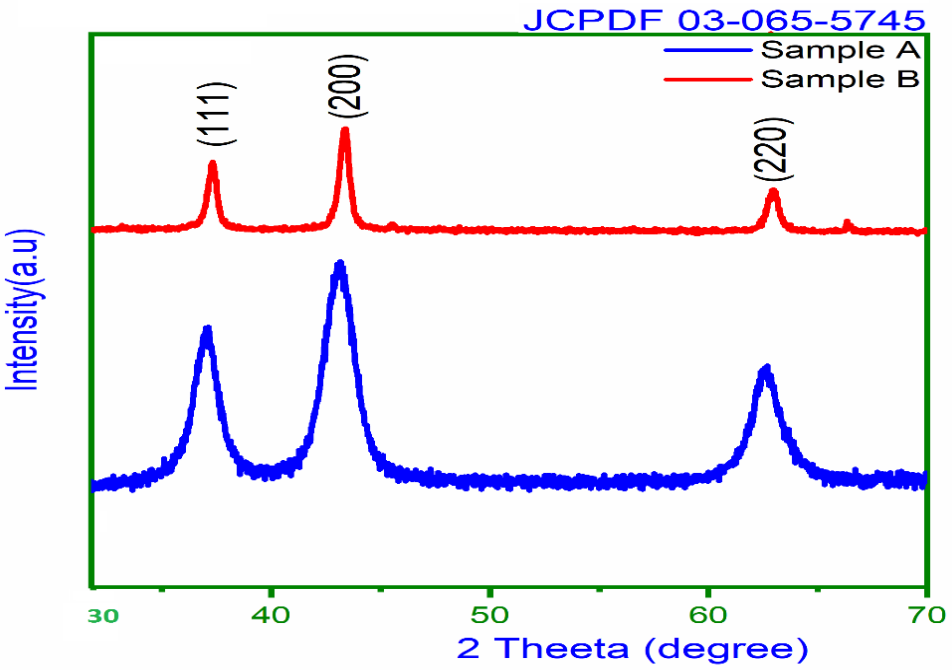

Figure 1: XRD Spectra for Sample A & Sample B

4.1.2. Morphological Characterization

SEM (VEGA 3 LMU, TESCAN) was used to understand the surface morphology and surface quality. Studies have been done using SEM, at a magnification of up to 500 nm with an accelerating voltage of about 20 kV and a magnification of about 50 kX. SEM Results of Co-precipitation prepared sample showed needle like structure width varying from 64.19 nm up to 97.61 nm and length up to 901.71 nm was found while the SEM Results of hydrothermally synthesized sample showed clusters of small particles attached to large particles. Particle size of radius ranging from 34.89 nm, 71.20 nm were found at 500 nm Scale. Information obtained through SEM has been justified from literature. H. Xiao et al. also used $NiCl_2.6H_2O$ as precursor and fabricated large scale ultrathin NiO nanoflakes through combining a hydrothermal reaction and a thermal annealing process [15]. A. Manikandan et al. fabricated NiO Nano sized flakes, the average size and void space diameter of single NiO nanoflake was found to be 15–20 nm [16]. Nanostructured nickel oxide (NiO) synthesized by similar hydrothermal route by using similar chloride precursor yielded attractive nanosphere which were made up of fine nanoflakes [17]. Q. Zhou et al. also used typical hydrothermal procedure to synthesize hierarchical NiO nanostructures, which are constructed by many ultrathin nanoflakes with thickness

ranging from 10 to 15nm [18]. Research group of S. Safa observed that morphology and size of NiO nanostructures can be controlled effectively by changing the hydrothermal temperature [19]. Rahdar et al. also used co-precipitation method with similar precursors i.e. $NiCl_2.6H_2O$ and NaOH and synthesized nanostructured nickel oxide (NiO) in spherical shape, average size of the NiO nanoparticles is 24 nm [6]. The formed NPs show agglomeration at different locations due to large surface energy and high reactivity [20].

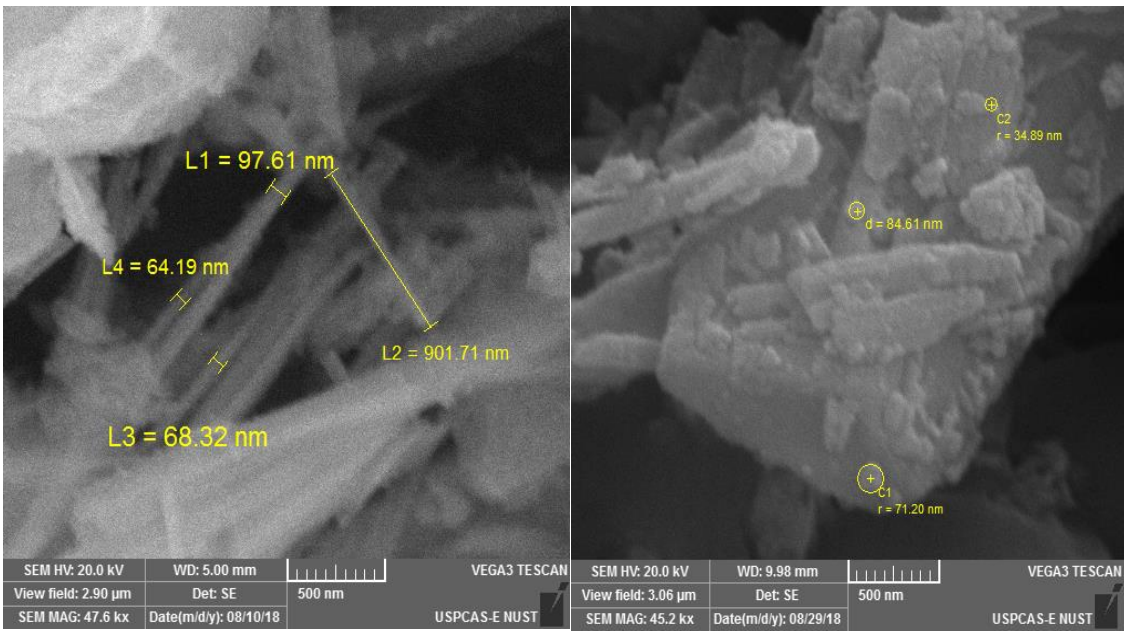

Figure 2:SEM Images (a) Sample prepared through co-precipitation technique (b) Sample prepared through hydrothermal synthesis.

4.2. Optimization of NiO Nanoparticles through variation in process conditions

Uniform and fine structured NiO nanoparticles obtained by optimizing process conditions during co-precipitation technique have been subjected to structural and morphological characterizations in order to select the best material for further film deposition.

4.2.1. Structural Characterization

4.2.1.1. X-ray Diffraction Spectroscopy

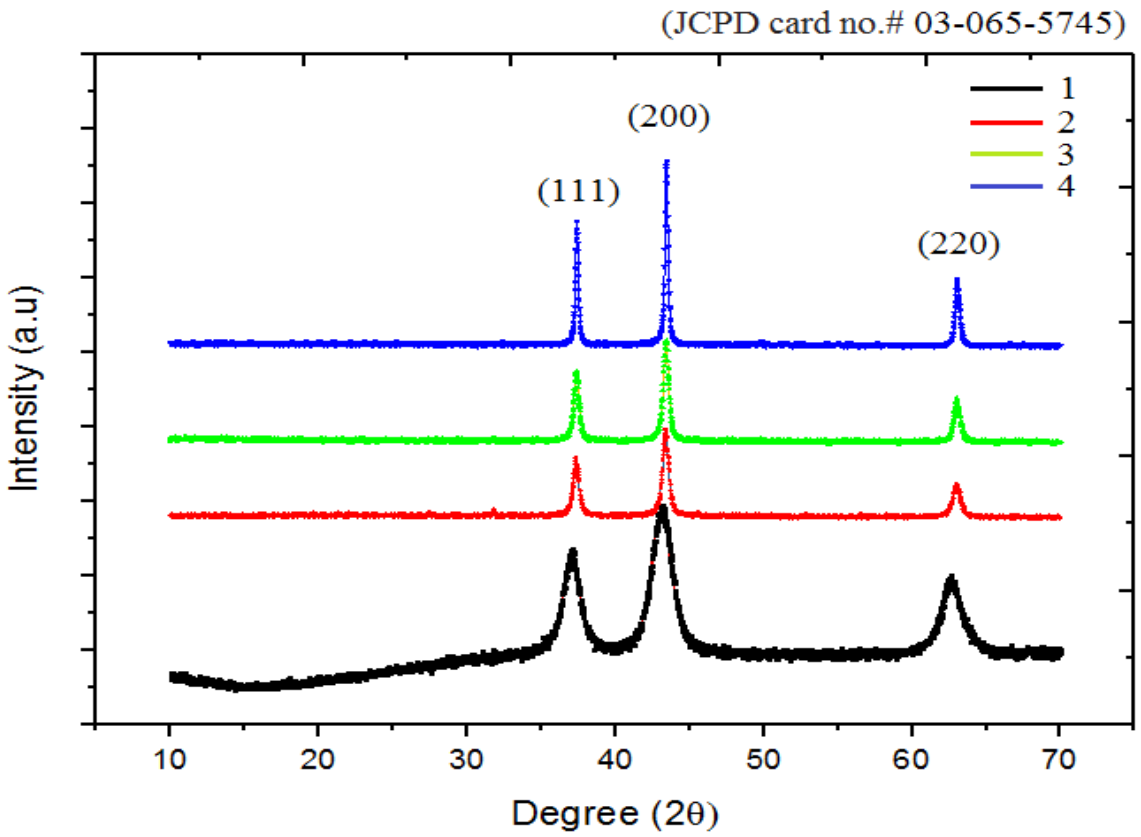

Figure 3: XRD Spectra for Sample 1, Sample 2, Sample 3, Sample 4

XRD (D8 Advance, BRUKER) was incorporated for structural characterization, 2Θ angle is used from 10° to 70°. XRD patterns of the synthesized Nickel Oxide nanoparticles are shown in Figure 3. The characteristic peaks seen at 2θ of 37.0°. 43.1°, 62.6° could be indexed to (111), (200), and (220) diffraction planes respectively. Reflections in the XRD pattern are attributable to cubic phase of NiO (JCPD card no.# 03-065-5745). XRD results have been justified through literature. Rahdar A. et al. also synthesized nanostructured Nickel oxide (NiO) by co-precipitation method. XRD pattern revealed the face-centered cubic (FCC) structure of NiO and ensured high degree of crystallinity. Results have been compared before and after calcination, NiO nanoparticles calcined at 500 C exhibit high crystalline quality as compared to non-calcined samples [6][21]. Research group of Pilban synthesized Nickel oxide nanoparticles through a facile sol gel method, calcined at varied temperatures of 300, 400, 500 °C and compared the results. Similar diffraction peaks

obtained through XRD at crystal planes (111), (200), (220), (311), and (222) correspond to face-centered-cubic structure of NiO [13]. XRD Spectra indicates that diffraction peaks intensity has improved with the calcination temperature, which indicates that nickel oxide prepared at a higher calcination temperature exhibit better crystallinity. No peaks from other phases are detected ensuring high purity of the product.

4.2.1.2. Crystallite Size Calculation

Scherrer equation was used to calculate average crystallite size;

$$\mathbf{Dp = (0.94\ X\ \lambda) / (\beta\ X\ Cos\theta)}$$

Where, Dp = Average Crystallite size, β = Line broadening in radians, θ = Bragg angle, λ = X-Ray wavelength.

Table 2: Crystallite Size Calculation

Sample 1:

Pos. [°2Th.]	FWHM	Crystal size
37.0310	0.9446	9.26
43.1166	1.2595	7.09
62.5951	1.1520	8.45

Sample 2:

Pos. [°2Th.]	FWHM	Crystal size
37.3298	0.9446	9.28
43.3694	0.9446	9.46
62.9826	1.1520	8.45

Sample 3:

Pos. [°2Th.]	FWHM	Crystal size
37.3545	0.9446	9.28
43.3923	0.9446	9.46
63.0247	1.1520	8.45

Sample 4:

Pos. [°2Th.]	FWHM	Crystal size
37.3864	0.9446	9.28
43.4183	0.9446	9.46
63.0445	1.1520	8.45

The average crystallite size calculated using the Scherrer equation is about 8.27 nm, 9.063 nm, 9.063 nm, 9.06 nm for sample 1, sample 2, sample 3, sample 4 respectively.

4.2.2. Morphological Characterization

SEM (VEGA 3 LMU, TESCAN) was used to understand the surface morphology and surface quality. Studies have been done using SEM, at a magnification of up to 500 nm with an accelerating voltage of about 20 kV and a magnification of about 50 kX. Scanning electron microscope images of samples are given in fig. 4. SEM images of sample 1

resulted in flake like structure with width varying from 64.19 nm up to 97.61 nm and length up to 901.71 nm was found. SEM images of Sample 2 showed Grain Like Nano structures with Grain size of d= 27.28 nm, 28.50 nm, 25.53 nm observed at 500 nm scale. SEM images of Sample 3 showed Grain Like Nano structure with Grain size of d= 23.62 nm, 25.79 nm, 27.08 nm observed at 500 nm scale. SEM images of Sample 4 showed Grain Like Nano structures with Grain size of d= 32.27nm, 37.17 nm, 39.20 nm observed at 500 nm scale.

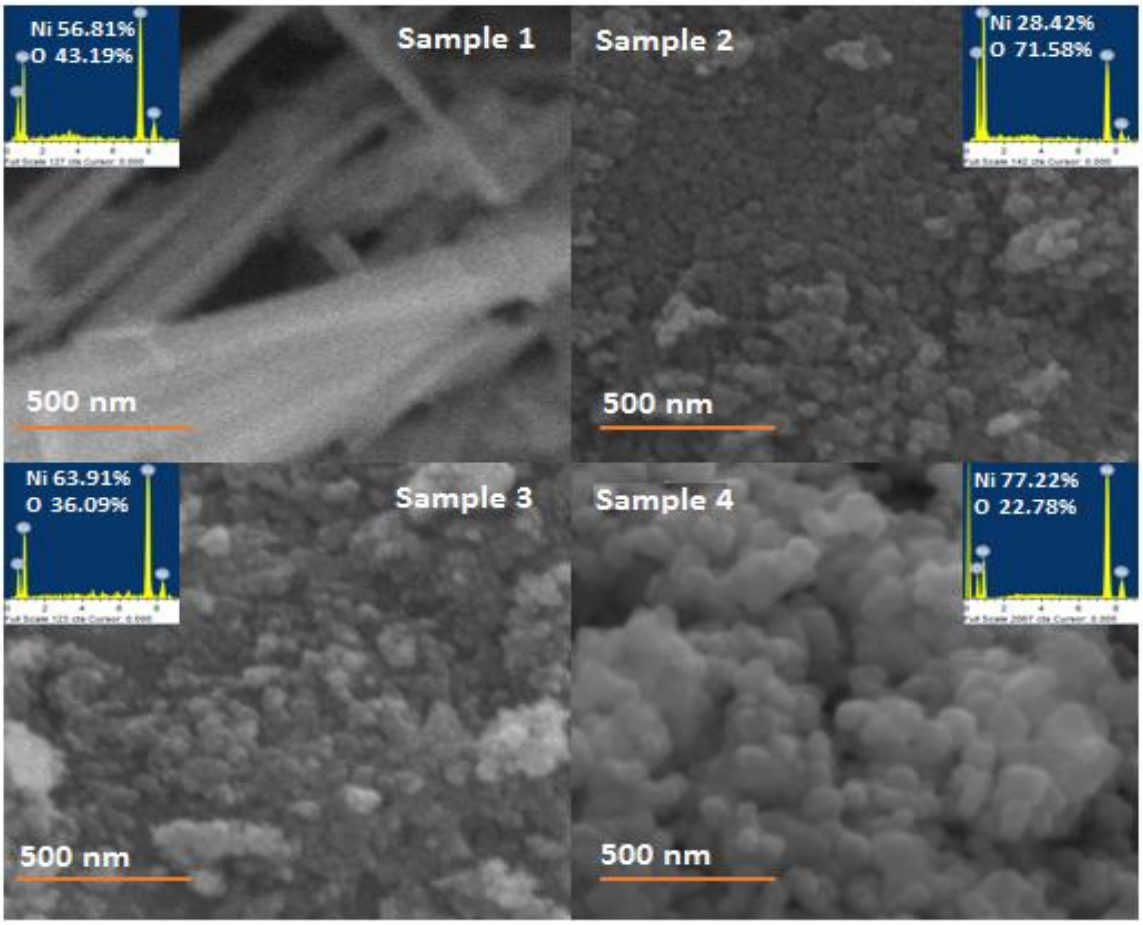

Figure 4: SEM Images (a) Sample 1 (b) Sample 2 (c) Sample 3 (d) Sample 4

Results obtained through morphological characterization have been justified through literature. S.V. Ganachari et al. synthesized NiO nanoparticles at low temperature. The particles obtained have irregular spherical shape in nanosized range of 20-40 nm [22]. Uniform and well dispersed cubic nickel oxide (NiO) nanoparticles with size 40–50nm have been synthesized by N. Dharmaraj et al. SEM image show similar uniform sized

grain like structure with diameter around 40–50nm obtained due to heat treatment [23]. Research group of A.Rahdar synthesized nanostructured Nickel oxide (NiO) by using same technique and same precursors i.e. co-precipitation method , $NiCl_2.6H_2O$ and NaOH respectively. SEM results indicated spherical shape of nanoparticles with average size~24nm [6]. S. Sagadevan et al. also used co-precipitation technique for NiO nanoparticles synthesis, SEM images showed small and homogeneous spherical shaped grains [24]. NiO nanoparticles synthesized by research group of Khalaji are approximately spherical with the diameter varying between 35 and 60 nm [25]. Similar structure has been observed in this work.

4.3. HTL Characterizations

NiO film deposited by spin coating, MWCNT film fabricated through ultrasonic spray coating and Bi-layer which is formed by combining NiO film and MWCNT film have been subjected to structural, morphological, electrical and optical characterization.

4.3.1. Structural Characterization

XRD (D8 Advance, BRUKER) was incorporated for structural characterization, 2θ angle is used from 10° to 70°. The characteristic peaks seen at 2θ of 37.0°. 43.1°, 62.6° could be indexed to (111), (200), and (220) diffraction planes respectively. XRD pattern reflections can be attributed to cubic phase of NiO (JCPD card no.# 03-065-5745). Peak appeared at 26° can be indexed to (002) plane of MWCNTs. The other peaks observed in non-sintered films at 2θ of 31.6° have been identified as Ni_2O_3 corresponds to [002] crystal planes. Peaks observed at 2θ of 45.315° have been identified for Ni [111] phase. These peaks have disappeared after sintering, this shows that sintering has converted Ni and Ni_2O_3 to NiO. Shrivastav et al. observed similar peaks for Ni and Ni_2O_3 in his work for fabrication NiO [26]. High peak intensity indicates that the NiO nanoparticles are of high crystallinity. Z. Liu et al used NiO nanocrystals dispersed in chlorobenzene to spin coat a 30 nm-thick layer of a NiO film at 3000 rpm, synthesized NiOx film exhibit diffraction peak at 36.9°, 42.9°, 62.2°, which are attributable to crystal planes (111), (200) and (220) of NiO, respectively [27]. Similar XRD spectra for spin coated NiO film has been observed by Kwon U et al. XRD spectrum showed intense peaks at 2θ = 37.2°, 43.3°,

and 62.9°, which are assigned to (111), (200), (220) planes of NiO cubic crystal structure [28].

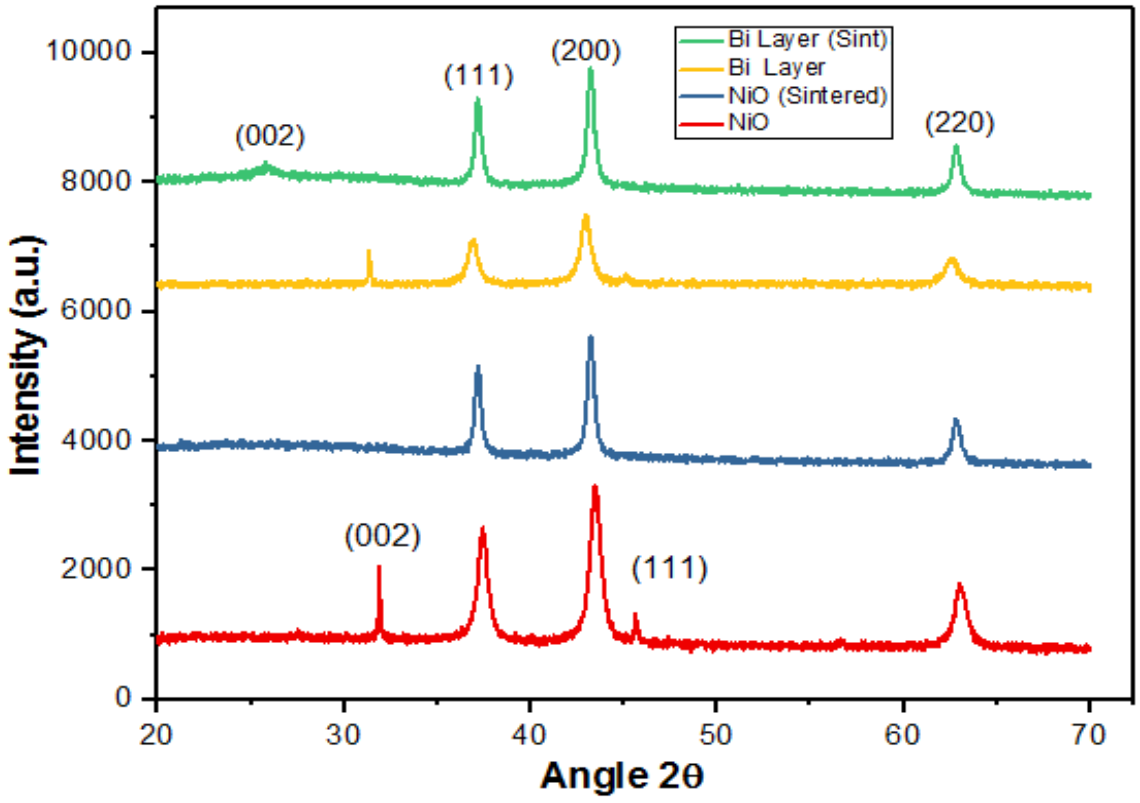

Figure 5: XRD Spectra for hole transporting layer

4.3.2. Morphological Characterization

SEM (VEGA 3 LMU, TESCAN) was used to understand the surface morphology and surface quality. Studies have been done using SEM, at a magnification of up to 500 nm with an accelerating voltage of about 20 kV and a magnification of about 50 kX. SEM images show that a uniform film of NiO nanoparticles has been obtained through spin coating at r1=700rpm -r2=3000rpm for t1=t2=30 seconds. Uniform film of MWCNTs has been obtained through Ultrasonic spray coating. SEM images of MWCNT film shows MWCNT films were coated uniformly and densely on NiO film by forming well-interconnected network structure.

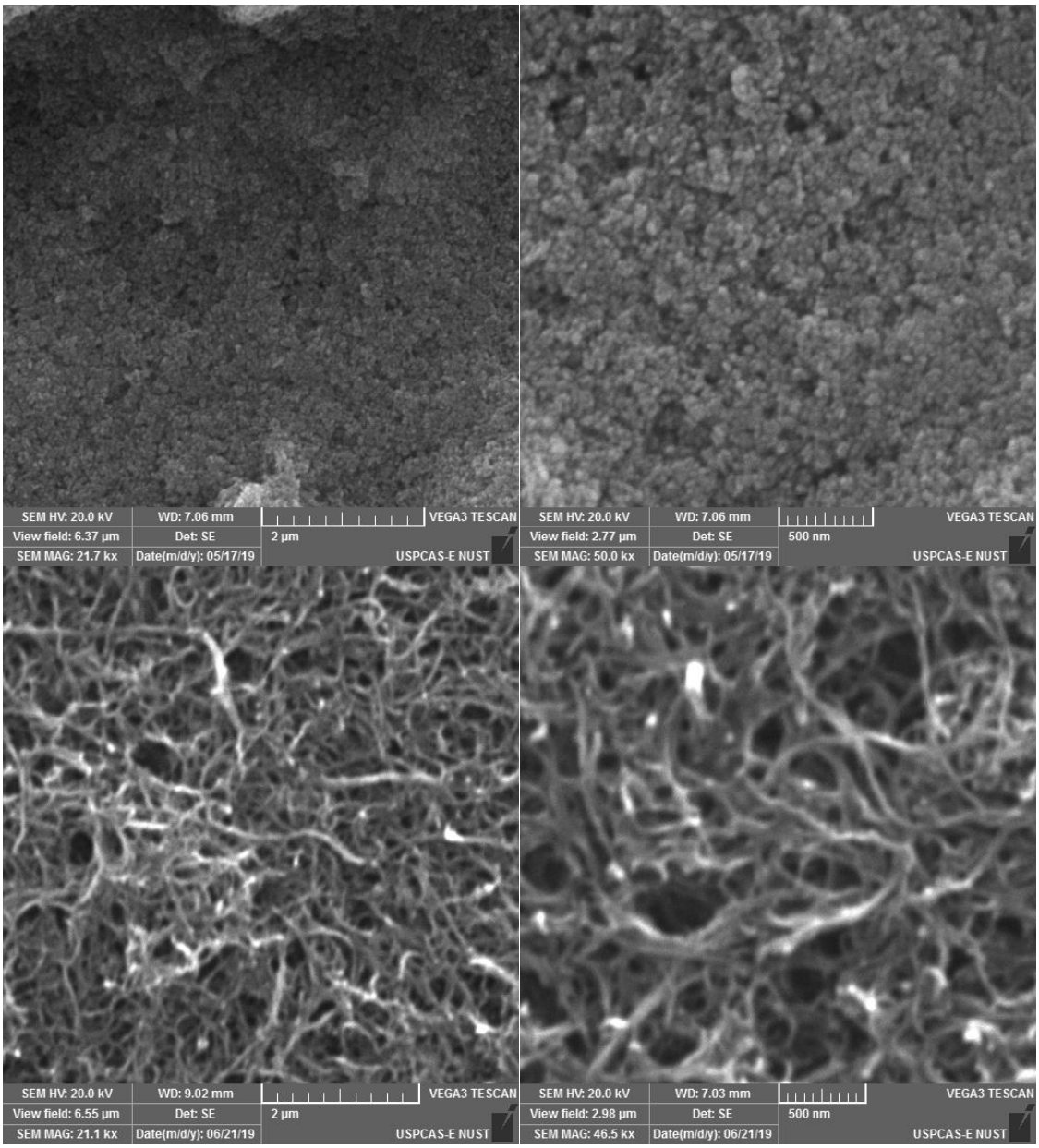

Figure 6: SEM Images (a) NiO thin film (b) MWCNTs thin film

Morphological characterization results in this work has been justified through literature. Z. Liu et al used NiO nanocrystals dispersed in chlorobenzene to spin coat a 30 nm-thick layer of a NiO film at 3000 rpm for 30 s, annealed it at 150 °C, resultantly similar film structure was observed through SEM [27]. Kwon U et al. spin-coated NiO nanoparticles at 3000 rpm for 30 s, similar morphology was observed in SEM images [28]. Research group of M. Ruscello used similar solvent for NiO nanoparticles i.e. ethanol, spin-coated at 2000 rpm for 40 s, annealed at 100 C and treated it with oxygen plasma. Fine NiO film

was observed in SEM images [29]. M. Wasik et al. also used sodium dodecyl sulfate as a surfactant for MWCNT Solution, the thin films forming random networks were formed by employing vacuum filtration method. Similar morphology of random MWCNT network was observed in SEM results [30]. J. Di et al. also prepared MWCNT film with similar morphology of random MWCNT network [31]. Research group of Young J. fabricated similar structurally stable multiwalled carbon nanotube thin films through spin-coating [32]. Y. Yang et al. fabricated NiO and MWCNTs bi-layer by using ultrasound spray method while using chlorobenzene as a solvent. Morphology observed through SEM results shows random MWCNT Network on NiO nanoparticles [10].

4.3.3. Electrical Characterization

Ecopia Hall Effect Measurement System (HMS-3000 ver. 3.2) was used to understand the conductivity of the films. In order to examine electrical properties of NiO thin films, we measured the conductivity, resistivity, carrier concentrations and the Hall mobility using Hall-effect measurements. Tabulated data shows that non-sintered NiO film offers high resistivity i.e. 6.481×10^{4} Ω cm and low conductivity i.e. 1.543×10^{-5}/ Ω cm, on the other hand sintered NiO film offers conductivity~1.067×10^{-6}/ Ω cm and resistivity~9.370×10^{5} Ω cm. Electrical properties can be co-related with film thickness. Electrical resistivity of nickel oxide thin films has been reported in the range of $10 - 10^{6}$ (Ω·cm) [33]. The Hall resistivity decreases with increase in film thickness of Nickel [34]. Bulk concentration for non-sintered NiO film was found to be $1.036 \times 10^{12}/cm^{3}$, it was found to be 1.288×10^{12} $/cm^{3}$ for sintered NiO film. It is an p-type material. Research group of Chanae studied the effect of sintering on NiO film, film resistivity was 24.7 Ω·cm before sintering, it decreased to 4.23 Ω·cm after sintering~100 ºC. Nio film was found to have increased conductivity i.e. 1.78×10^{16} cm^{-3} after sintering, before sintering the value for conductivity was 2.41×10^{15} cm^{-3}.Decrease in mobility from 104 $cm^{2}V^{-1}s^{-1}$ to 82.85 $cm^{2}V^{-1}s^{-1}$ was observed before and after sintering respectively [35]. Research group of JianRen reported that hybrid films conductivity depends on the conductive network formed by the MWCNTs. MWCNTs provide network for the electron transfer due to which electrical resistance decreases [36]. Bulk concentration for CNT film was found to be $7.715 \times 10^{18}/cm^{3}$ which shows it is an p-type material as well but bulk concentration for bi-layer with non-sintered NiO film was found to be $5.22 \times 10^{18}/cm^{3}$, which increased to

$7.872x10^{19}/cm^3$ with sintered NiO film. It is an p-type film and it can be incorporated as an HTL in PSCs. Bi-layer has improved results as compared to NiO film, sintering has enhanced the electrical properties for both NiO film and bi-layer as well. Bi-layer shows p-type behavior with decreased resistivity, improved conductivity, and carrier concentration.

Table 3: Electrical Characterization Results

Parameters	NiO Film	NiO Film (Sintered)	MWCNT Film	Bi Layer (NiO & MWCNTs)	Bi Layer (sintered)
Resistivity (Ω cm)	$6.481x10^{4}$	$9.370x10^{5}$	$9.867x10^{-1}$	$5.382x10^{0}$	$1.555x10^{-1}$
Conductivity (1/ Ω cm)	$1.543x10^{-5}$	$1.067x10^{-6}$	$1.014x10^{0}$	$1.858x10^{-1}$	$5.994x10^{0}$
Mobility ($cm^2 V_s^{-1}$)	$9.299x10^{1}$	5.174x10	$8.200x10^{-1}$	$2.229x10^{-1}$	$4.753x10^{-1}$
Carrier Concentration (cm^{-3})	$1.036x10^{12}$	$1.288x10^{12}$	$7.715x10^{18}$	$5.22x10^{18}$	$7.872x10^{19}$

4.3.4. Optical Characterization

For optical characterization, UV-VIS-NIR Spectrophotometer (UV-3600 Plus, SHIMADZU) is used to understand the absorbance and percent transmittance of the layers. Non sintered NiO film shows <1% transmittance in visible region. Bi-layer with non-sintered NiO film shows transmittance ~1%. Transmittance for MWCNT film was found to be ~4% in visible region. Sintering effect improved transmittance for NiO Film ~11%. Transmittance of bi-layer with sintered NiO film was ~4%. Optical characterization results in this work have been justified through literature. Oscillations arise in transmittance spectra because of refractive index difference between thin films and substrate [37]. Abdel et al. reported that with increase in Ni concentration, transmittance of the Ni-doped ZnO decreased because of increased lattice defects [38]. Research group of Safwat A. observed an anomalous behavior at low substrate temperature that is disappearing absorption edge and lowering of the transmittance [39]. Absorption edge disappears in the films deposited at low temperature leading to decreased

transmittance; by lowering substrate temperature bigger clusters are formed and the scattered radiation increase because of surface roughness. This can be a reason of low transmittance in this work as well. Anyaegbunam et al. reports that decrease in transmittance can be linked with being metal oxide since the metal films reflect the incident radiation. The decrease in transmittance could also be attributed to increased molarity of the solution [40]. Generally, optical transmittance increases with decrease in film thickness. This behavior may be ascribed to the stoichiometry and perfection of the films. The reduction in the optical transmittance due to irradiation might result from increase in nickel to oxygen ratio and it can be related to increased lattice defects.

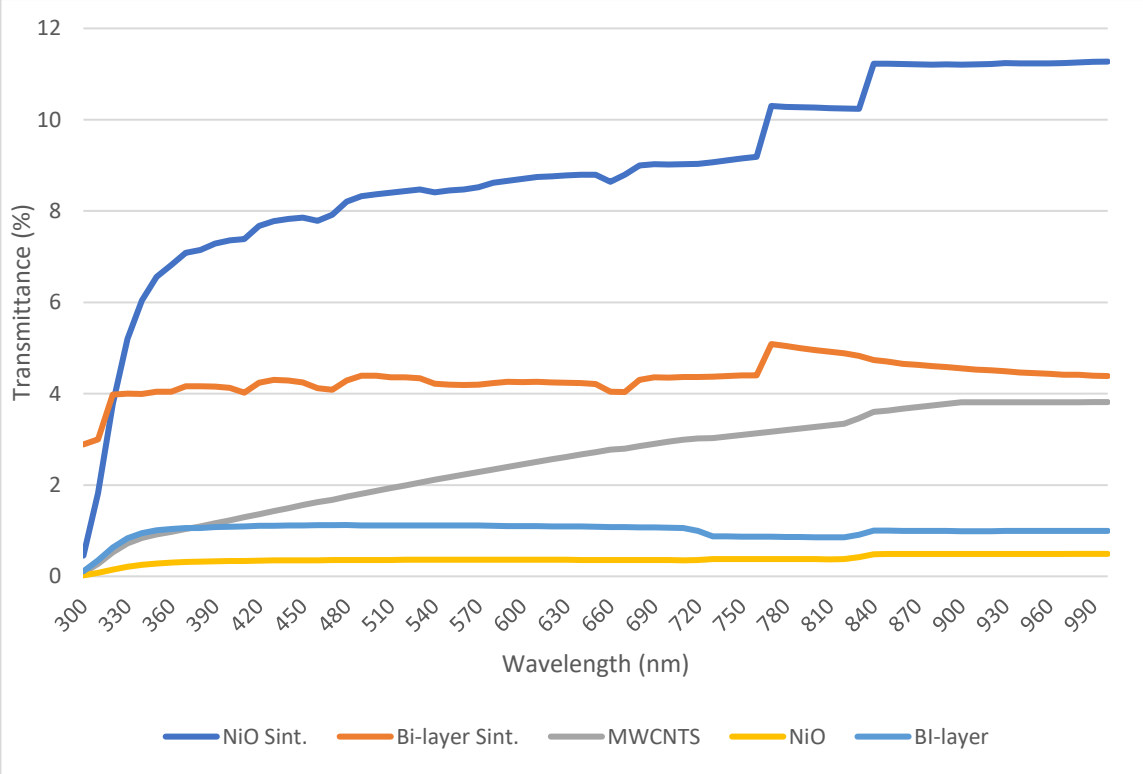

Figure 7: UV-Vis Spectra of NiO Thin film, MWCNT Thin film and Bi-layer.

4.3.5. Contact Angle Measurement

Contact angle for the fabricated NiO film and Bi-layer was observed before and after sintering by using a Kruss Drop Shape Analyzer DSA100. A 3-µm sized water droplet was poured upon the surface of slide. The contact angle of non-sintered NiO film was found to be <10°. After step sintering from 30°- 90° the contact angle improved to ~40°. The contact angle of bi-layer with non-sintered NiO film was found to be ~49°. The

contact angle of bi-layer with sintered NiO film improved from 49° to 68.4°. Contact angle could be improved if the sintering temperature is raised but in this work the film is being deposited on perovskite layer, raising temperature above 90° can destroy the perovskite layer.

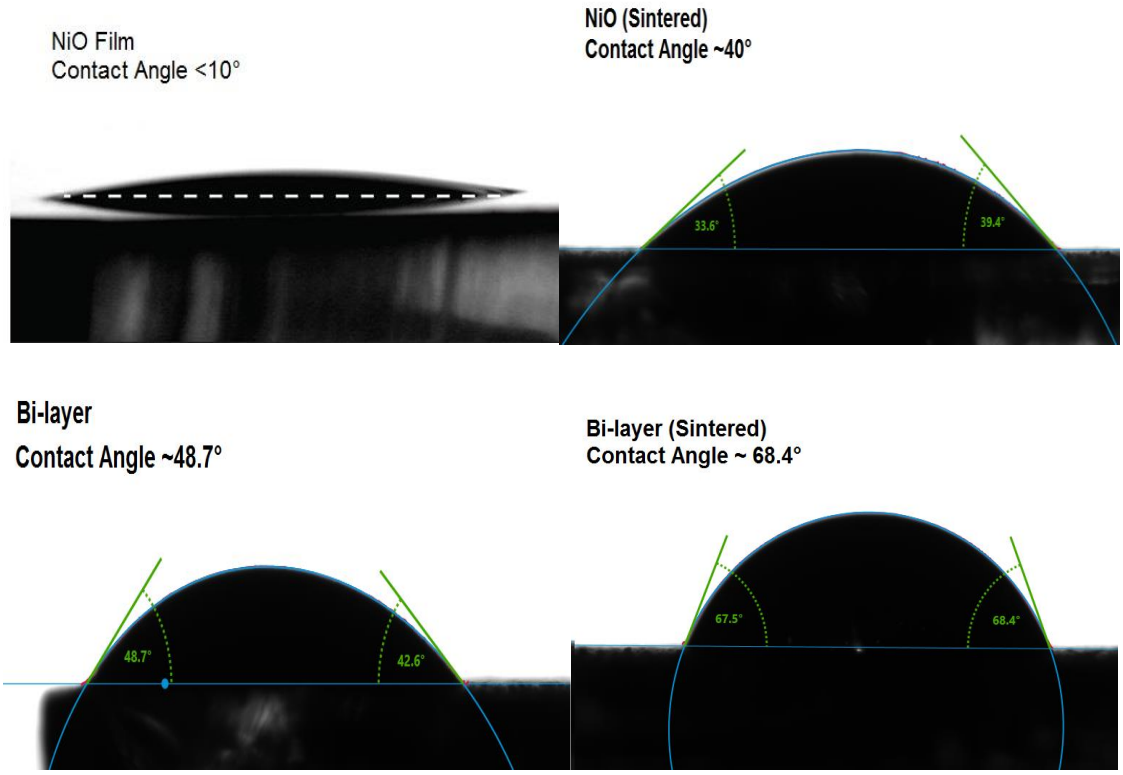

Figure 8: Contact Angles (a) NiO Film (b) Sintered NiO FILM (c) Bi-Layer (d) Sintered Bilayer

5. Conclusion

Nickel oxide nanoparticles with grain like structures with grain size of d= 32.27nm, 37.17 nm, 39.20 nm observed at 500 nm scale were synthesized through co-precipitation technique. Thin film comprising of nickel oxide nanoparticles was deposited through spin coating, at r1 1500 rpm - r2 3000 rpm for t1=t2=30seconds. Structural characterization results show that diffraction peaks are attributable to the face-centered cubic crystalline structure of NiO with relative peak position and characteristic peaks intensity as well. Increase in sharpness of XRD peaks has been observed by increasing sintering temperature of the particles and films. A Bi-layer comprising of NiO and MWCNTs was deposited by ultrasonic spray deposition of MWCNTs on NiO thin film.

Sintered and non-sintered NiO film and bi-layer were tested through structural, morphological, electrical and optical characterization. Comparatively, Bi-layer with sintered NiO film has showed better results to be employed as an HTL for solar cell applications.

References

[1] A. Mohammad Bagher, “Types of Solar Cells and Application,” *Am. J. Opt. Photonics*, vol. 3, no. 5, p. 94, 2015.

[2] Z. H. Bakr, Q. Wali, A. Fakharuddin, L. Schmidt-Mende, T. M. Brown, and R. Jose, “Advances in hole transport materials engineering for stable and efficient perovskite solar cells,” *Nano Energy*, vol. 34, no. November 2016, pp. 271–305, 2017.

[3] A. F. Ahmad, Z. Abbas, S. A. Aziz, S. J. Obaiys, and M. F. Zainuddin, “Synthesis and characterisation of nickel oxide reinforced with polycaprolactone composite for dielectric applications by controlling nickel oxide as a filler,” *Results Phys.*, vol. 11, no. April, pp. 427–435, 2018.

[4] F. I. Dar, K. R. Moonooswamy, and M. Es-Souni, “Morphology and property control of NiO nanostructures for supercapacitor applications,” *Nanoscale Res. Lett.*, vol. 8, no. 1, pp. 1–7, 2013.

[5] N. Zaghian and B. S. Boroujeny, “The Effect of Saccharin on Microstructure and Corrosion Behavior of Nanocrystalline Nickel Thin Films in Alkaline Solution,” *J. Adv. Mater. Process.*, vol. 5, no. 2, pp. 25–37, 2017.

[6] D. Das and F. Gharib, “Cubic NiO Nanoparticles: Synthesis and Characterization,” *Int. J. Bio-Inorganic Hybrid Nanomater.*, vol. 4, no. 2, pp. 59–64, 2015.

[7] S. Zhou, X. Zhu, L. Ma, Q. Yan, and S. Wang, “Outstanding superhydrophobicity and corrosion resistance on carbon-based film surfaces coupled with multi-walled carbon nanotubes and nickel nano-particles,” *Surf. Sci.*, vol. 677, no. May, pp. 193–202, 2018.

[8] J. R. Manders *et al.*, “<NiOfilmの作り方.pdf>,” pp. 2993–3001, 2013.

[9] Y. S. Lee *et al.*, “Nitrogen-doped cuprous oxide as a p-type hole-transporting layer in thin-film solar cells,” *J. Mater. Chem. A*, vol. 1, no. 48, pp. 15416–15422, 2013.

[10] Y. Yang *et al.*, “Ultrasound-spray deposition of multi-walled carbon nanotubes on NiO nanoparticles-embedded perovskite layers for high-performance carbon-based

perovskite solar cells," *Nano Energy*, vol. 42, no. November, pp. 322–333, 2017.

[11] S. Ganeshan, R. Dhanalakshmi, and R. Vijayalakshmi, "Synthesis and characterization of LiCoO2 by sol gel method," *Int. J. ChemTech Res.*, vol. 7, no. 3, pp. 1085–1089, 2015.

[12] A. Barakat *et al.*, "One step synthesis of NiO nanoparticles via solid-state thermal decomposition at low-temperature of novel aqua(2,9-dimethyl-1,10-phenanthroline)NiCl2 complex," *Int. J. Mol. Sci.*, vol. 14, no. 12, pp. 23941–23954, 2013.

[13] S. Pilban Jahromi *et al.*, "Influence of particle size on performance of a nickel oxide nanoparticle-based supercapacitor," *RSC Adv.*, vol. 5, no. 18, pp. 14010–14019, 2015.

[14] Z. Wei, H. Qiao, H. Yang, C. Zhang, and X. Yan, "Characterization of NiO nanoparticles by anodic arc plasma method," *J. Alloys Compd.*, vol. 479, no. 1–2, pp. 855–858, 2009.

[15] H. Xiao, F. Qu, and X. Wu, "Ultrathin NiO nanoflakes electrode materials for supercapacitors," *Appl. Surf. Sci.*, vol. 360, pp. 8–13, 2016.

[16] G. Raja, S. Gopinath, R. A. Raj, A. K. Shukla, M. S. Alhoshan, and K. Sivakumar, "Comparative investigation of CuFe2O4 nano and microstructures for structural, morphological, optical and magnetic properties," *Phys. E Low-Dimensional Syst. Nanostructures*, vol. 83, pp. 69–73, 2016.

[17] K. Mahendraprabhu and P. Elumalai, "Nanoscience and Nanotechnology : An International Journal ISSN : 2278-1374 Original Article Influence of precursors on formation of NiO nanostructures in hydrothermal synthesis," vol. 5, no. 2, pp. 29–33, 2015.

[18] Q. Zhou, Z. Lu, Z. Wei, L. Xu, Y. Gui, and W. Chen, "Hydrothermal synthesis of hierarchical ultrathin NiO nanoflakes for high-performance CH4 sensing," *Front. Chem.*, vol. 6, no. MAY, pp. 2–5, 2018.

[19] S. Safa, R. Hejazi, M. Rabbani, and R. Azimirad, "Hydrothermal synthesis of NiO

nanostructures for photodegradation of 4-nitrophenol," *Desalin. Water Treat.*, vol. 57, no. 46, pp. 21982–21989, 2016.

[20] A. Shamim, Z. Ahmad, S. Mahmood, U. Ali, T. Mahmood, and Z. A. Nizami, "Synthesis of nickel nanoparticles by sol-gel method and their characterization," *Open J. Chem.*, vol. 2, no. 1, pp. 16–20, 2019.

[21] H. Yan *et al.*, "Solution growth of NiO nanosheets supported on Ni foam as high-performance electrodes for supercapacitors," *Nanoscale Res. Lett.*, vol. 9, no. 1, pp. 1–7, 2014.

[22] R. D. and V. A. Sharanabasava V.Ganachari, Ravishankar Bhat, "Synthesis and characterization of nickel oxide nanoparticles by self-propagating low temperature combustion method," *Recent Res. Sci. Technol.*, vol. 04, no. 04, pp. 50–53, 2012.

[23] N. Dharmaraj, P. Prabu, S. Nagarajan, C. H. Kim, J. H. Park, and H. Y. Kim, "Synthesis of nickel oxide nanoparticles using nickel acetate and poly(vinyl acetate) precursor," *Mater. Sci. Eng. B Solid-State Mater. Adv. Technol.*, vol. 128, no. 1–3, pp. 111–114, 2006.

[24] S. Sagadevan and J. Podder, "Investigations on structural, optical, morphological and electrical properties of nickel oxide nanoparticles," *Int. J. Nanoparticles*, vol. 8, no. 3–4, pp. 289–301, 2015.

[25] A. D. Khalaji, K. Jafari, and S. M. Rad, "Synthesis of NiO nanoparticles via a solid state thermal decomposition of nickel(II) schiff base complex Ni(caph) (N3)(NO3) as a new precursor," *Synth. React. Inorganic, Met. Nano-Metal Chem.*, vol. 45, no. 6, pp. 875–878, 2015.

[26] N. Srivastava and P. C. Srivastava, "Realizing NiO nanocrystals from a simple chemical method," *Bull. Mater. Sci.*, vol. 33, no. 6, pp. 653–656, 2010.

[27] Z. Liu *et al.*, "Nickel oxide nanoparticles for efficient hole transport in p-i-n and n-i-p perovskite solar cells," *J. Mater. Chem. A*, vol. 5, no. 14, pp. 6597–6605, 2017.

[28] U. Kwon *et al.*, "Solution-Processible Crystalline NiO Nanoparticles for High-Performance Planar Perovskite Photovoltaic Cells," *Sci. Rep.*, vol. 6, no. April, pp.

1–10, 2016.

[29] M. Ruscello *et al.*, "Nanocomposite of nickel oxide nanoparticles and polyethylene oxide as printable hole transport layer for organic solar cells," *Sustain. Energy Fuels*, vol. 3, no. 6, pp. 1418–1426, 2019.

[30] M. Wąsik *et al.*, "Ultraviolet to far-infrared transmission properties of thin film multi-walled carbon nanotube random networks," *Journal of Materials Science*, vol. 52, no. 6. pp. 3086–3094, 2017.

[31] J. Di *et al.*, "Dry-processable carbon nanotubes for functional devices and composites," *Small*, vol. 10, no. 22, pp. 4606–4625, 2014.

[32] Y. J. Kim, S. J. Yu, and Y. G. Jeong, "Carbon nanotube/polyimide bilayer thin films with high structural stability, optical transparency, and electric heating performance," *RSC Adv.*, vol. 6, no. 36, pp. 30106–30114, 2016.

[33] A. J. Hassan, "Study of Optical and Electrical Properties of Nickel Oxide (NiO) Thin Films Deposited by Using a Spray Pyrolysis Technique," *J. Mod. Phys.*, vol. 05, no. 18, pp. 2184–2191, 2014.

[34] M. K. Dasoundhi, R. P. Jena, D. Kumar, and A. Lakhani, "Anomalous hall effect in nickel thin film at low temperatures," *AIP Conf. Proc.*, vol. 2100, no. April, 2019.

[35] C. Park, J. Kim, K. Lee, S. K. Oh, H. J. Kang, and N. S. Park, "Electronic, Optical and Electrical Properties of Nickel Oxide Thin Films Grown by RF Magnetron Sputtering," *Appl. Sci. Converg. Technol.*, vol. 24, no. 3, pp. 72–76, 2015.

[36] J. Huang, S. C. Her, X. Yang, and M. Zhi, "Synthesis and characterization of multi-walled carbon nanotube/graphene nanoplatelet hybrid film for flexible strain sensors," *Nanomaterials*, vol. 8, no. 10, 2018.

[37] S. T. Tan *et al.*, "Blueshift of optical band gap in ZnO thin films grown by metal-organic chemical-vapor deposition," *J. Appl. Phys.*, vol. 98, no. 1, pp. 1–5, 2005.

[38] M. S. Abdel-Wahab, A. Jilani, I. S. Yahia, and A. A. Al-Ghamdi, "Enhanced the photocatalytic activity of Ni-doped ZnO thin films: Morphological, optical and

XPS analysis," *Superlattices Microstruct.*, vol. 94, pp. 108–118, 2016.

[39] S. A. Mahmoud, A. Shereen, and M. A. Tarawnh, "Structural and Optical Dispersion Characterisation of Sprayed Nickel Oxide Thin Films," *J. Mod. Phys.*, vol. 02, no. 10, pp. 1178–1186, 2011.

[40] F. N. C. Anyaegbunam and C. Augustine, "A study of optical band gap and associated Urbach energy tail of chemically deposited metal oxides binary thin films," *Dig. J. Nanomater. Biostructures*, vol. 13, no. 3, pp. 847–856, 2018.